NASA Technical Memorandum 86719

NASA-TM-86719 19850025802

An Evaluation of Three Helicopter Rotor Sections

Raymond M. Hicks and Leslie J. Collins

August 1985

National Aeronautics and
Space Administration

NASA Technical Memorandum 86719

An Evaluation of Three Helicopter Rotor Sections

Raymond M. Hicks, Ames Research Center, Moffett Field, California
Leslie J. Collins, Informatics General Corp., Palo Alto, California

August 1985

National Aeronautics and
Space Administration

Ames Research Center
Moffett Field, California 94035

AN EVALUATION OF THREE HELICOPTER ROTOR SECTIONS

Raymond M. Hicks and Leslie J. Collins[1]

Ames Research Center

SUMMARY

Three helicopter rotor sections were tested in the NASA Ames Research Center 2- by 2-Foot Transonic Wind Tunnel over a Mach number range from 0.2 to 0.88. The sections tested had maximum thickness/chord ratios of 0.078, 0.09, and 0.10. The thickest section was of early technology and had been tested previously in other wind tunnels. This section was included in the investigation to establish a basis for comparing the two thinner sections, which were of recent design. The results of the investigation showed that the pitching-moment characteristics for the three airfoil sections were acceptable. The drag divergence Mach numbers for the three sections were 0.80, 0.825, and 0.845 in order of decreasing thickness.

NOMENCLATURE

c	airfoil chord, m (ft)
C_d	section drag coefficient
C_ℓ	section lift coefficient
C_m	section pitching-moment coefficient referenced to quarter chord
C_p	pressure coefficient $\frac{P_1 - P_\infty}{q_\infty}$
h	tunnel height, m (ft)
M_∞	free-stream Mach number
P	static pressure, N/m^2 (lb/ft^2)
q	dynamic pressure, N/m^2 (lb/ft^2)
R	Reynolds number based on free-stream conditions and airfoil chord

[1]Informatics General Corp., Palo Alto, Calif.

x airfoil abscissa, m (ft)

y airfoil ordinate, m (ft)

α angle of attack

δ wall correction factor

Subscripts

Max maximum

L lower

l local

U upper

∞ free stream

INTRODUCTION

The use of modern Computational Fluid Dynamic (CFD) codes for designing advanced airfoil sections has become fairly common over the past few years (refs. 1 and 2). These CFD codes are based on numerical solutions of the potential-flow equation (ref. 3). Viscous effects are usually included by iteratively correcting the potential-flow solution by use of an integral boundary-layer equation. The airfoil design can be accomplished by use of an inverse potential-flow code (ref. 4) or a numerical optimization algorithm coupled with a direct potential-flow code (ref. 1). The numerical optimization method permits the designer to consider multiple design conditions simultaneously during the design process, but has a limited design space. Inverse design codes usually permit consideration of only a single design condition, but offer a much larger design space; hence a greater variety of airfoil contours is available. The success or failure of a design is often determined by the experience of the designer in using and interpreting the computed results from these various techniques.

AIRFOIL DESIGNS

Three airfoil sections with low camber and maximum thickness/chord ratios of 0.078, 0.09, and 0.10 were evaluated during this study. The 7.8%-thick section, designated the A-2 airfoil, was designed by the numerical optimization method described in reference 1. The design goals for this airfoil were a drag-divergence Mach number of 0.86; quarter-chord pitching-moment coefficients of approximately

zero at low lift coefficients; and maximum lift coefficients of 1.2, 1.1, 1.0, and 1.0 at Mach numbers of 0.2, 0.3, 0.4, and 0.5, respectively. The 9%- thick section, designated the SSC-A09 airfoil, was designed by R. J. Flemming (Sikorsky Aircraft Division, United Technologies Corporation, Stratford, CN). This airfoil was designed by an inverse potential-flow code with the following goals: drag-divergence Mach number of 0.83, low pitching moments, and high maximum-lift coefficients at Mach numbers between 0.3 and 0.5. The 10%-thick section, designated the SC1095 airfoil, was designed by D. T. Balch (also of Sikorsky). This airfoil is an early technology airfoil and was included in the study to permit comparison of 2- by 2-ft wind tunnel data with data from other tunnels. This section also served as a baseline to assess the aerodynamic advantages of the newer A-2 and SSC-A09 airfoils.

The experimental data obtained during this investigation have been compared with a widely used, nonconservative, potential-flow code which includes an iterated boundary-layer correction (ref. 5).

APPARATUS AND TEST PROCEDURE

Models

Three airfoil models with the contours shown in figure 1 were machined from stainless steel billets. The profile coordinates are given in table 1. The models had 6-in. chords and 24-in. spans. Each model was equipped with 24 upper-surface orifices and 22 lower-surfaces orifices, drilled normal to the surface to determine the surface pressure distributions.

Wind Tunnel

The test was conducted in the Ames 2- by 2-Foot Transonic Wind Tunnel, a variable-speed, continuous-flow, ventilated-wall, variable-pressure facility. The tunnel can be used for two-dimensional testing by replacing the ventilated side walls with solid walls where thick, model-supporting glass windows are mounted. The windows are rotated by a motorized drive system to change the angle of attack. A drag rake of 82-tubes located 1.75 chords behind the model's trailing edge was used to survey the model wake. Airfoil models are mounted spanning the horizontal dimension of the tunnel test section so that the center of rotation is near the 25% chord station on the model. The gaps between the side walls and the end of the model were sealed.

Instrumentation

Measurements of the model surface pressures and the wake-rake pressures were made by a system of scanivalves utilizing precision pressure transducers. Basic tunnel parameters were measured with precision mercury manometers. The angle of attack was measured with a potentiometer coupled to the rotating side window by a

drive gear. Data were obtained by a high-speed, data-acquisition system and reduced on an IBM 360 computer.

Tests

The aerodynamic coefficients of the three airfoils were obtained at Mach numbers ranging from 0.2 to 0.88, and Reynolds numbers of 1.9 million at Mach 0.2 to Reynolds numbers of 4 million for Mach numbers greater than 0.5. The angles of attack ranged from approximately -2° to stall. It was not possible to obtain data at angles of attack near and beyond stall at moderate and high Mach numbers because of severe vibration of the wake rake. The vibration was caused by the unsteady loads induced by massive separation from the models. Data were obtained at all test conditions with transition fixed at 13% of the chord.

Pressure coefficients were determined from surface pressure measurements. Section normal-force coefficients, chord-force coefficients, and pitching-moment coefficients were obtained from an integration of pressure coefficients. An angle-of-attack correction, $\Delta\alpha$, was used to account for the presence of the tunnel walls by the following equation:

$$\Delta\alpha = \delta(c/h)C_{\ell}$$

where δ, c/h, and C_{ℓ} are the correction-factor coefficient, model chord/tunnel height ratio, and section lift coefficient, respectively. (This correction was established by L. S. Stivers, Jr., in a private communication.) The angle-of-attack coefficient for the correction factor, δ, is a function of Mach number. The values used are as follows:

M	δ
0.2	5.4
.3	8.5
.4	10.6
.5	11.9
.6	12.5
.7	12.8
.75	12.9
.77	12.9
.79	12.9
.80	13.0
.81	13.0
.82	13.0
.83	13.1
.84	13.1
.86	13.1
.88	13.1

The $\Delta\alpha$ correction corresponding to each value of δ was added algebraically to the model geometric angle of attack expressed in degrees.

RESULTS AND DISCUSSION

SC1095 Airfoil

The theoretical and experimental aerodynamic-force coefficients for the SC1095 airfoil are shown in figures 2(a) through 2(l). Repeat data taken during testing are represented by different symbols in the figures.

Plots of lift coefficient versus angle of attack indicate a fairly abrupt stall at Mach numbers below 0.5 with the stall becoming more gentle at higher Mach numbers (figs. 2(a)-2(e)). The stall characteristics and maximum lift coefficients were difficult to determine at high Mach numbers because of severe vibration of the wake rake caused by extensive flow separation over the model upper surface. The experiment-theory correlation for lift-curve slope is acceptable only at Mach 0.2. The correlation becomes progressively worse as the Mach number is increased because of the use of inaccurate wind tunnel wall corrections for the model angle of attack. Sufficient time was not available to rewrite the data-reduction program to eliminate the corrections. The experimental lift curve at Mach 0.88 shows a decrease in slope near -1° angle of attack caused by a shock wave on the lower surface which disappears as the angle of attack is increased (fig. 2(l)). This nonlinearity is not predicted by theory. As stated earlier, the theory used here is a transonic potential code with a boundary-layer, displacement-thickness correction.

The pitching moments show a slight increase with increasing lift coefficient below stall at low Mach numbers (figs. 2(a) through 2(e)) because of decreasing pressures near the leading edge on the upper surface. At high Mach numbers the pitching-moment curves show a negative slope at low lift coefficients because of the rearward movement of the upper-surface shock wave with increasing lift coefficient (figs. 2(i) and 2(j)). The theory predicts the magnitude of the pitching moments fairly well for attached flow (fig. 2(h)), but shows poor correlation with experiment when separation is present (fig. 2(j)).

The theoretical drag level is approximately 20% lower than the experimental level at Mach numbers below drag divergence for attached flow conditions (figs. 2(a)-2(g)). The drag correlation becomes worse at high lift coefficients because the theory used here does not model the separated flow. The shape of the theoretical drag curves is similar to the experimental curves at Mach numbers near drag divergence for attached flow conditions, indicating the shock strength is reasonably well predicted. The level of drag is not well predicted at Mach numbers above drag rise because of shock-induced separation and underprediction of shock strength (figs. 2(i)-2(l)). The theoretical drag values given included shock drag obtained from an integration of surface pressures with a far-field flux correction and form drag obtained from the Squire-Young formula (ref. 5).

A-2 Airfoil

The theoretical and experimental aerodynamic-force data for the A-2 airfoil are presented in figures 3(a) through 3(j).

The maximum lift coefficient at Mach 0.2 is fairly high considering the low maximum-thickness/chord ratio (0.078) and the relatively low test Reynolds number for this airfoil (fig. 3(a)). However, the decrease in maximum lift coefficient with increasing Mach number is large, showing that the shape of the leading edge of this airfoil is effective in delaying flow separation only at low Mach numbers where the stall is not determined by shock-induced separation. Note that the stall of the A-2 airfoil is considerably more gradual than that for the SC1095 section at moderate Mach numbers (compare fig. 2(c) with 3(c)). The leading-edge shape of the A-2 airfoil is also effective in promoting an isentropic compression at Mach numbers near drag rise at low lift coefficients.

The theoretical pitching-moment curves for the A-2 section show a more positive slope than the experimental curves at Mach numbers less than 0.70 (fig. 3(c)). Above Mach 0.70 the correlation of theoretical with experimental pitching moments improves until flow separation is encountered near Mach 0.86. The improved correlation at Mach numbers between 0.70 and 0.86 is due to a fortuitous balancing of errors in upper- and lower-surface theoretical pressures. Note that the pitching-moment coefficients are near zero at low lift coefficients for all Mach numbers below drag rise, which fulfills one of the design goals for this airfoil.

The predicted drag coefficients for the A-2 airfoil are consistently less than the experimental values at all test conditions (figs. 3(a)-3(j)). As expected, the degree of correlation becomes progressively worse with increasing Mach number and lift coefficient because of the onset of flow separation. In spite of the error in the magnitude of the calculated drag, the shape of the theoretical curves is similar to experiment for attached and mildly separated flows (figs. 3(a)-3(i)). Poor correlation is noted at Mach 0.88 where flow separation is present at nearly all lift coefficients.

SSC-A09 Airfoil

The section aerodynamic characteristics for the SSC-A09 airfoil are presented in figures 4(a) through 4(l).

As observed with the two previously discussed airfoils, the lift-curve slope is underestimated by theory at all Mach numbers except 0.2 because of an error in the experimentally determined wall corrections for the wind tunnel. Note that the stall of the SSC-A09 section is more gradual than that of the SC1095 airfoil at most test Mach numbers (compare figs. 2(d) and 4(d)). The maximum lift coefficients of the SC1095 and SSC-A09 airfoils are nearly the same at subcritical Mach numbers (compare figs. 2(a)-2(d) with 3(a)-3(d)).

The experiment-theory correlation for pitching moments for the SSC-A09 airfoil is fairly good for test conditions with attached flow (figs. 3(a)-3(h)). The theoretical slope is slightly more positive than the experimental slope, caused in part by inaccurately predicted boundary-layer quantities near the trailing edge. At Mach numbers greater than 0.84, the nonlinear characteristics of the pitching-moment curves are not well predicted by theory mainly because of shock-induced, boundary-layer separation which is not modeled by the theory. Note that this airfoil gives near-zero pitching moments for low and moderate lift coefficients at Mach numbers below 0.77.

The drag level for the SSC-A09 airfoil at lift coefficients near zero remains nearly constant until the drag-rise Mach number of approximately 0.82 is reached. This is a desirable characteristic of transonic rotor sections because of the wide range of flow conditions encountered by a rotor blade in flight. Theoretical drag curves are shown for both natural and fixed transition. Note that the experiment-theory correlation is good for fixed transition at all test conditions which exhibited attached flow (figs. 4(a)-4(i)). There is no obvious reason why the experiment-theory correlation for the SSC-A09 airfoil is better than for the SC1095 and A-2 airfoils discussed previously. As observed with the previously described results, the level of drag is not well predicted at Mach numbers above drag rise because of a lack of a shock-boundary-layer interaction model in the theory.

Pressure Distributions

Experimental pressure distributions for selected test conditions for the three airfoil sections tested are shown in figures 5 through 38 (the Reynolds numbers indicated in the figures are in millions). Theoretical pressure distributions are shown along with the experimental distributions for some test conditions. Theoretical curves are not shown for all conditions because of the high cost and time involved in generating the calculations and because the shape of the pressure distributions does not change rapidly with Mach number or angle of attack. The theoretical calculations were performed at the experimental-lift coefficients; hence, the computed angles of attack would be different from the experimental angles at all Mach numbers except 0.2. As stated previously, this discrepancy between experimental and theoretical angle of attack is due to inaccurate wind tunnel wall corrections. Such forced matching of experimental and theoretical lift coefficients can cause poor correlation of leading-edge pressures because of different experimental and theoretical stagnation point locations. The fact that the experimental leading-edge pressures correlate fairly well with the theoretical pressures for most cases shown here is further evidence of the inaccuracy of the experimental angles of attack shown in the figures of this report. In general, the theoretical pressure distributions show better correlation with the experimental distributions at subcritical Mach numbers than at transonic conditions (compare figs. 6(f) and 15(a)). This is somewhat surprising since the theoretical method used here was "tuned" for transonic flow. However, the presence of discontinuities in transonic flow makes accurate theoretical simulation more difficult than for smooth subcritical flow. As expected, the correlation becomes poor for separated flow conditions (fig. 15(e)).

The correlation is poor for some test conditions which exhibit good trailing-edge pressure recovery, which is indicative of attached flow (fig. 10(g)). The poor experiment-theory correlation in such cases may be due to the existence of a separation bubble at the base of the shock, which is not modeled by the theory. Pressure distributions are not presented for high lift conditions at low Mach numbers, because the pressure coefficients near the leading edge were off scale on the machine-generated plots. Selected pressure distributions for cases which exhibit massive flow separation have been included to give those engaged in the theoretical modeling of such flows some data to consider (fig. 17(g)).

Drag Summary

Summary curves of drag coefficient versus Mach number at lift coefficients of 0.0 and 0.2 are shown in figure 39 for the three airfoil sections tested. Both theoretical and experimental data are shown. Note that the theory predicts the drag-divergence Mach number fairly well, but underpredicts the subcritical drag level for the SC1095 and A-2 airfoils. The rate of drag increase beyond the drag-divergence Mach number is not accurately predicted for all airfoils. The fact that the drag-divergence Mach number is fairly well predicted allows the aerodynamicist to use this method for preliminary design work. A more exact theory would be needed to assess the airfoil performance at flight conditions above the design Mach number and at high lift coefficients.

CONCLUDING REMARKS

The following conclusions result from the investigation reported here:

1. The A-2 airfoil was found to have a drag-divergence Mach number of 0.845, which is lower than the design goal of 0.86.

2. The A-2 airfoil exhibited quarter-chord pitching moments of nearly zero at all Mach numbers below drag divergence for low and moderate lift coefficients.

3. The maximum lift coefficient for the A-2 airfoil is 1.30 at Mach 0.2 and falls rapidly as the Mach number is increased. The A-2 airfoil exhibited a gentle stall at low and moderate Mach numbers.

4. The SSC-A09 airfoil exhibited better pitching-moment characteristics and a higher drag-divergence Mach number than the SC1095 airfoil.

5. The experiment-theory correlation for lift-curve slope was good only at Mach 0.2 because of inaccurate wall corrections of the wind tunnel.

6. The experiment-theory correlation for pitching moment was found to be fairly good for attached flow conditions.

7. The shape of the theoretical drag curves agreed fairly well with the shape of the experimental curves for attached flow even when shock waves were present. However, the theoretical drag level was less than the experimental level for all test conditions for the SC1095 and A-2 airfoils. The experiment-theory correlation for drag level was fairly good for the SSC-A09 airfoil for attached flow.

8. The experiment-theory correlation for drag-divergence Mach number was good. However, the rate of increase in drag at Mach numbers greater than drag rise was not well predicted by theory.

REFERENCES

1. Hicks, R. M.; and McCroskey, W. J.: An Experimental Evaluation of a Helicopter Rotor Section Designed by Numerical Optimization. NASA TM-78622, 1980.

2. Dadone, Leo: Rotor Airfoil Optimization: An Understanding of the Physical Limits. 34th Annual Nat. Forum of Amer. Helicopter Soc., 1978.

3. Jameson, Antony: Transonic Flow Calculations for Airfoils and Bodies of Revolution. Grumman Aerodynamics Report 390-71, 1971.

4. Carlson, Leland A.: Trandes: A Fortran Program for Transonic Analysis or Design. NASA CR-2821, 1977.

5. Bauer, F.; Garabedian, P.; and Jameson, A.: Supercritical Wing Sections II. Lecture Notes in Economics and Mathematical Systems, vol. 108, Springer-Verlag, 1975.

TABLE 1.- AIRFOIL COORDINATES

SC1095			A-2			SSC-A09		
x_U/C	y_U/C	y_L/C	x_U/C	y_U/C	y_L/C	x_U/C	y_U/C	y_L/C
0.000000	0.000000	0.000000	.0000000	.0000000	.0000000	0.000000	0.000000	0.000000
0.000200	0.001888	-0.001618	.0002000	.0044476	-.0027696	0.000199	0.002000	-0.001454
0.000500	0.003070	-0.002573	.0004000	.0054877	-.0037937	0.000798	0.003946	-0.002869
0.001000	0.004430	-0.003685	.0006000	.0062609	-.0044036	0.001994	0.006270	-0.004573
0.002000	0.006400	-0.005347	.0008000	.0068701	-.0048939	0.002991	0.008029	-0.005446
0.003500	0.008655	-0.007242	.0010000	.0074058	-.0053113	0.004487	0.009868	-0.006445
0.005000	0.010540	-0.008800	.0020000	.0094270	-.0068572	0.006979	0.012392	-0.007703
0.006500	0.012212	-0.010157	.0030000	.0109113	-.0079614	0.009970	0.014921	-0.008877
0.008000	0.013735	-0.011376	.0040000	.0121167	-.0088477	0.015952	0.019076	-0.010704
0.010000	0.015595	-0.012845	.0050000	.0131456	-.0095918	0.021934	0.022500	-0.012175
0.012500	0.017715	-0.014500	.0100000	.0169486	-.0122762	0.027916	0.025445	-0.013447
0.016000	0.020405	-0.016565	.0200000	.0219172	-.0156881	0.033898	0.028039	-0.014588
0.020000	0.023200	-0.018649	.0300000	.0253883	-.0180793	0.039881	0.030369	-0.015631
0.025000	0.026350	-0.020920	.0400000	.0280682	-.0199604	0.045863	0.032494	-0.016594
0.035000	0.031400	-0.024542	.0500000	.0302428	-.0215217	0.051845	0.034449	-0.017487
0.050000	0.036770	-0.028415	.0600000	.0320584	-.0228604	0.057827	0.036249	-0.018314
0.065000	0.040705	-0.031080	.0700000	.0336024	-.0240286	0.067797	0.038903	-0.019568
0.080000	0.043735	-0.032950	.0800000	.0349314	-.0250594	0.077767	0.041143	-0.020691
0.100000	0.046800	-0.034640	.0900000	.0360844	-.0259766	0.087737	0.043016	-0.021706
0.125000	0.049625	-0.036190	.1000000	.0370922	- 0268000	0.097707	0.044583	-0.022638
0.150000	0.051740	-0.037390	.1250000	.0391139	-.0285221	0.112663	0.046504	-0.023910
0.200000	0.054470	-0.038840	.1500000	.0406230	-.0298929	0.127618	0.048054	-0.025064
0.250000	0.055480	-0.039330	.1750000	.0417298	-.0309716	0.142573	0.049345	-0.026124
0.300000	0.055240	-0.039180	.2000000	.0425475	-.0318276	0.157529	0.050444	-0.027104
0.350000	0.054370	-0.038578	.2500000	.0435116	-.0329717	0.172485	0.051385	-0.028013
0.400000	0.052990	-0.037598	.3000000	.0438492	-.0335038	0.187440	0.052184	-0.028853
0.450000	0.051045	-0.036216	.3500000	.0436244	-.0333958	0.202395	0.052860	-0.029628
0.500000	0.048540	-0.034460	.4000000	.0429292	-.0326937	0.217350	0.053427	-0.030339
0.550000	0.045550	-0.032342	.4500000	.0417649	-.0313991	0.232305	0.053911	-0 030988
0 600000	0.042122	-0.029855	.5000000	.0401547	-.0295705	0.247261	0.054322	-0.031579
0.650000	0.038195	-0.027018	.5500000	.0381025	-.0272780	0.277171	0.054958	-0.032594
0.700000	0.033750	-0.023840	.6000000	.0355897	-.0245900	0.307082	0.055369	-0.033402
0.750000	0.028869	-0.020335	.6500000	.0325878	-.0215687	0.336992	0.055564	-0.034007
0.800000	0.023620	-0.016580	.7000000	.0290918	-.0182959	0.376873	0.055494	-0.034506
0.850000	0.018080	-0.012650	.7250000	.0271741	-.0166092	0.416754	0.055039	-0.034637
0.900000	0.012355	-0.008650	.7500000	.0251641	-.0149200	0.436694	0.054663	-0.034558
0.925000	0.009426	-0.006640	.7750000	.0230819	-.0132656	0.456635	0.054182	-0.034376
0.950000	0.006424	-0.004540	.8000000	.0209327	-.0116687	0.476575	0.053595	-0.034087
0.975000	0.003280	-0.002325	.8250000	.0186761	-.0101755	0.496515	0.052899	-0.033683
0.990000	0.001320	-0.000930	.8500000	.0163550	-.0087363	0.516456	0.052093	-0.033165
1.000000	0.000000	0.000000	.8750000	.0141148	-.0072907	0.536396	0.051176	-0.032532
			.9000000	.0120124	-.0058396	0.556336	0.050149	-0.031790
			.9250000	.0101222	-.0043838	0.576277	0.049009	-0.030949
			.9500000	.0085521	-.0029245	0.596217	0.047755	-0.030018
			.9600000	.0080436	-.0023402	0.616157	0.046381	-0.029002
			.9700000	.0076211	-.0017557	0.636097	0.044875	-0.027904
			.9800000	.0072965	-.0011699	0.656039	0.043220	-0.026720
			.9900000	.0070833	-.0005850	0.675979	0.041391	-0.025448
			.9950000	.0070250	-.0002930	0.695919	0.039368	-0.024088
			.0000000	.0070000	0.0000000	0.715860	0.037140	-0.022642
						0.735800	0.034719	-0.021121
						0.755740	0.032138	-0.019540
						0.775680	0.029445	-0.017918
						0.795621	0.026681	-0.016272
						0.815561	0.023871	-0.014617
						0.835501	0.021012	-0.012957
						0.855442	0.018089	-0.011289
						0.875382	0.015093	-0.009598
						0.895323	0.012051	-0.007863
						0.915264	0.009046	-0.006081
						0.935204	0.006229	-0.004290
						0.955144	0.003849	-0.002610
						0.975084	0.002288	-0.001325
						0.985055	0.001987	-0.000992
						0.995025	0.002135	-0.000863
						1.000000	0.002408	-0.000803

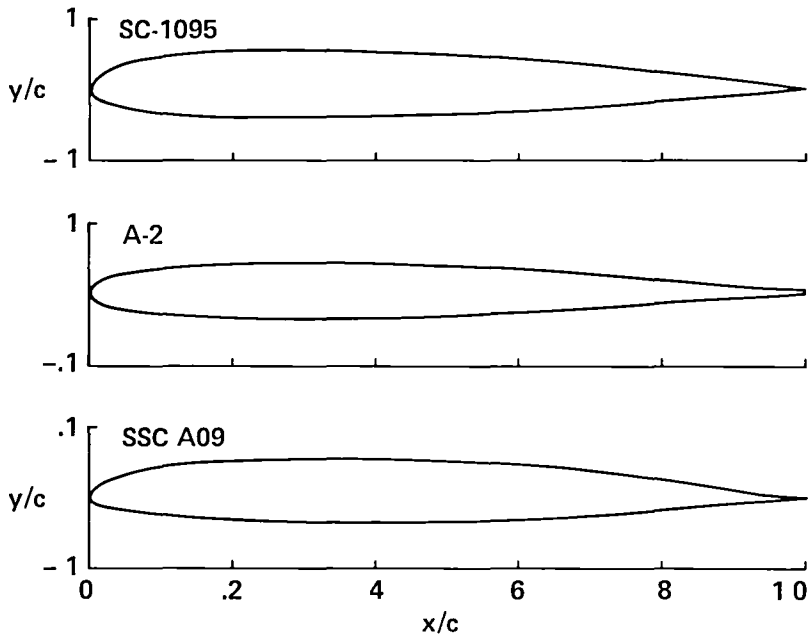

Figure 1.- Airfoil sections evaluated.

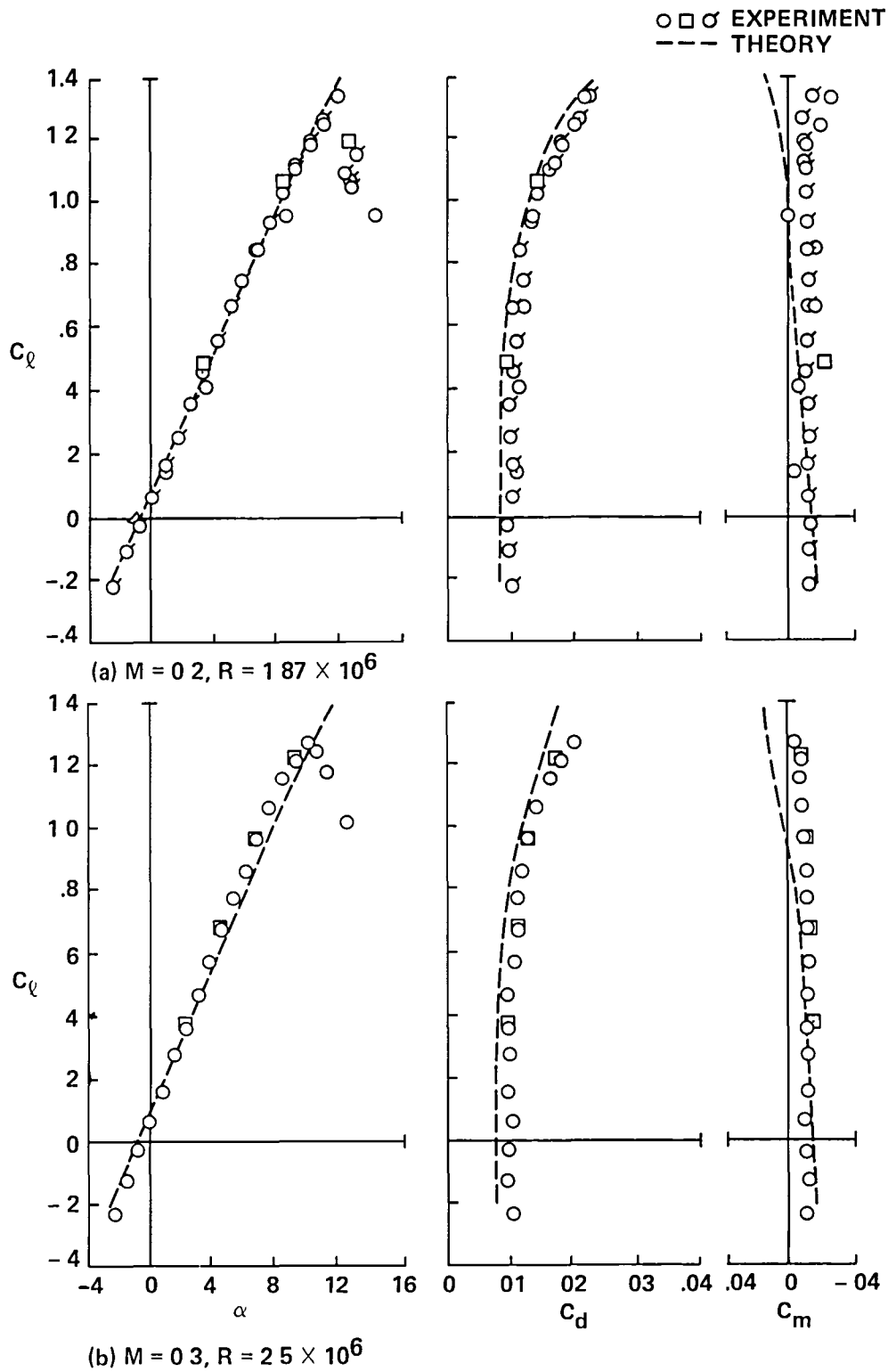

Figure 2.- Section aerodynamic characteristics of the SC1095 airfoil, transition fixed.

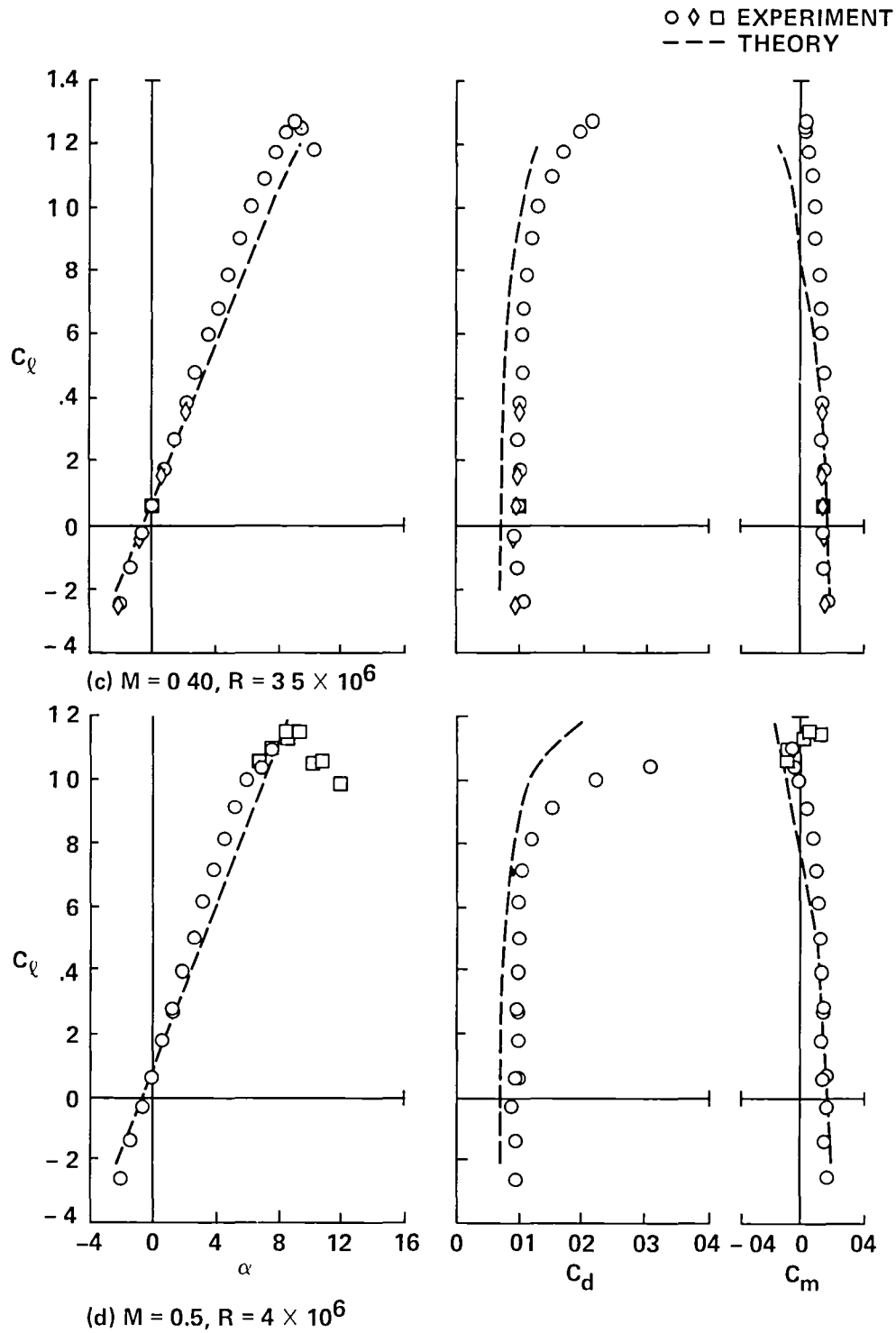

Figure 2.- Continued.

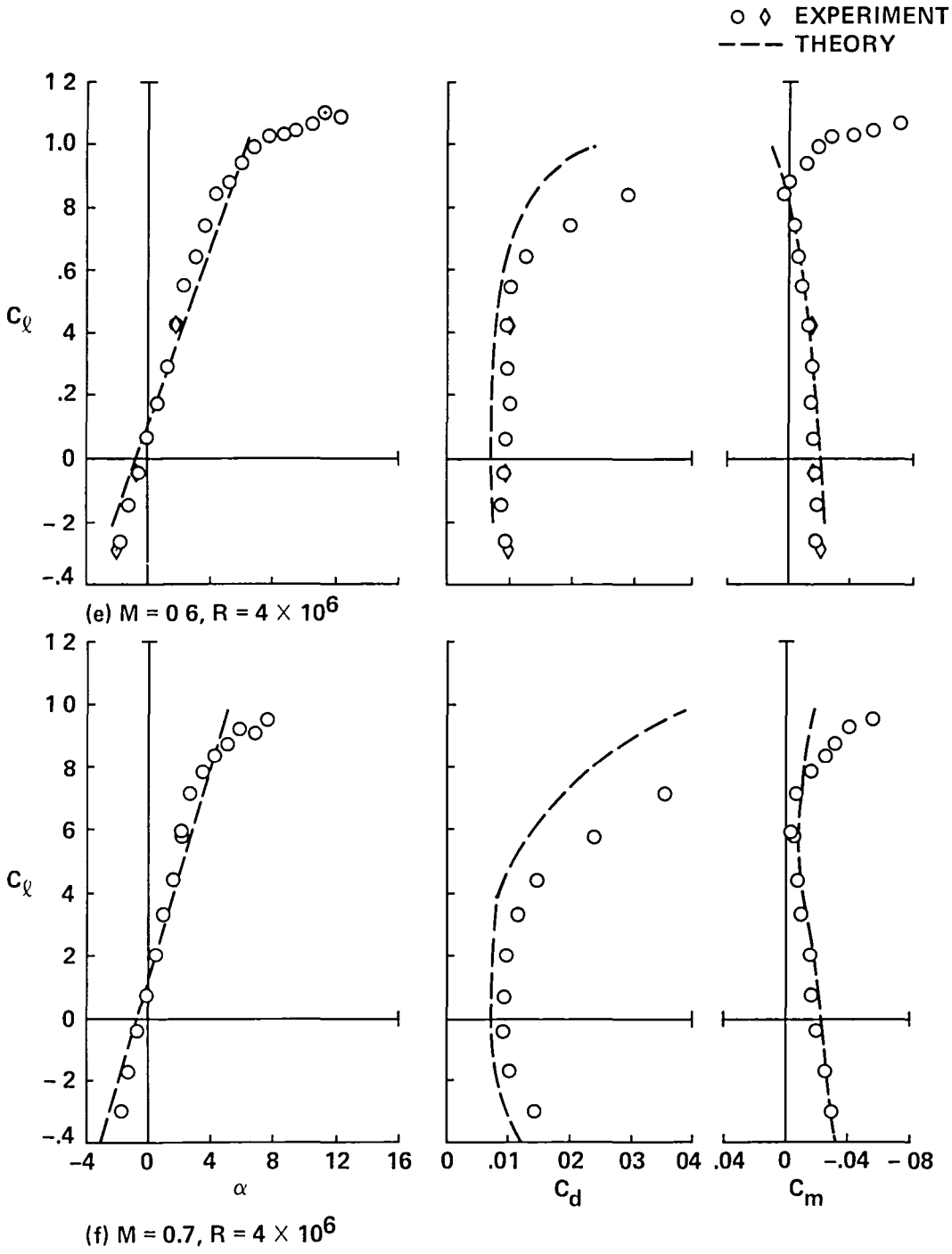

Figure 2.- Continued.

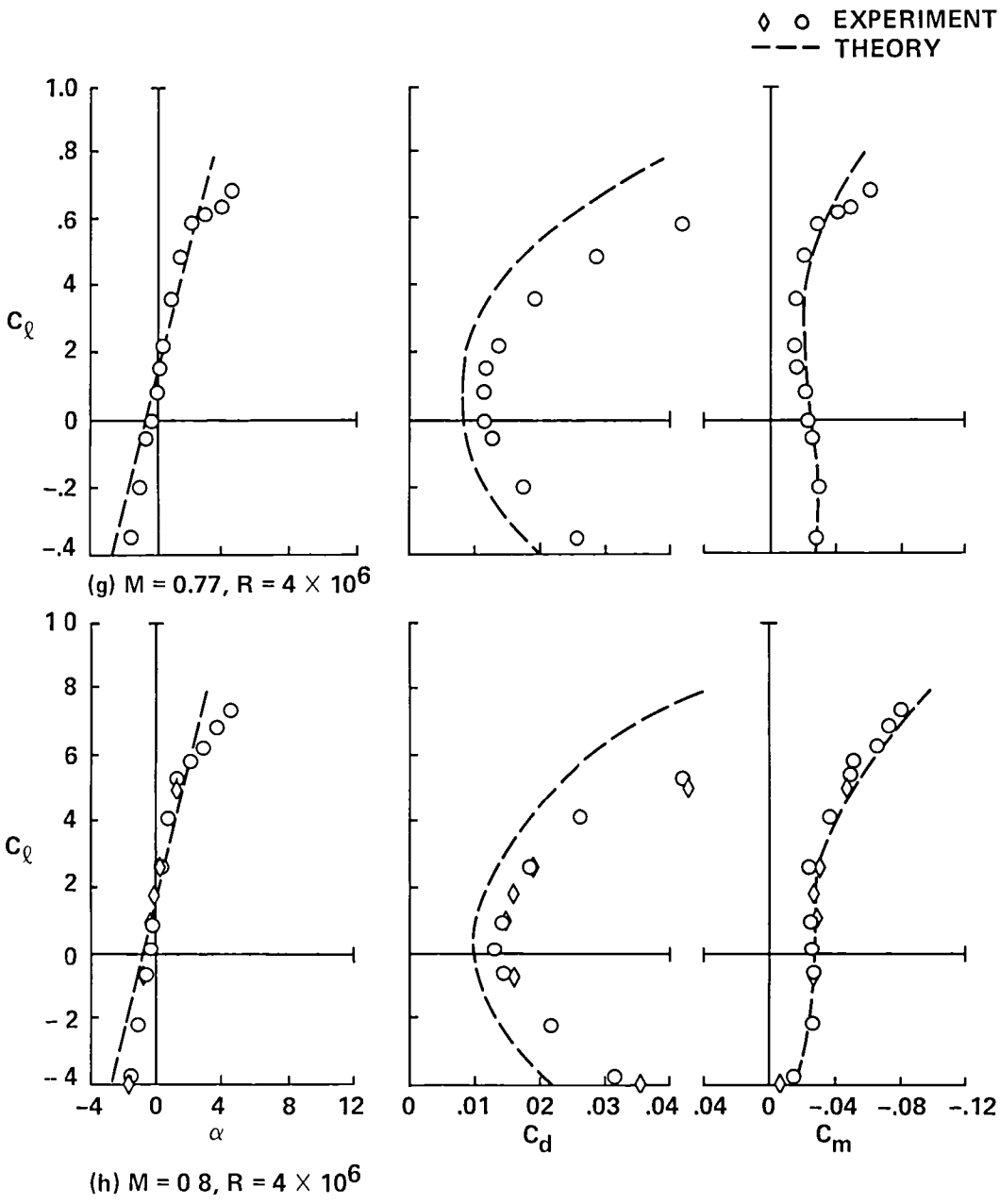

Figure 2.- Continued.

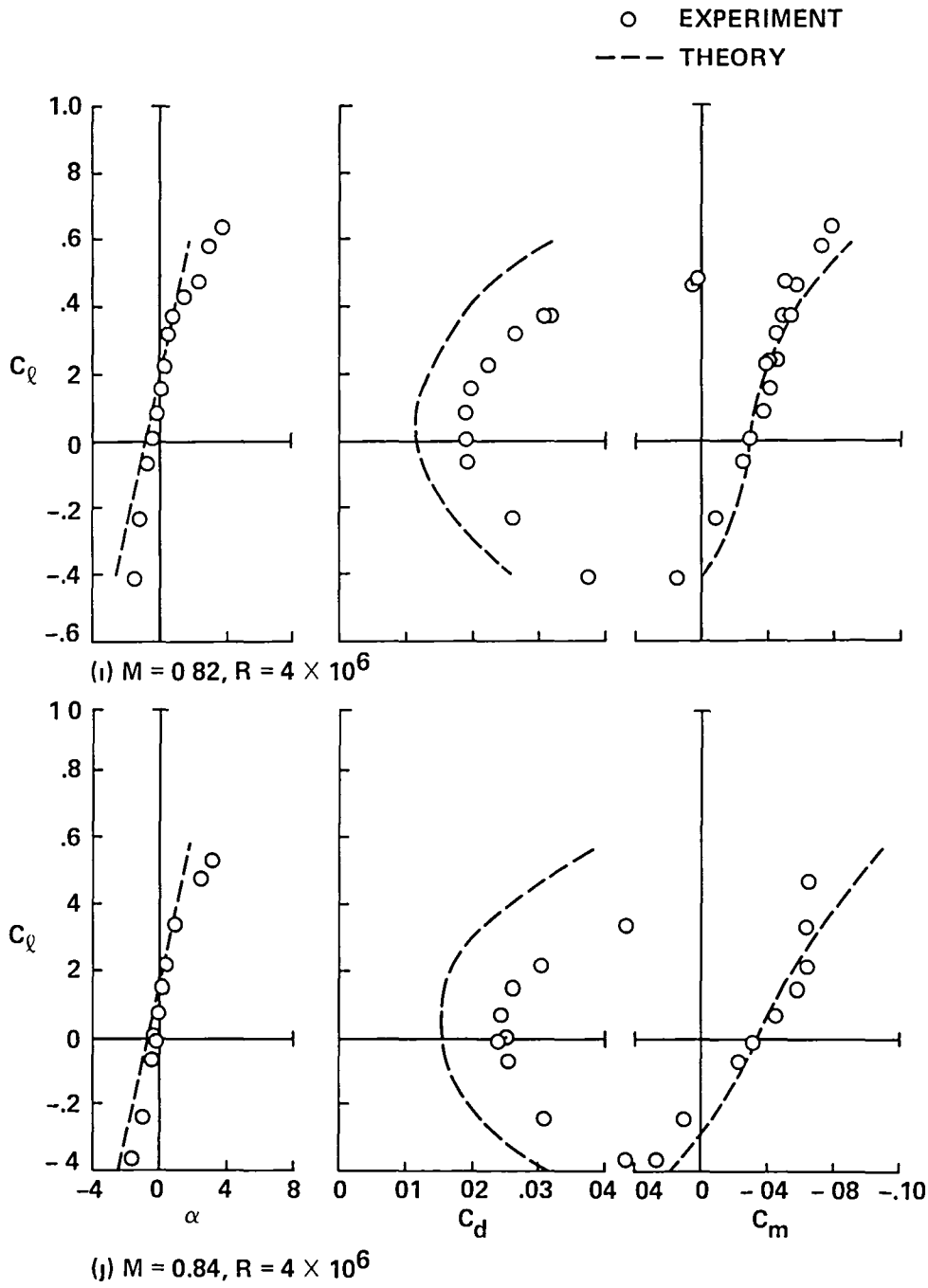

Figure 2.- Continued.

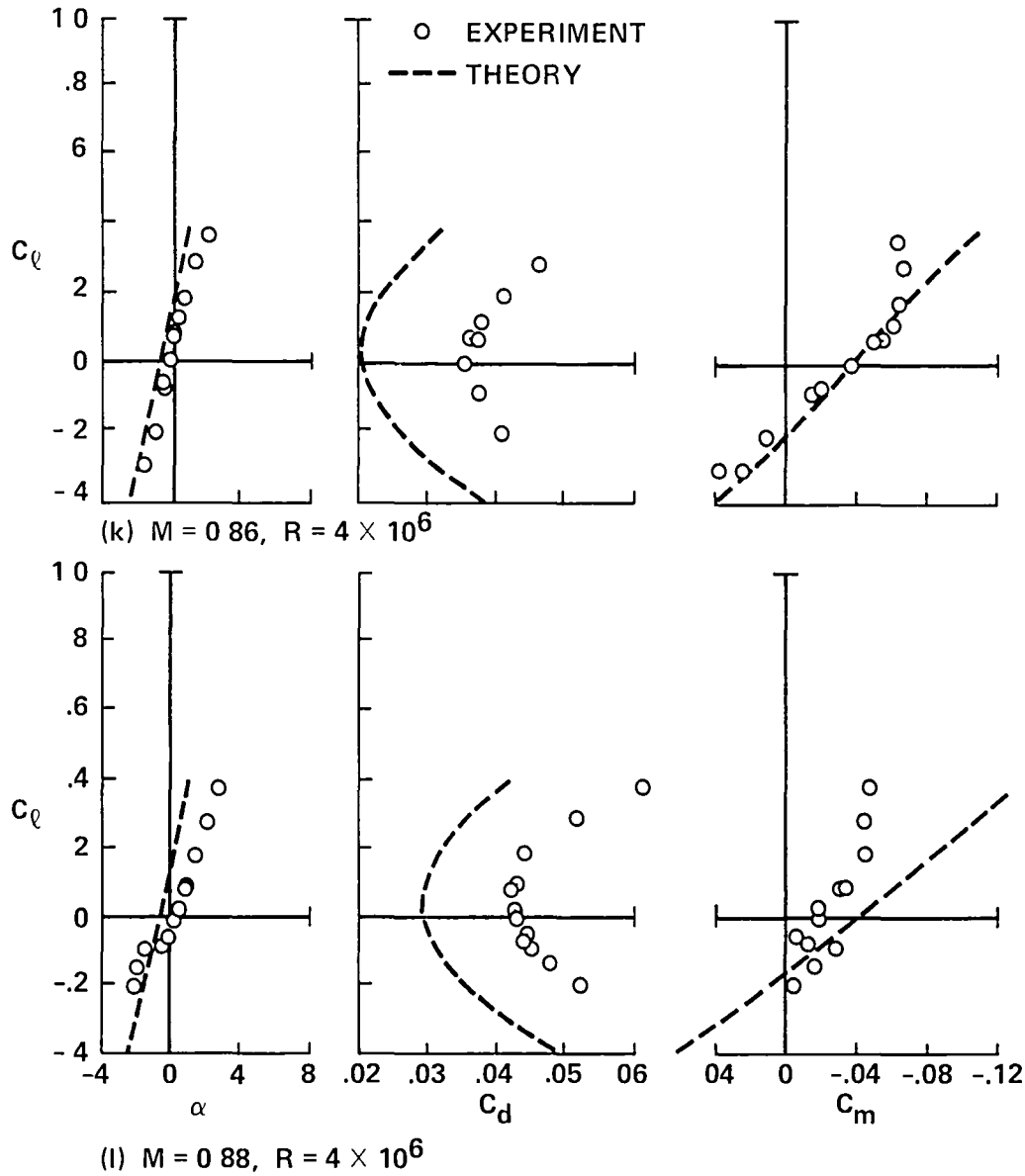

Figure 2.- Concluded.

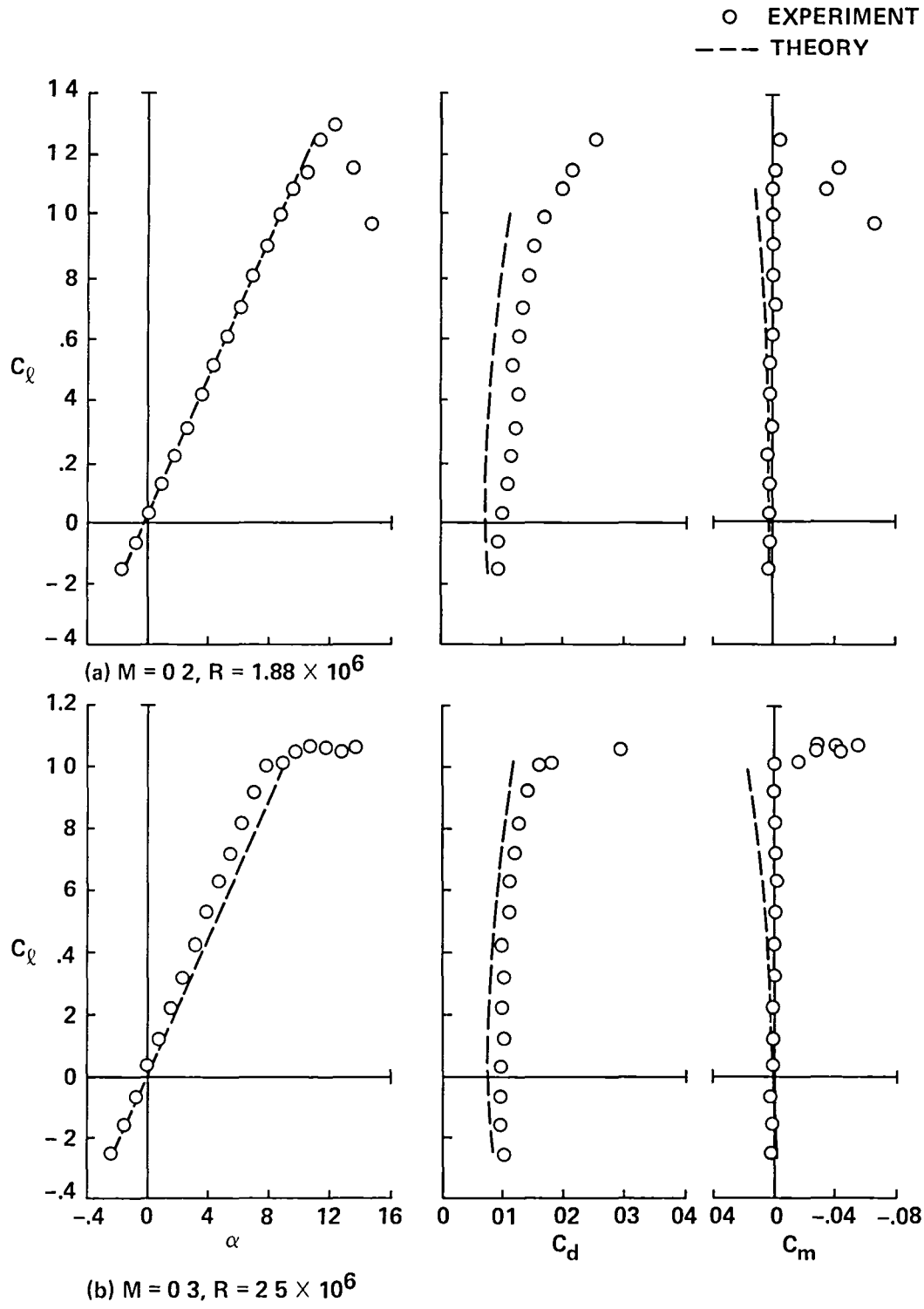

Figure 3.- Section aerodynamic characteristics of the A-2 airfoil, transition fixed.

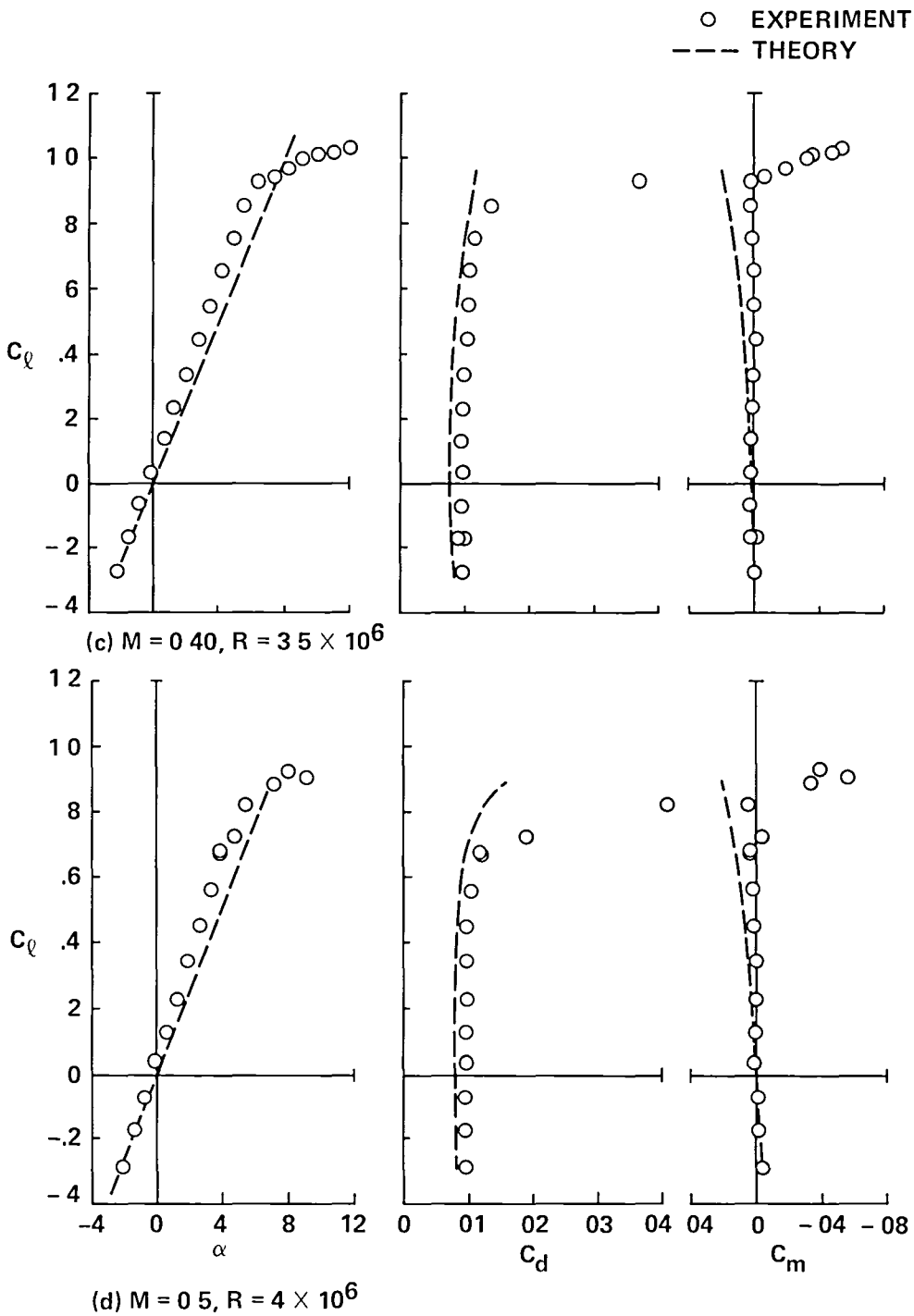

Figure 3.- Continued.

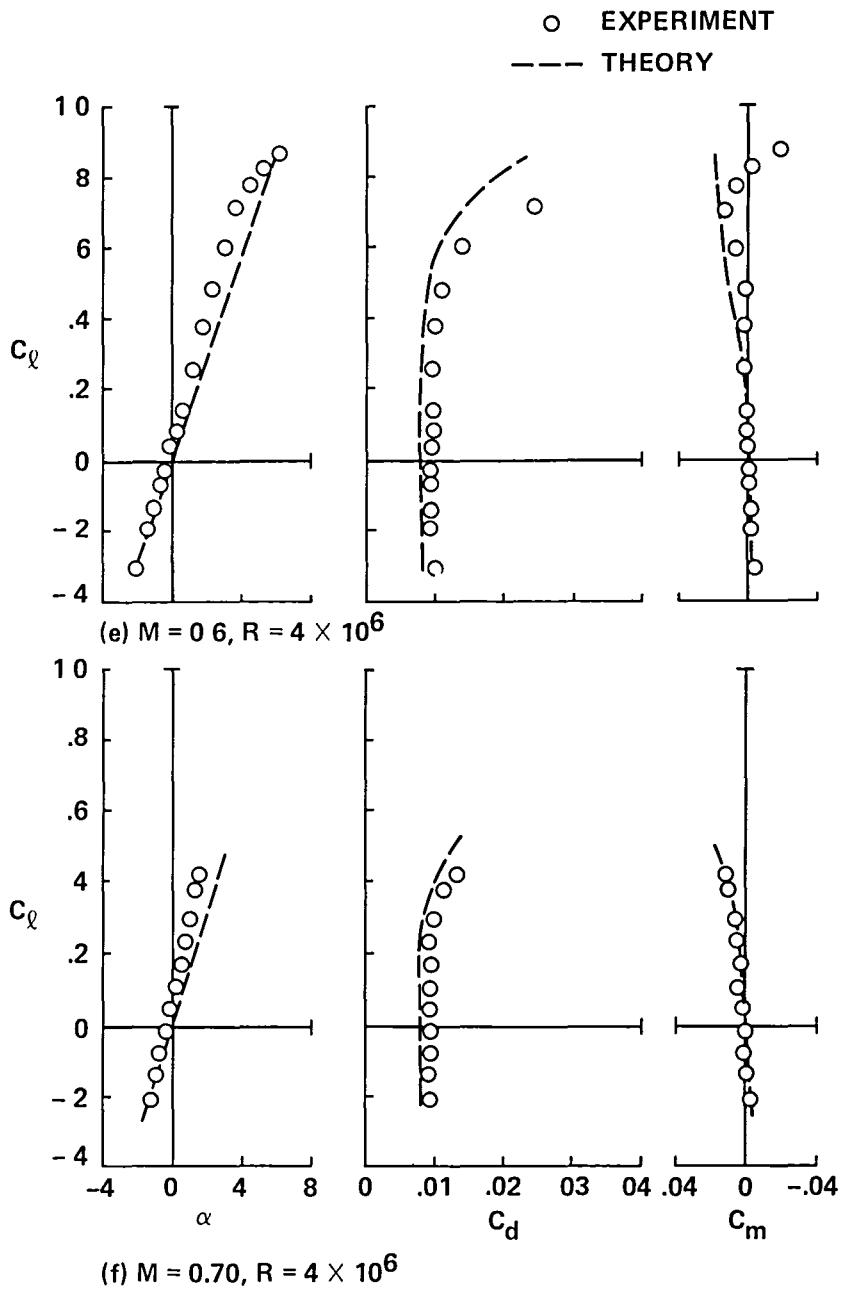

Figure 3.- Continued.

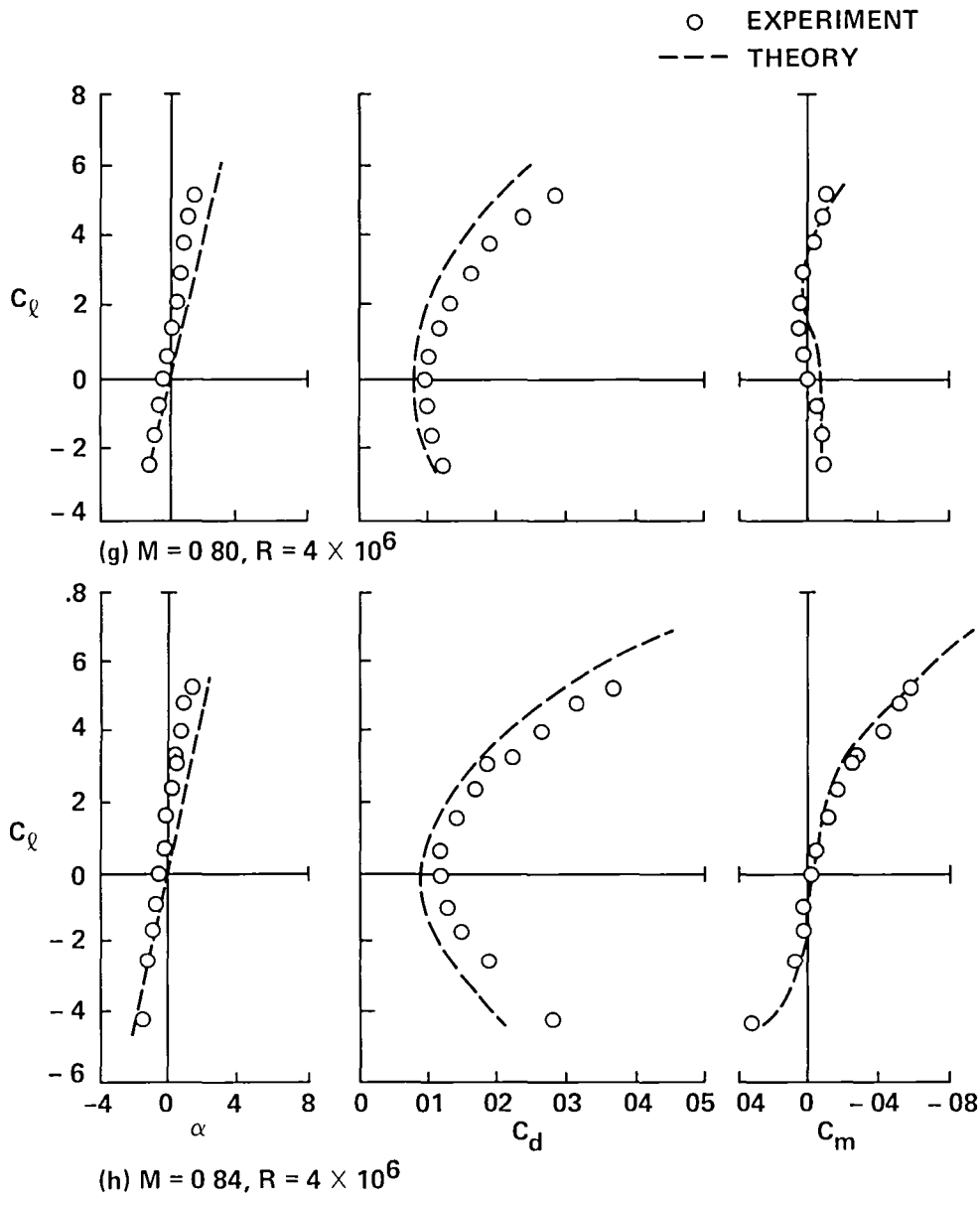

Figure 3.- Continued.

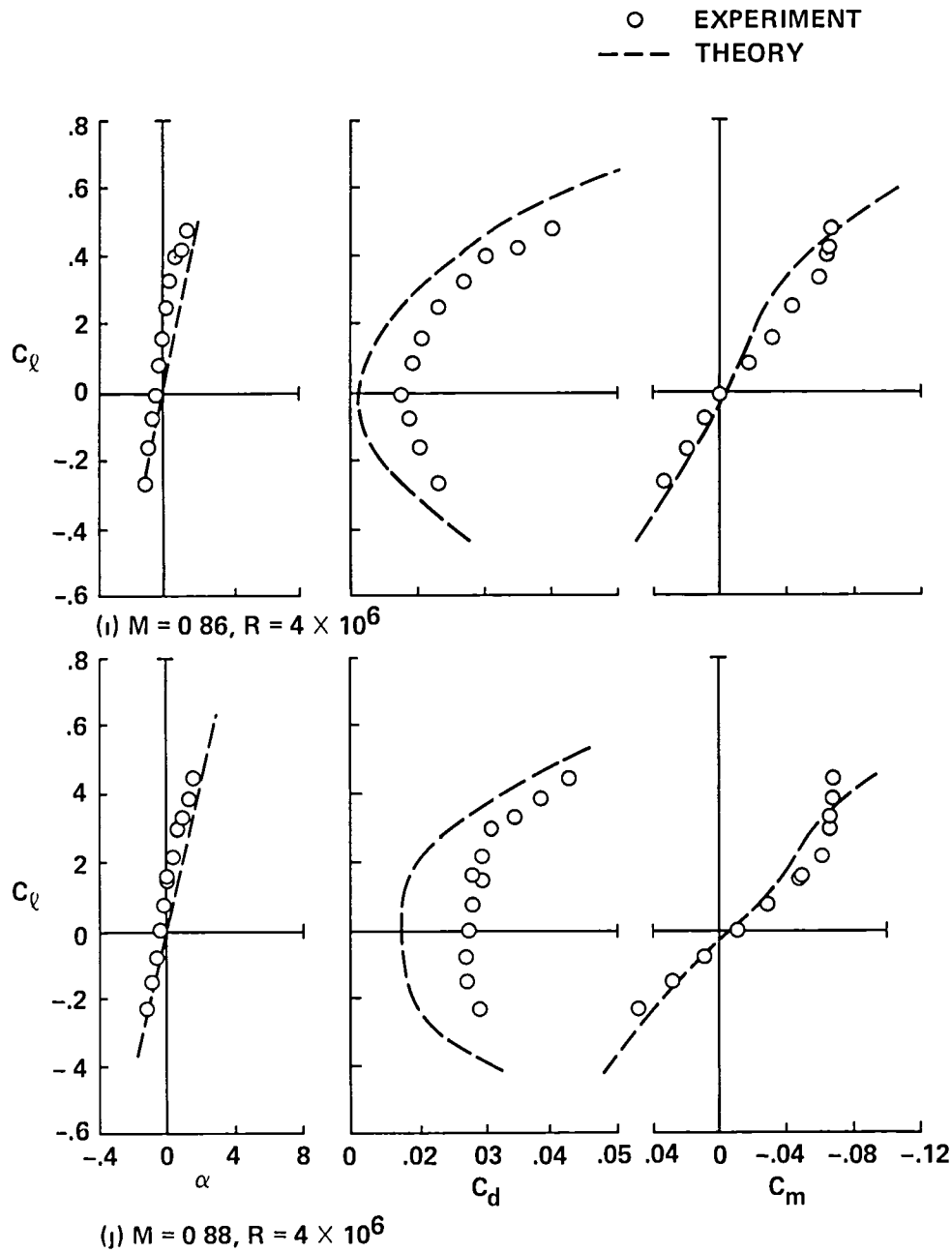

Figure 3.- Concluded.

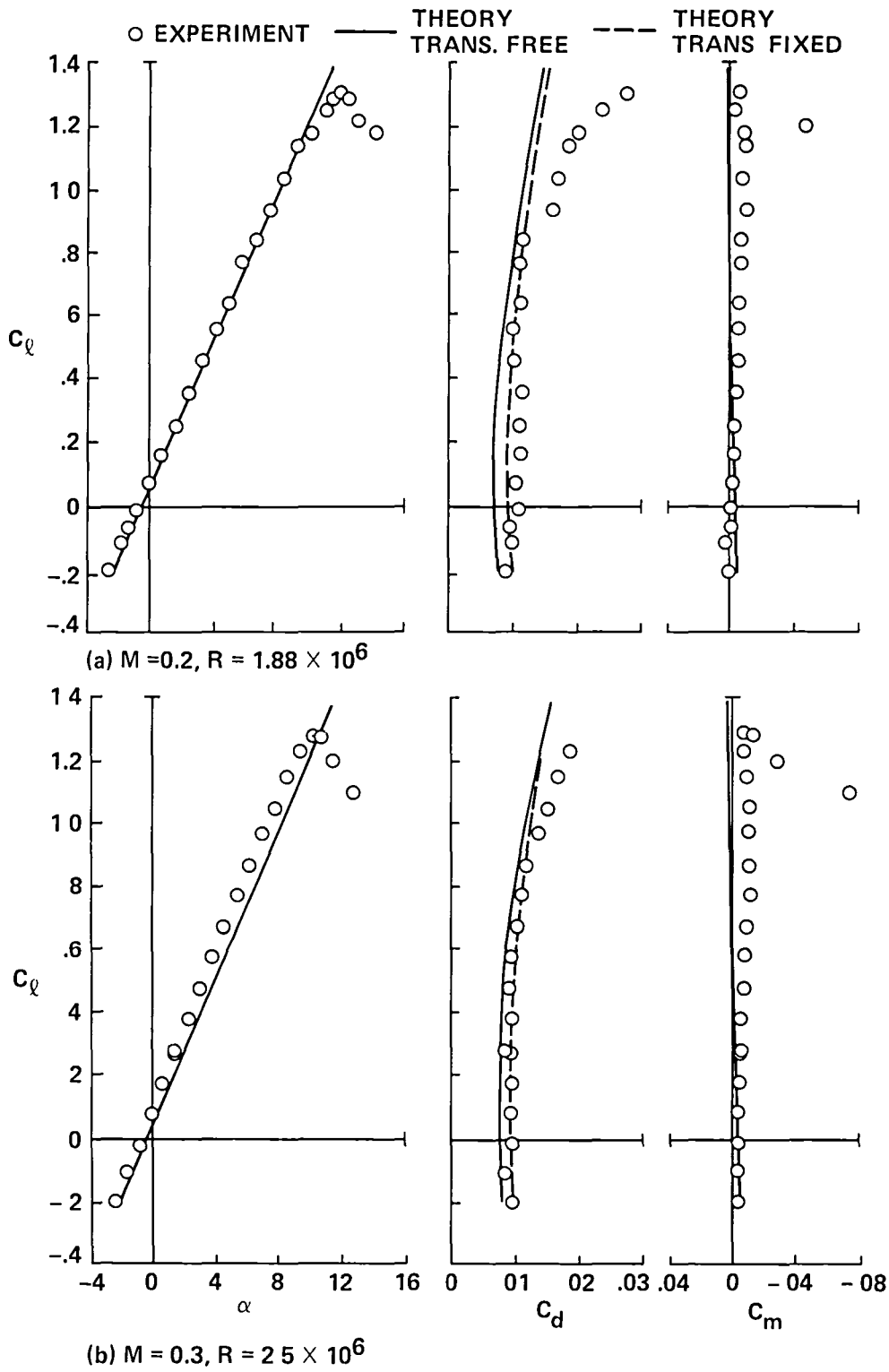

Figure 4.- Section aerodynamic characteristics of the SSC-A09 airfoil.

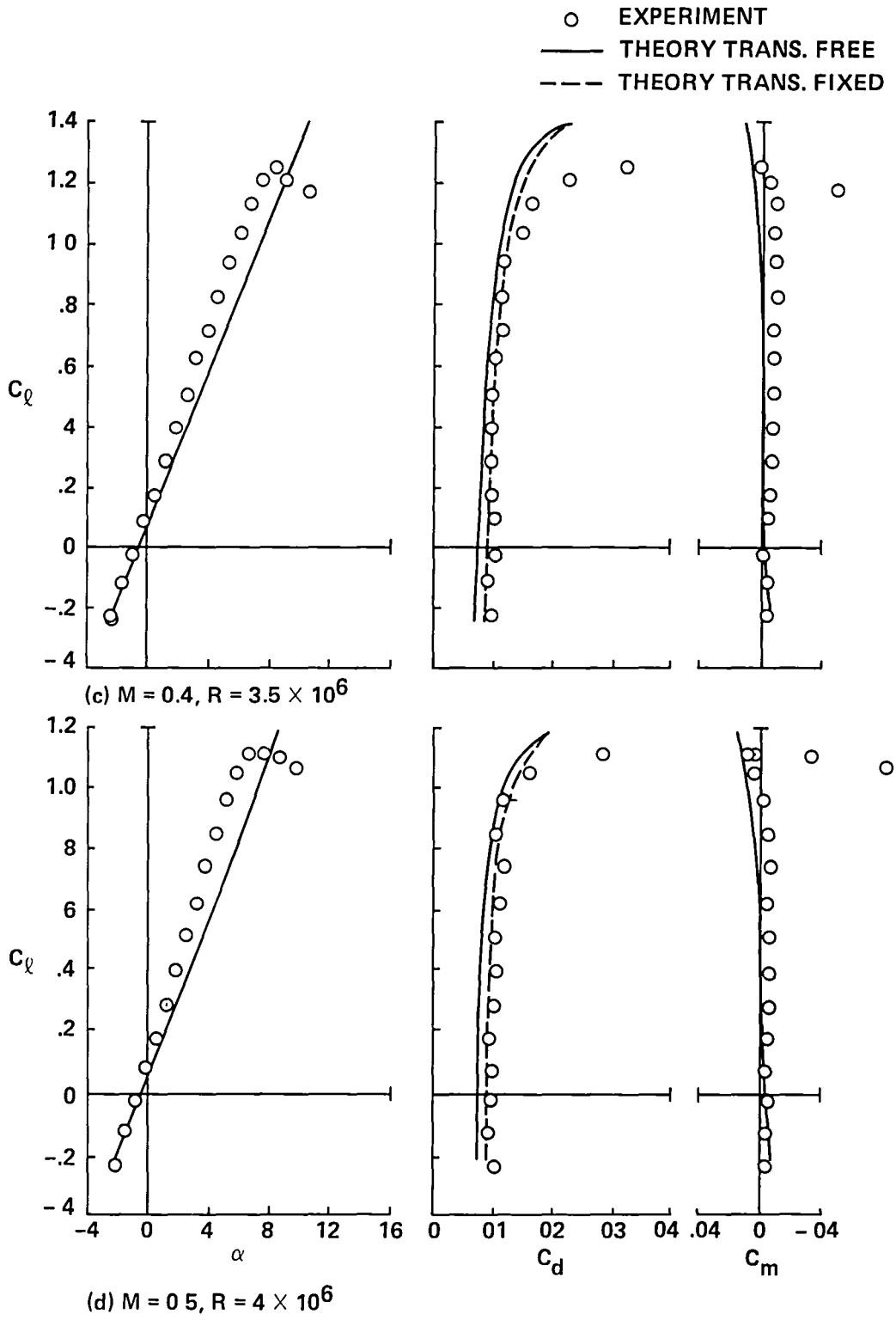

Figure 4.- Continued.

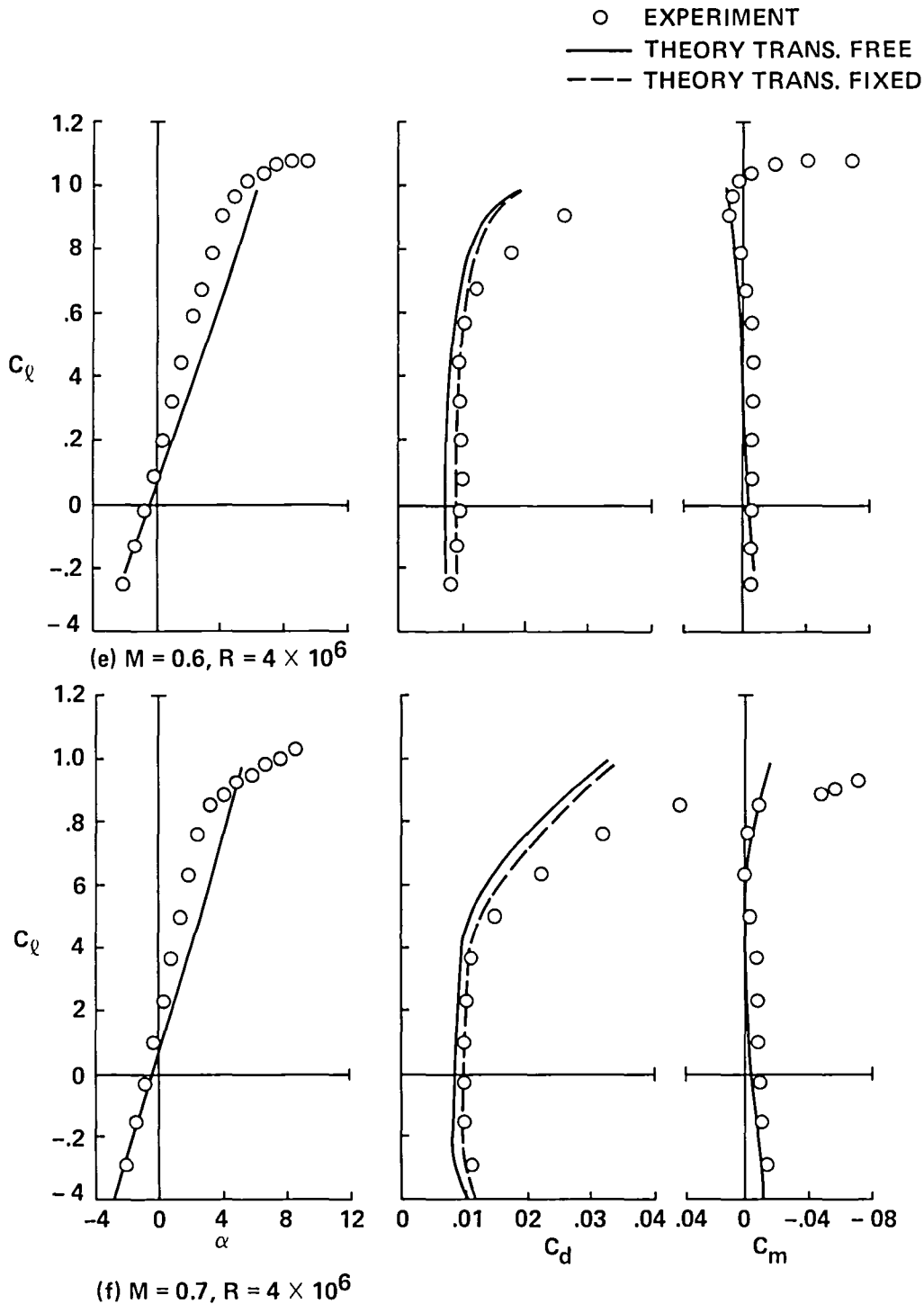

Figure 4.- Continued.

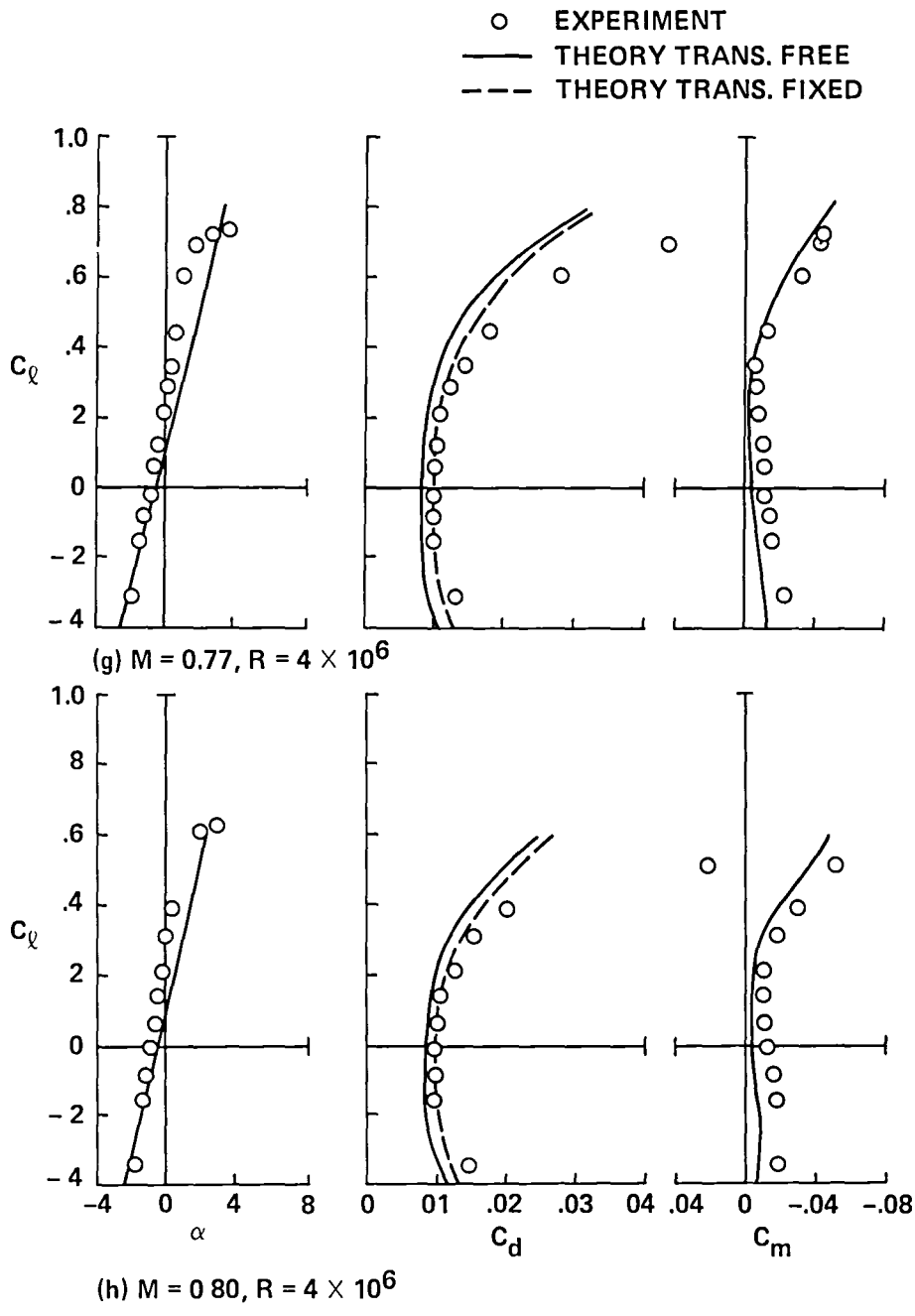

Figure 4.- Continued.

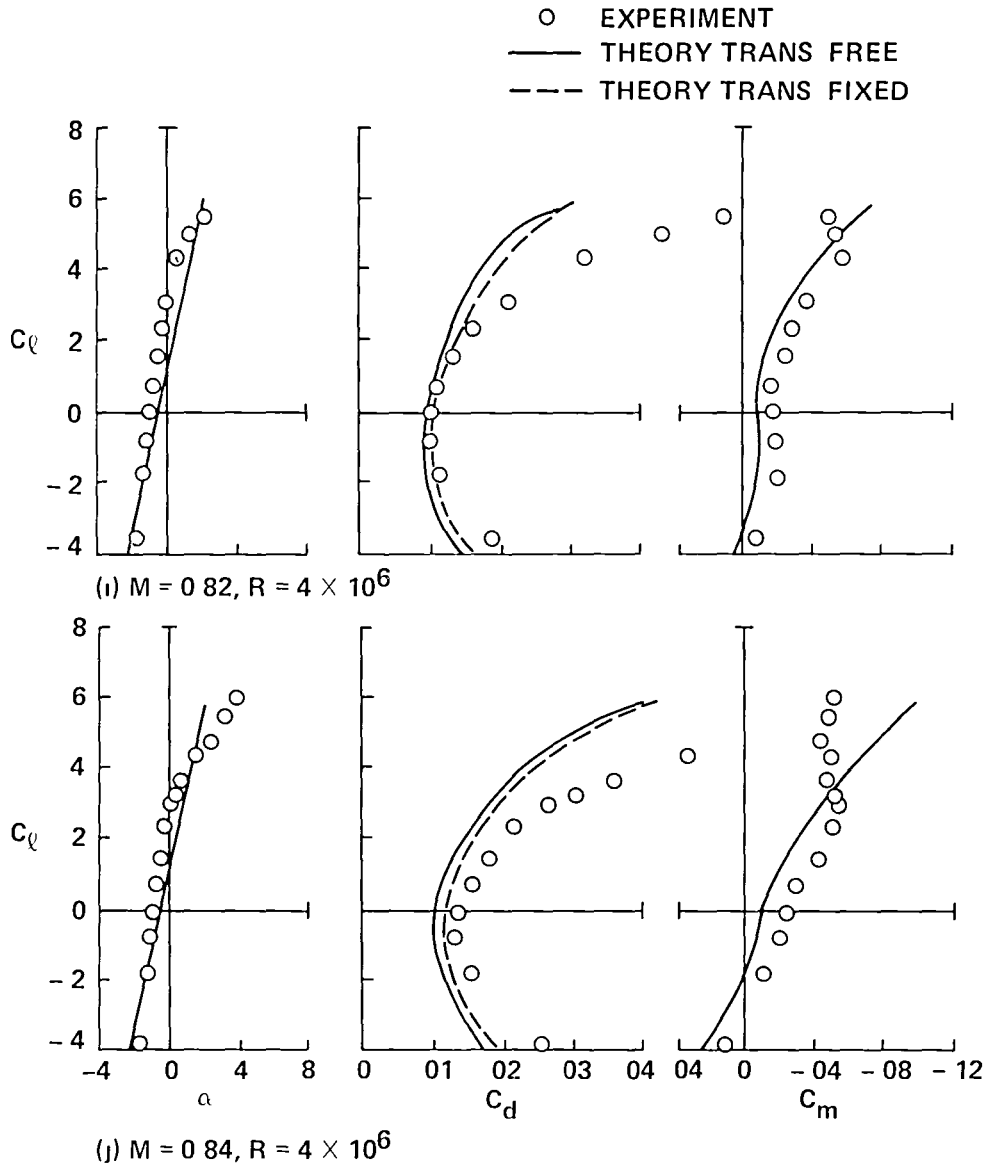

Figure 4.- Continued.

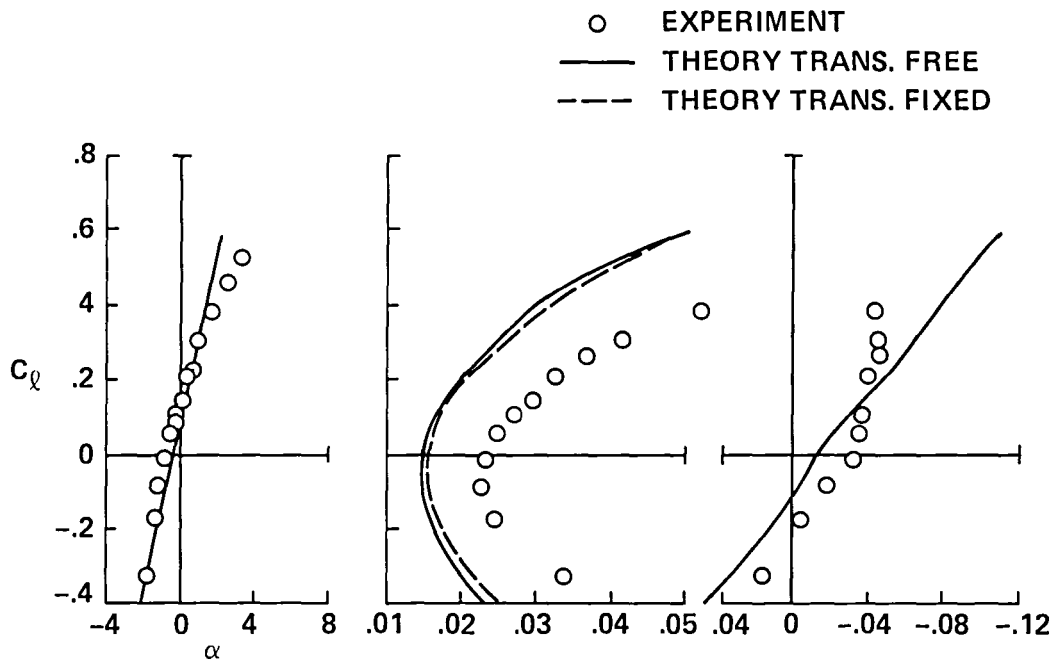

(k) M = 0.86, R = 4×10^6

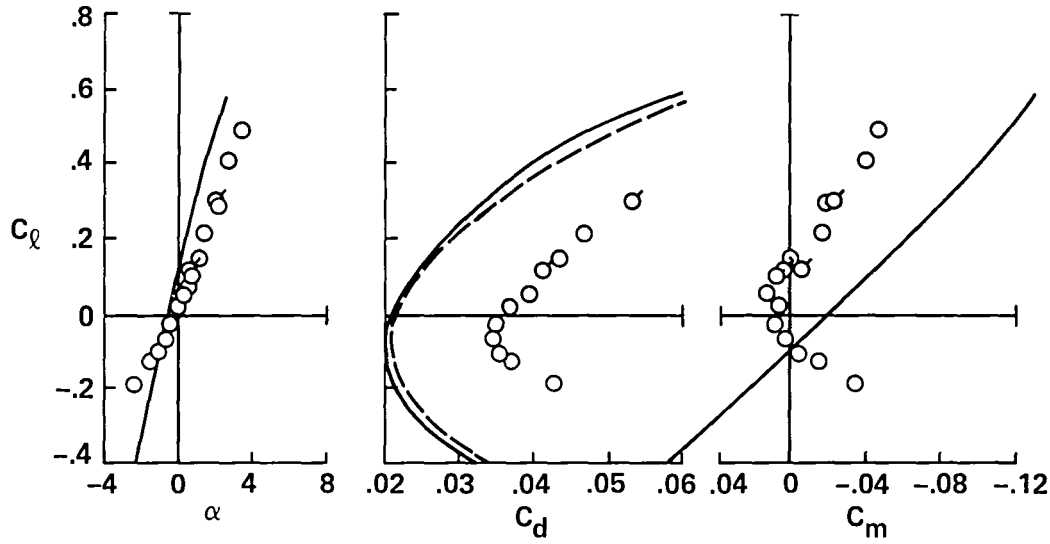

(l) M = 0.88, R = 4×10^6

Figure 4.- Concluded.

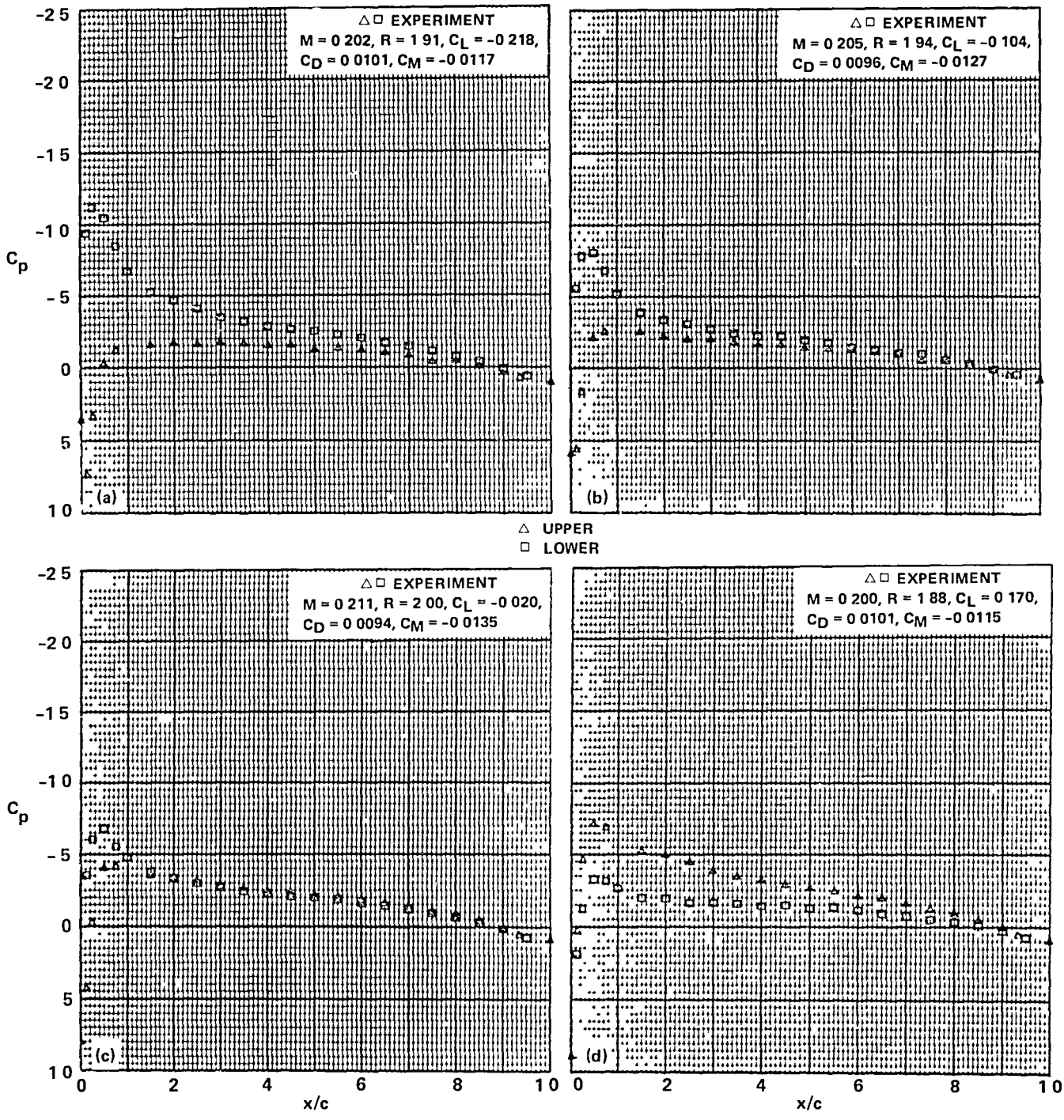

Figure 5.- Pressure distributions of the SC1095 airfoil, M_{set} = 0.2.

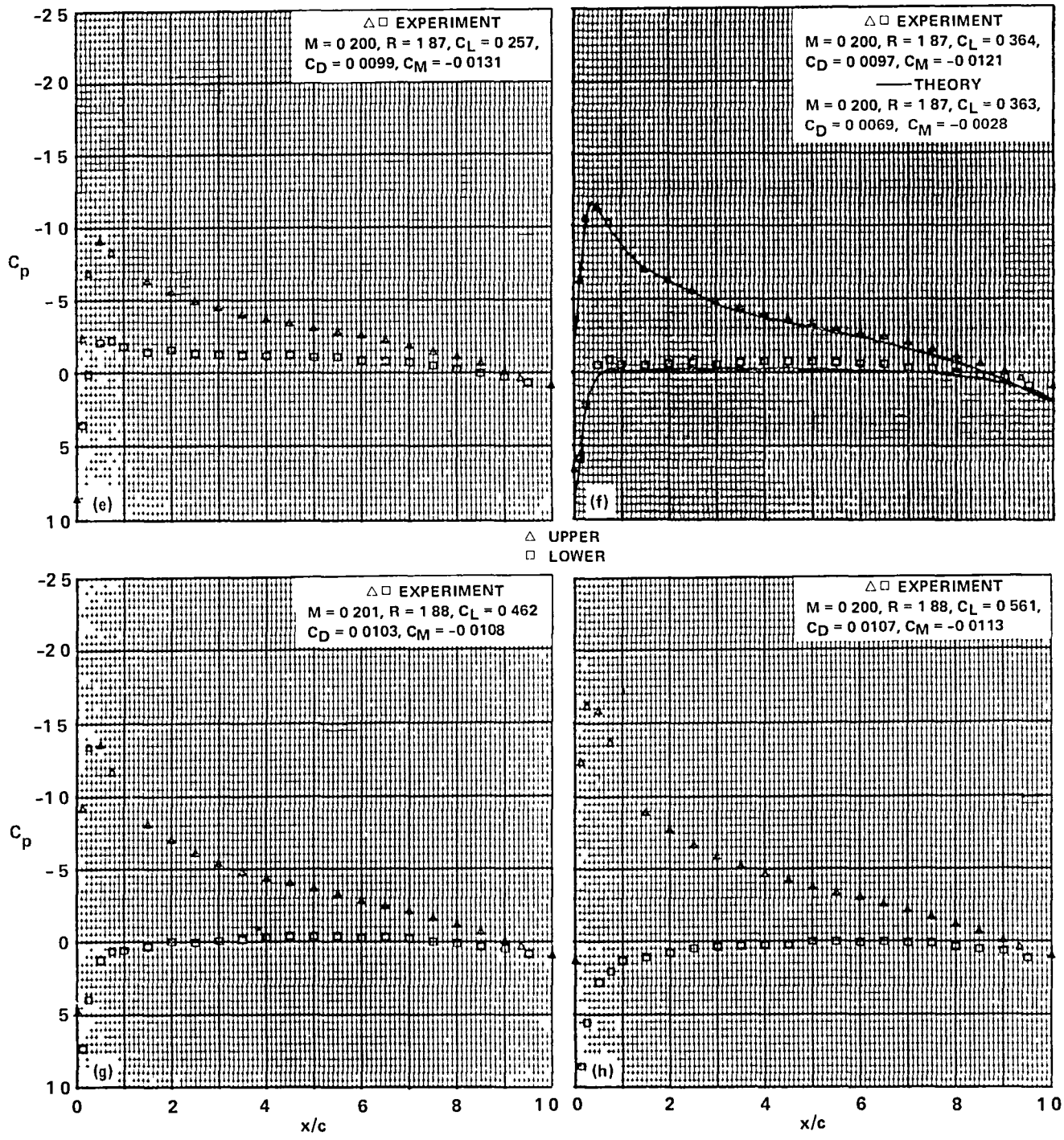

Figure 5.- Continued.

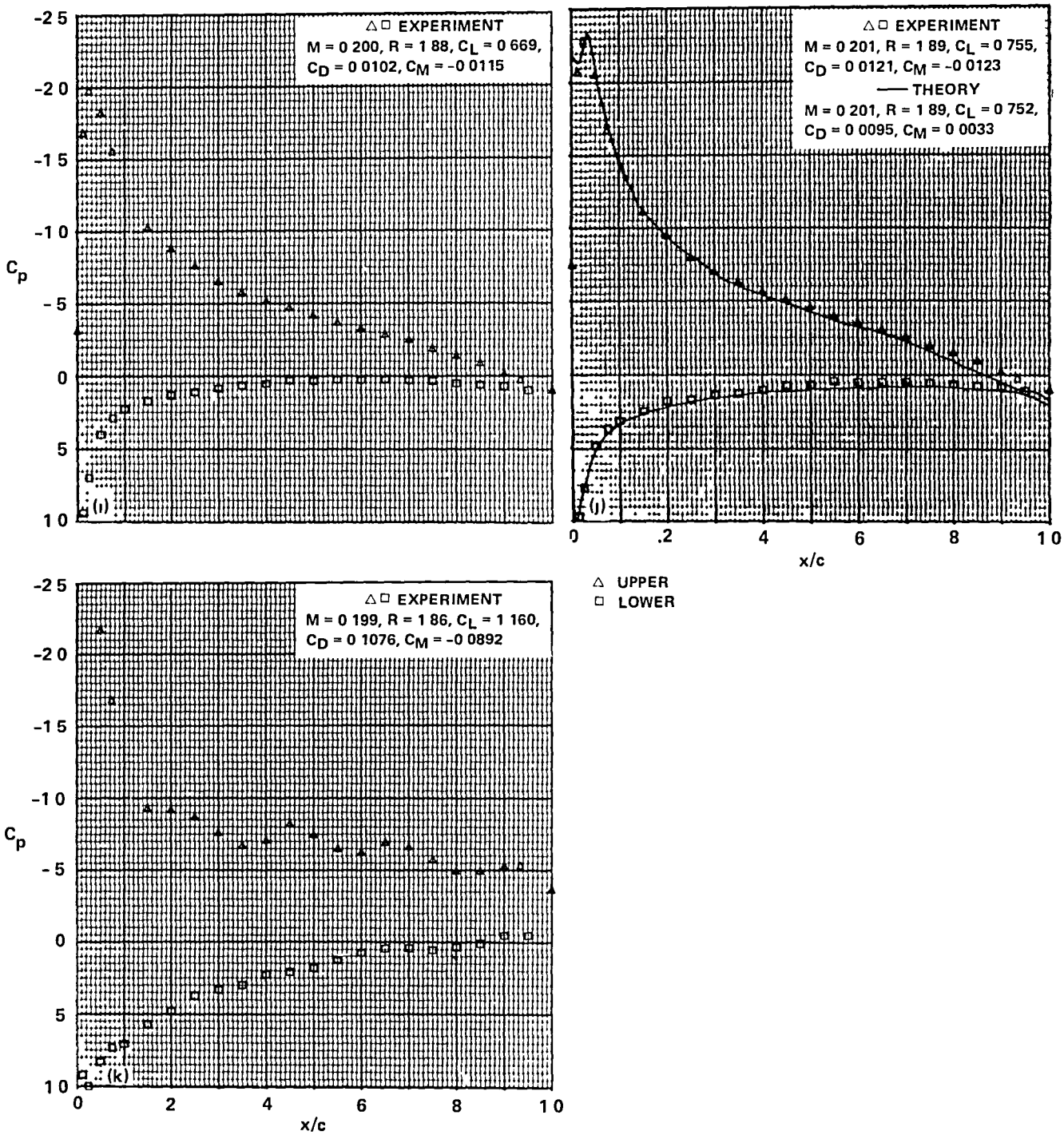

Figure 5.- Concluded.

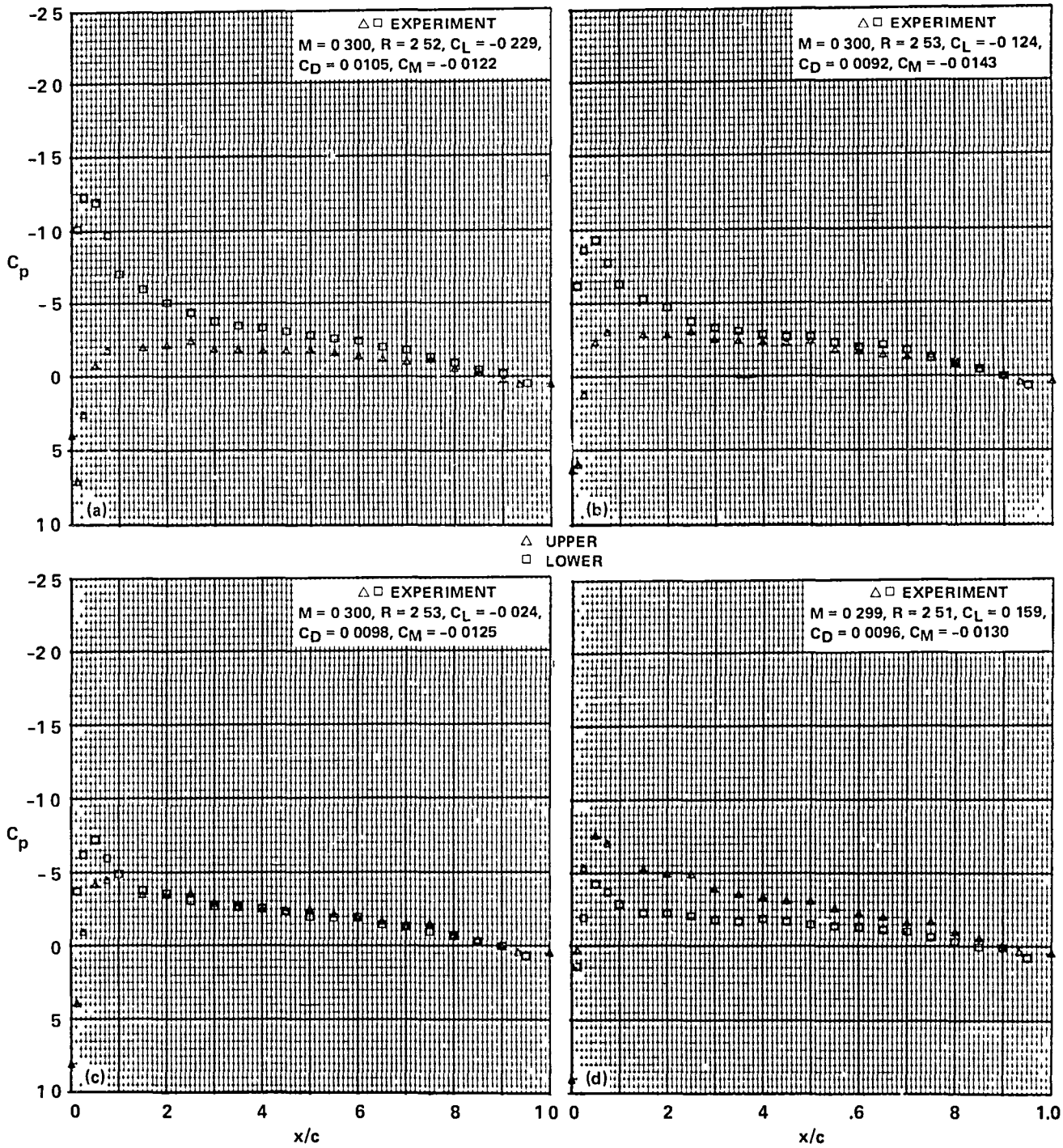

Figure 6.- Pressure distributions of the SC1095 airfoil, M_{set} = 0.3.

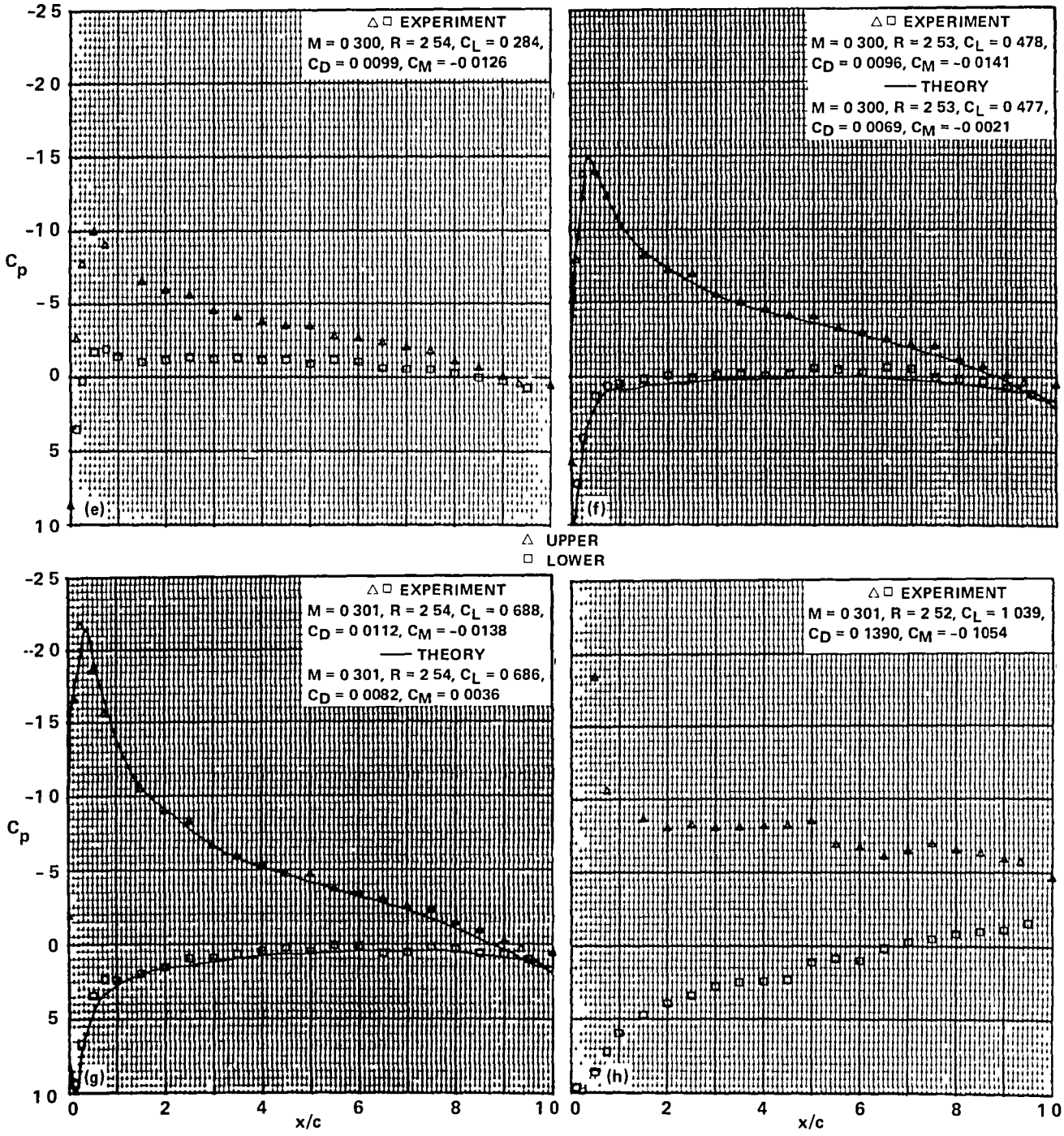

Figure 6.- Concluded.

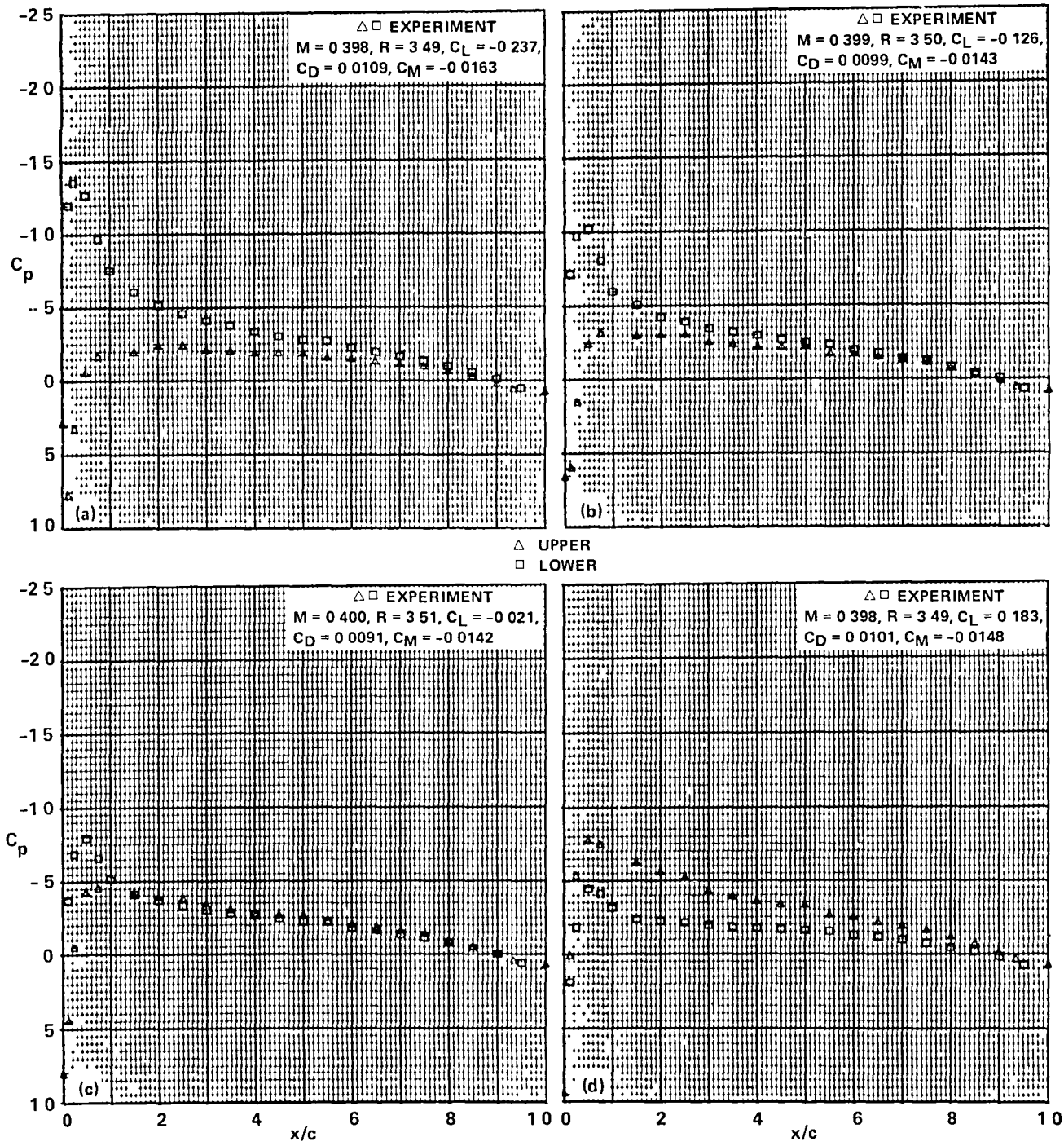

Figure 7.- Pressure distributions of the SC1095 airfoil, M_{set} = 0.4.

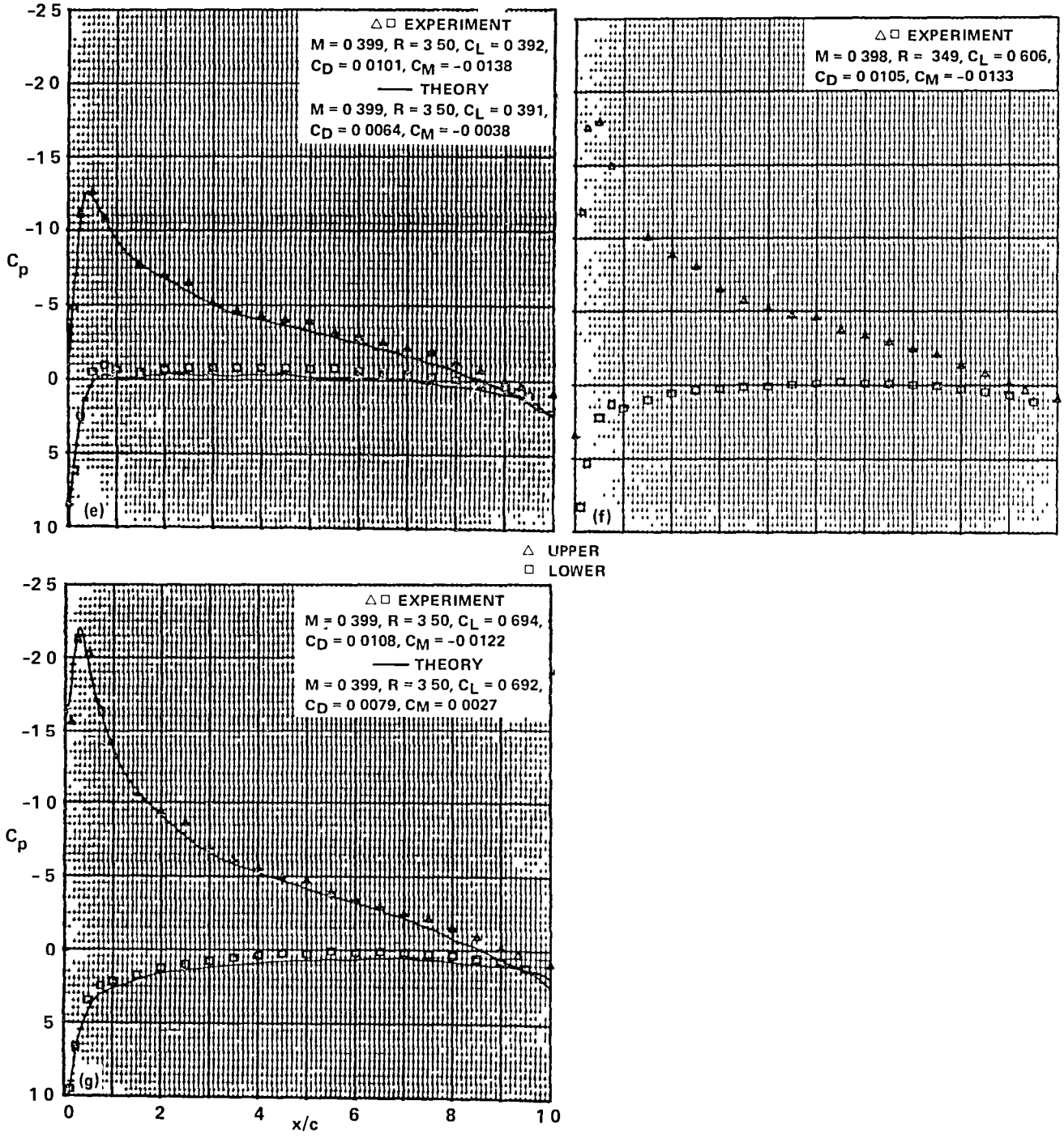

Figure 7.- Concluded.

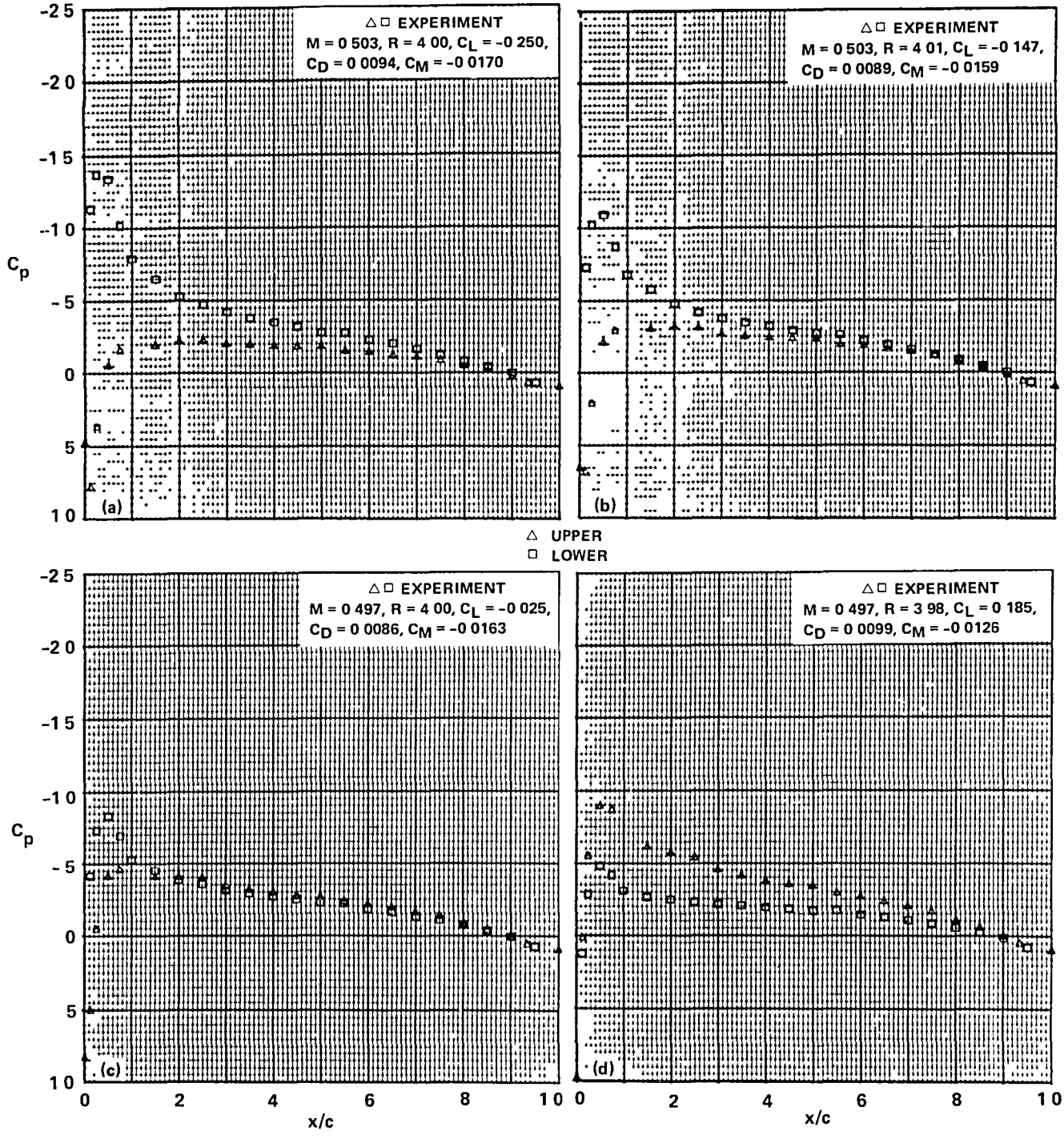

Figure 8.- Pressure distributions of the SC1095 airfoil, M_{set} = 0.5.

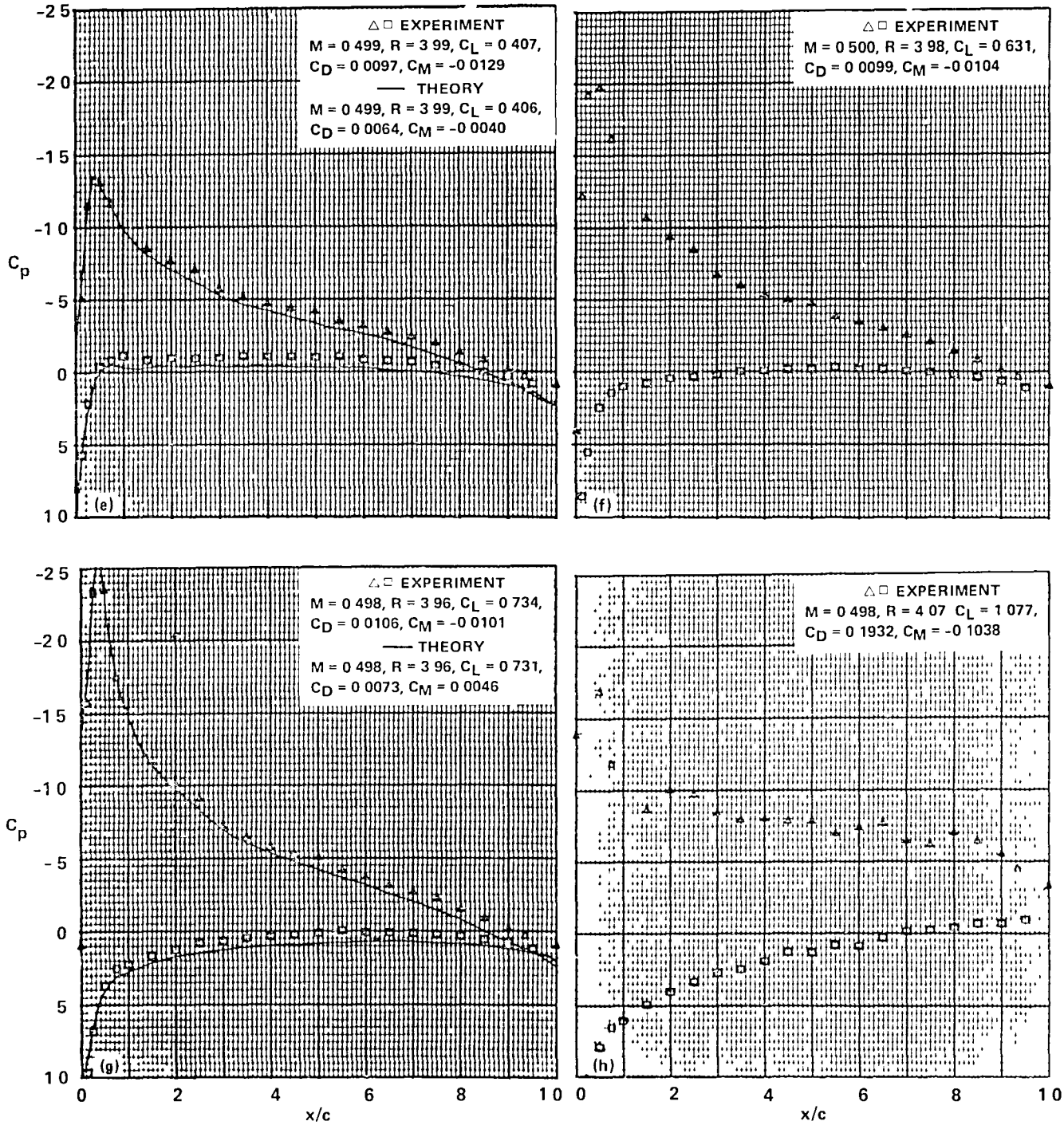

Figure 8.- Concluded.

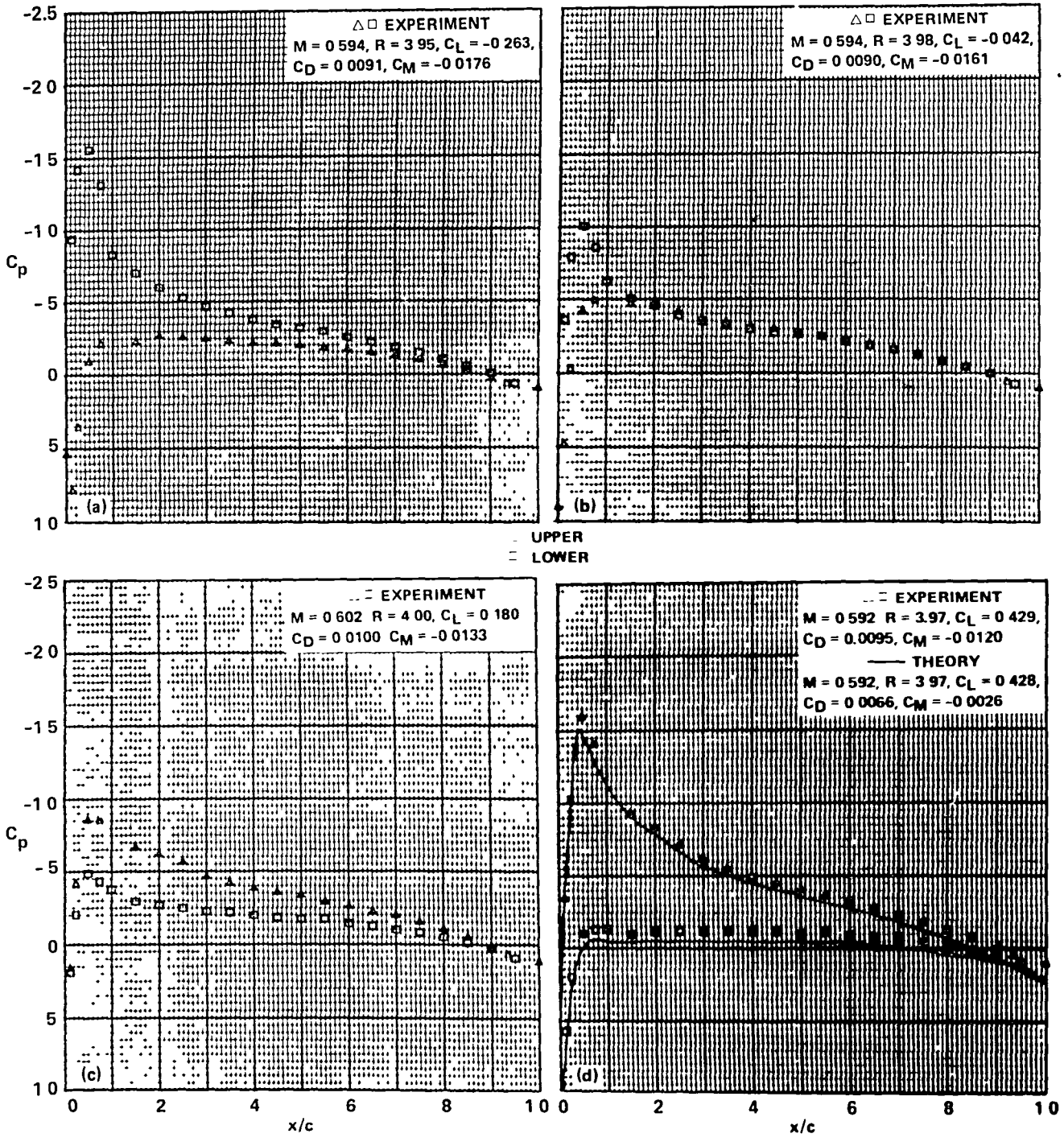

Figure 9.- Pressure distributions of the SC1095 airfoil, M_{set} = 0.6.

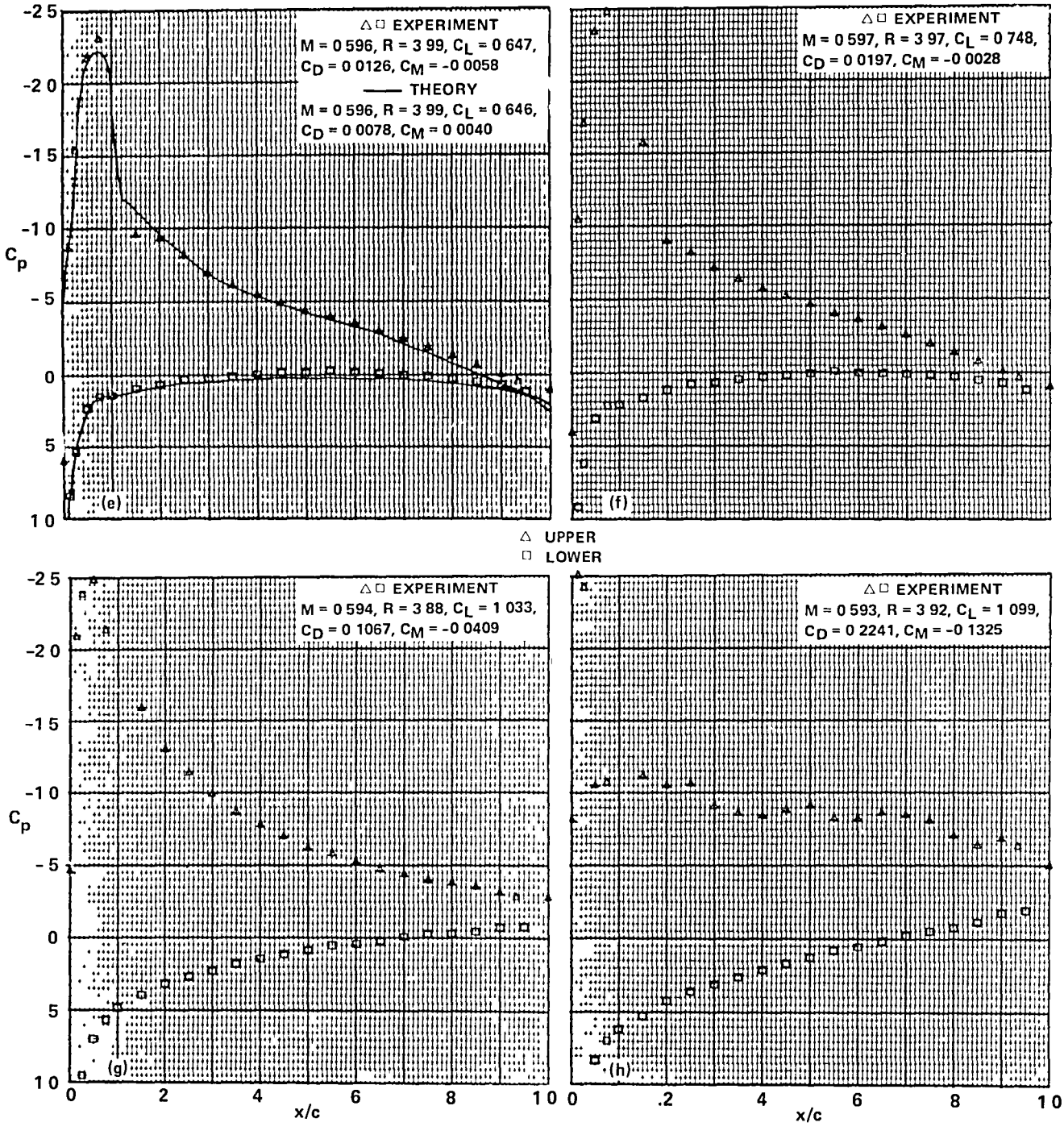

Figure 9.- Concluded.

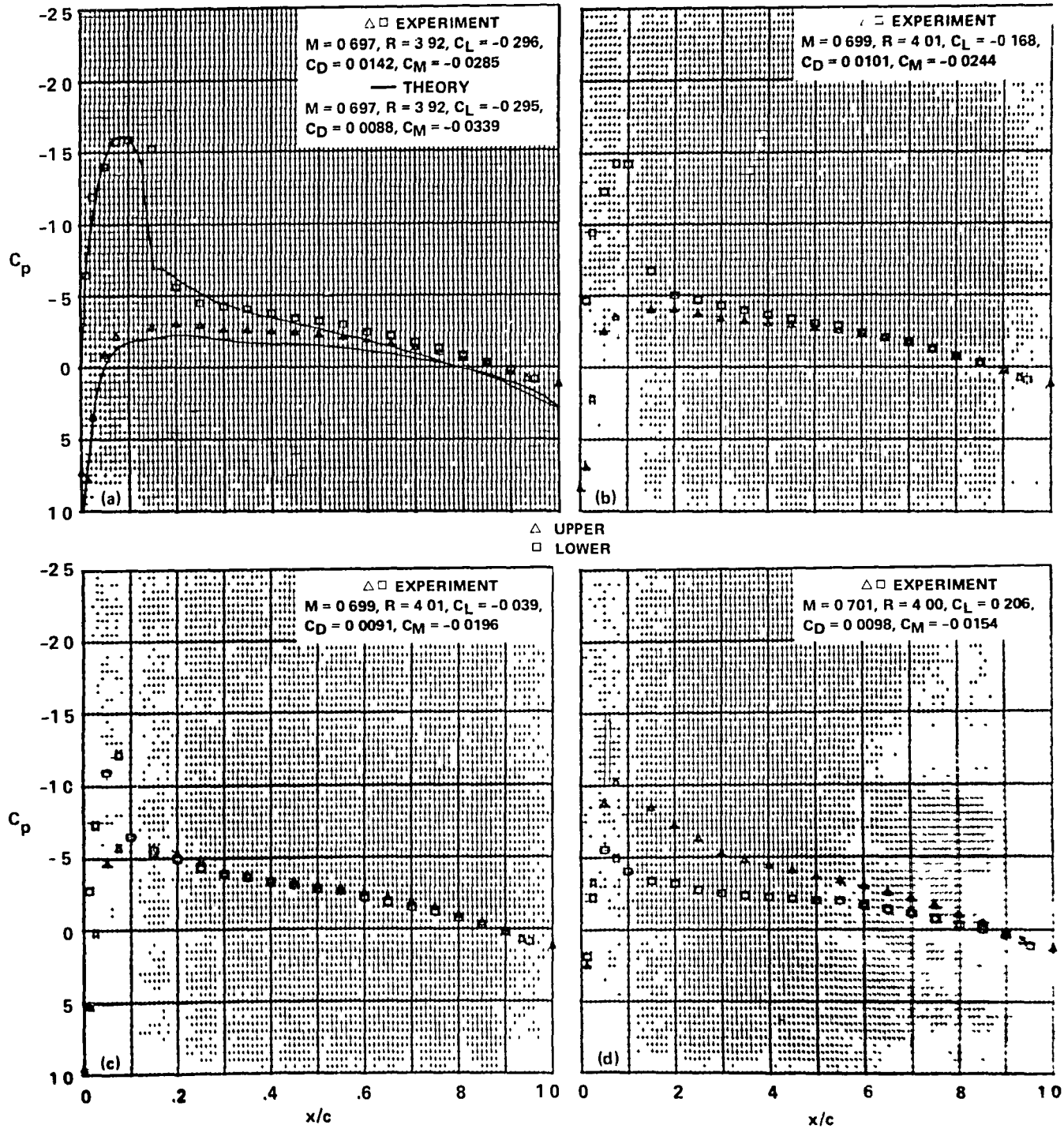

Figure 10.- Pressure distributions of the SC1095 airfoil, M_{sec} = 0.7

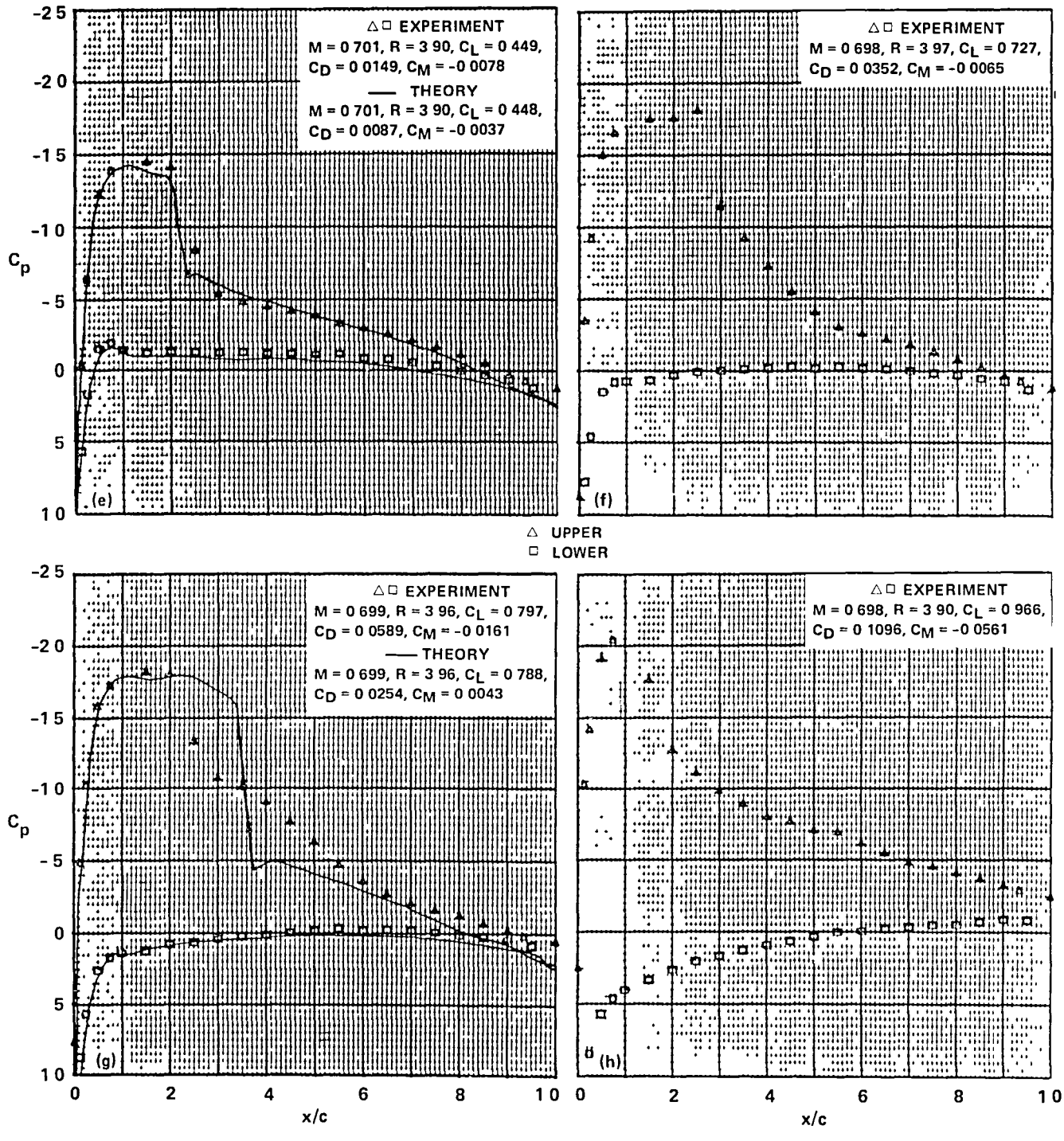

Figure 10.- Concluded.

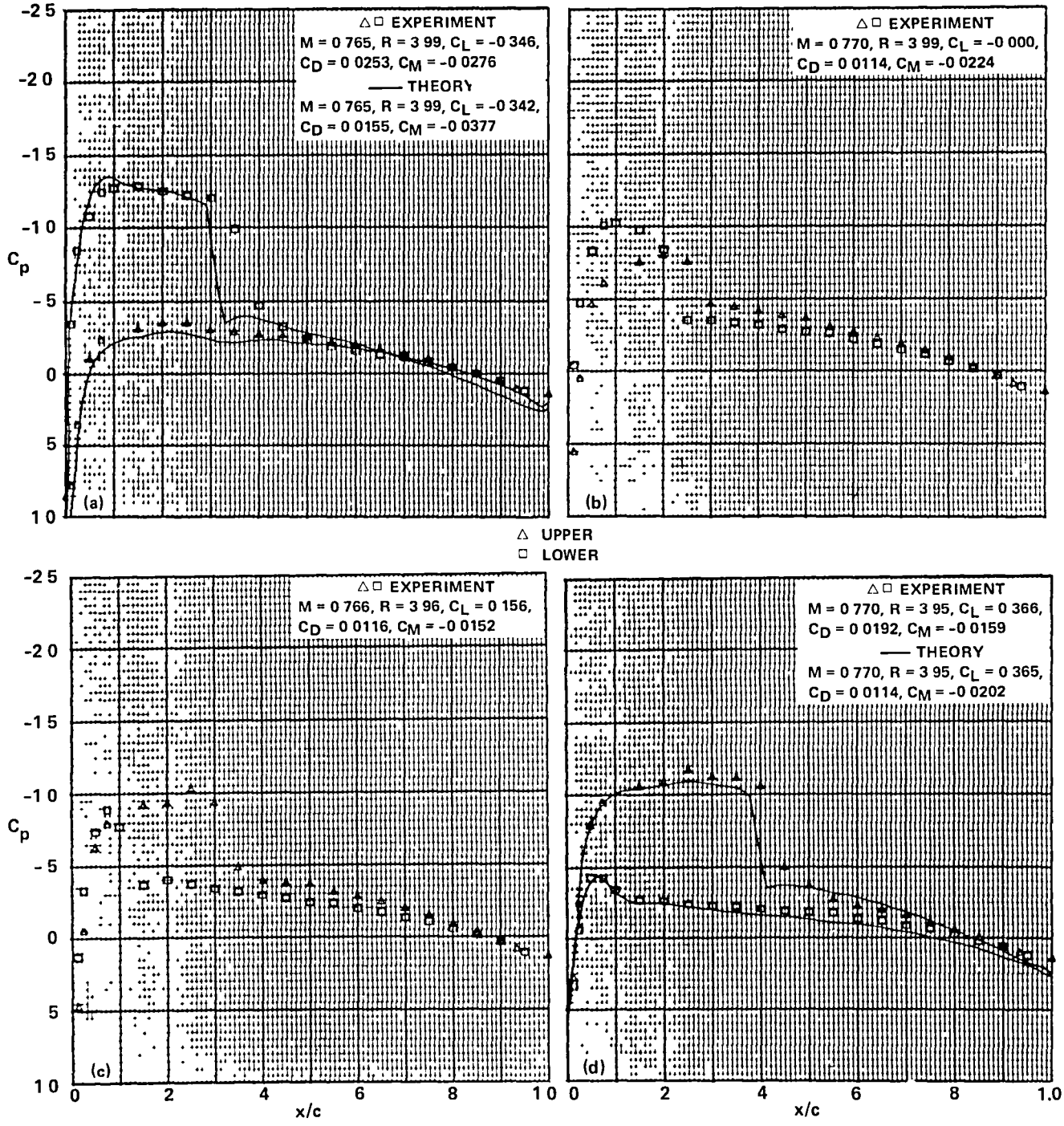

Figure 11.- Pressure distributions of the SC1095 airfoil, M_{set} = 0.77.

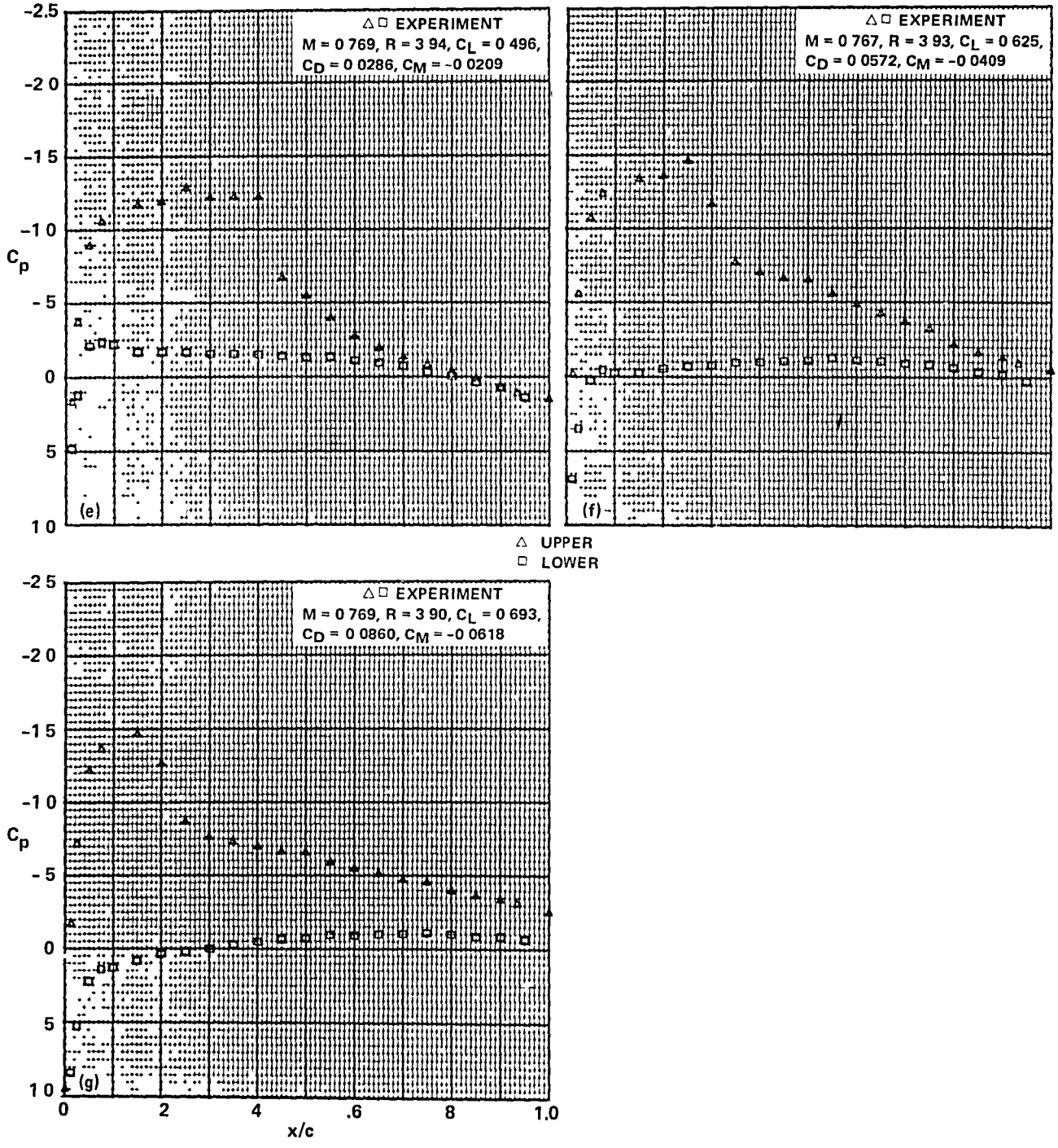

Figure 11.- Concluded.

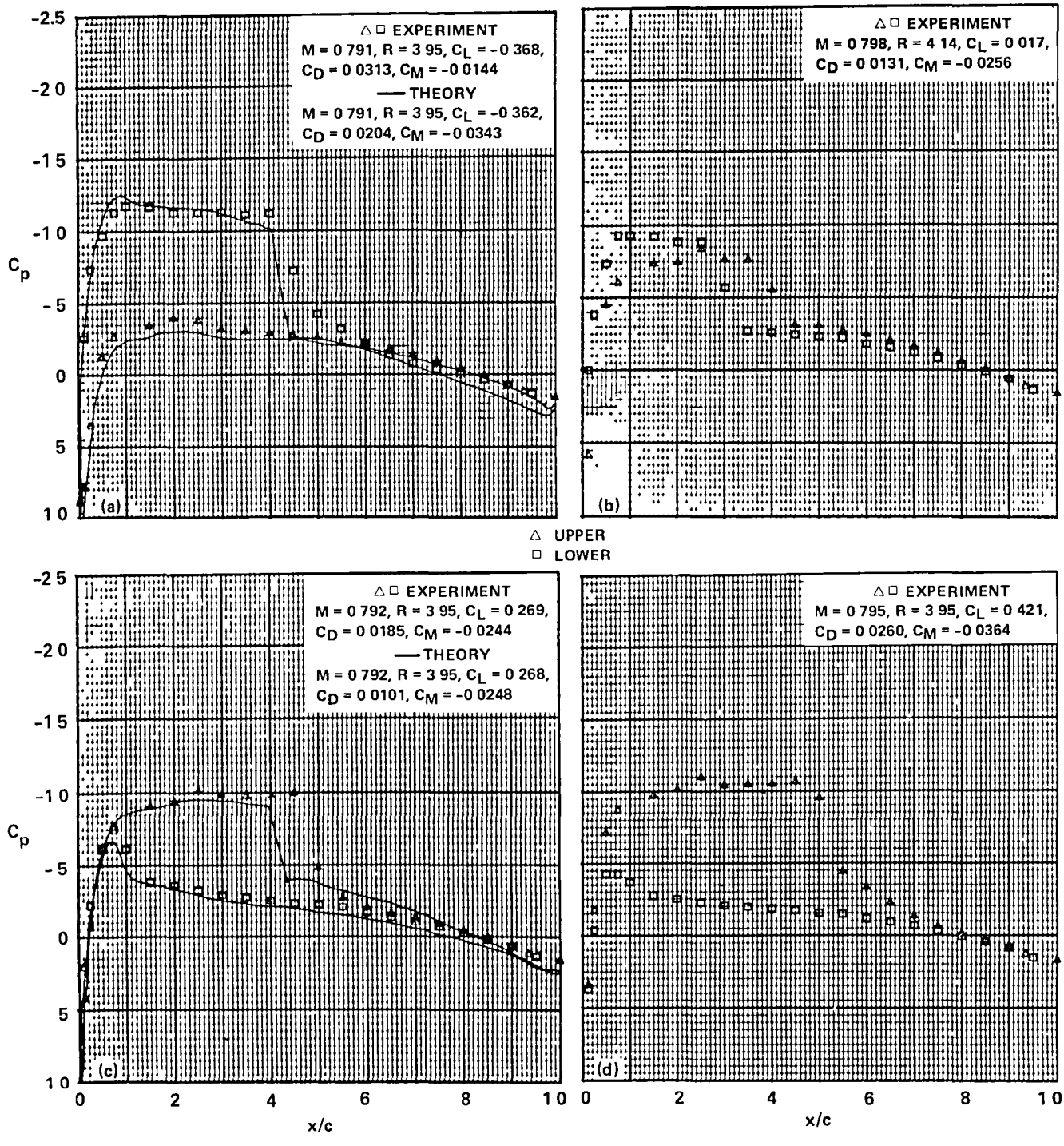

Figure 12.- Pressure distributions of the SC1095 airfoil, M_{set} = 0.8.

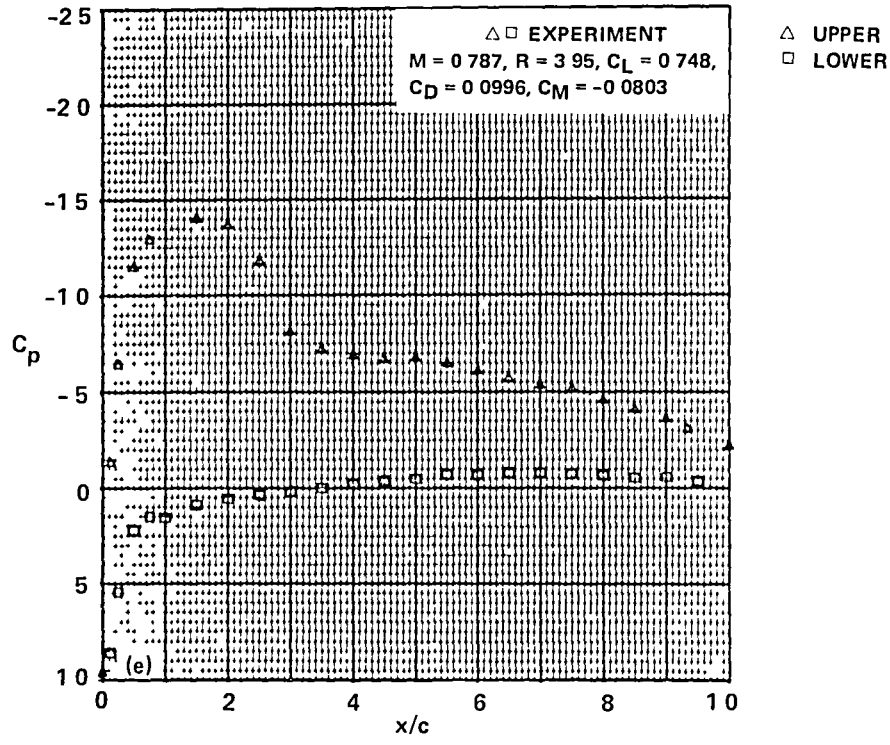

Figure 12.- Concluded.

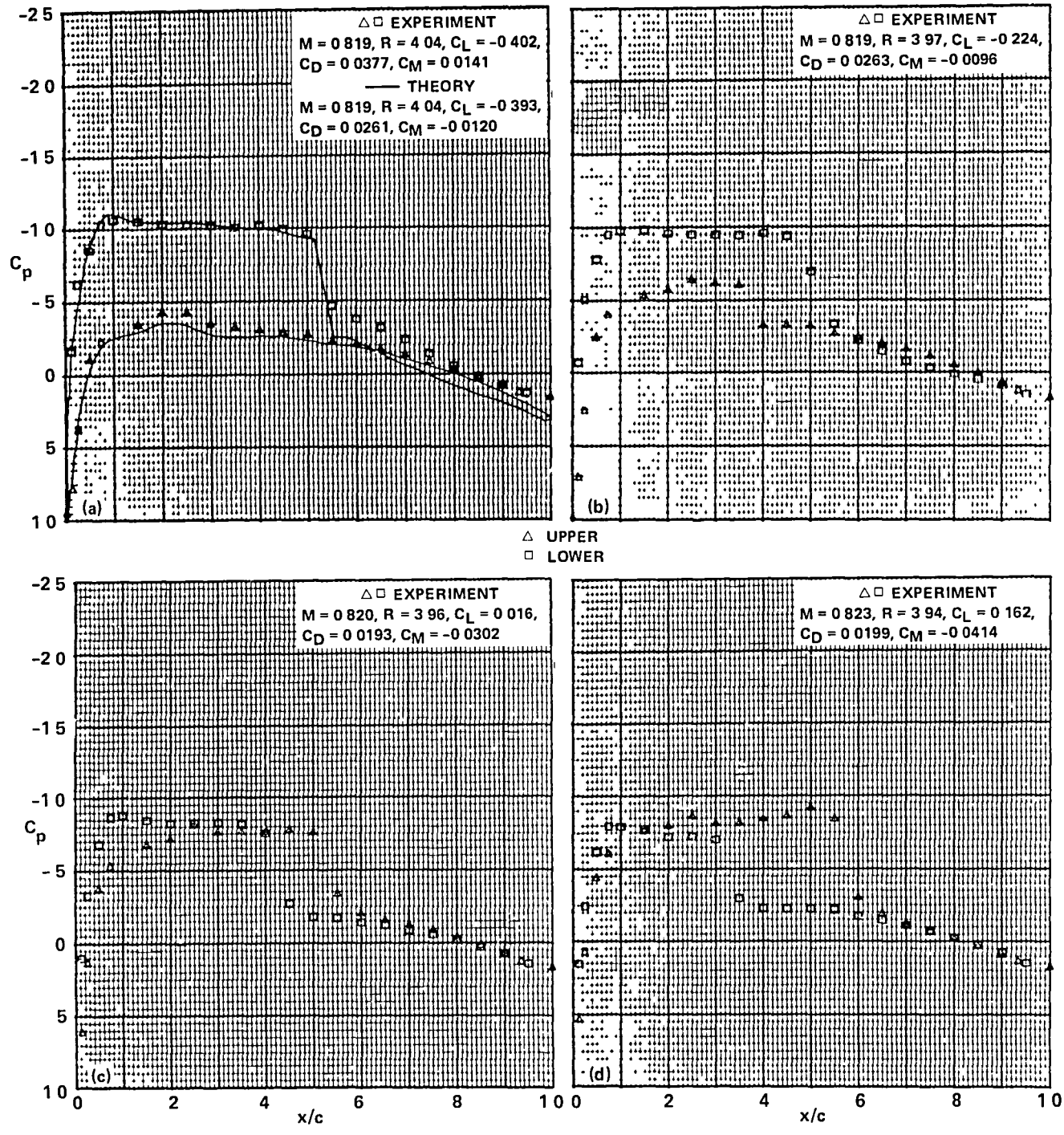

Figure 13.- Pressure distributions of the SC1095 airfoil, M_{set} = 0.82.

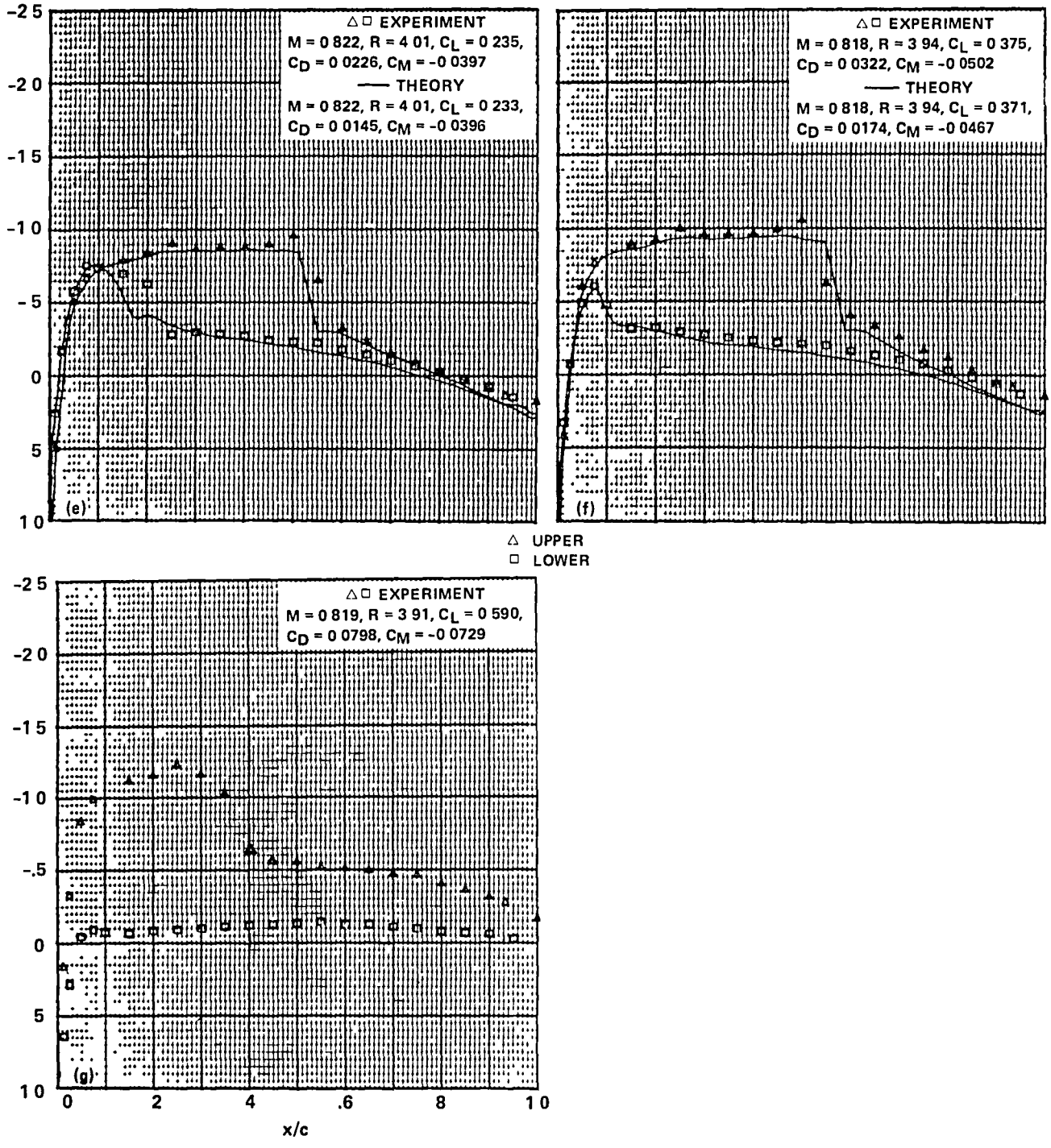

Figure 13.- Concluded.

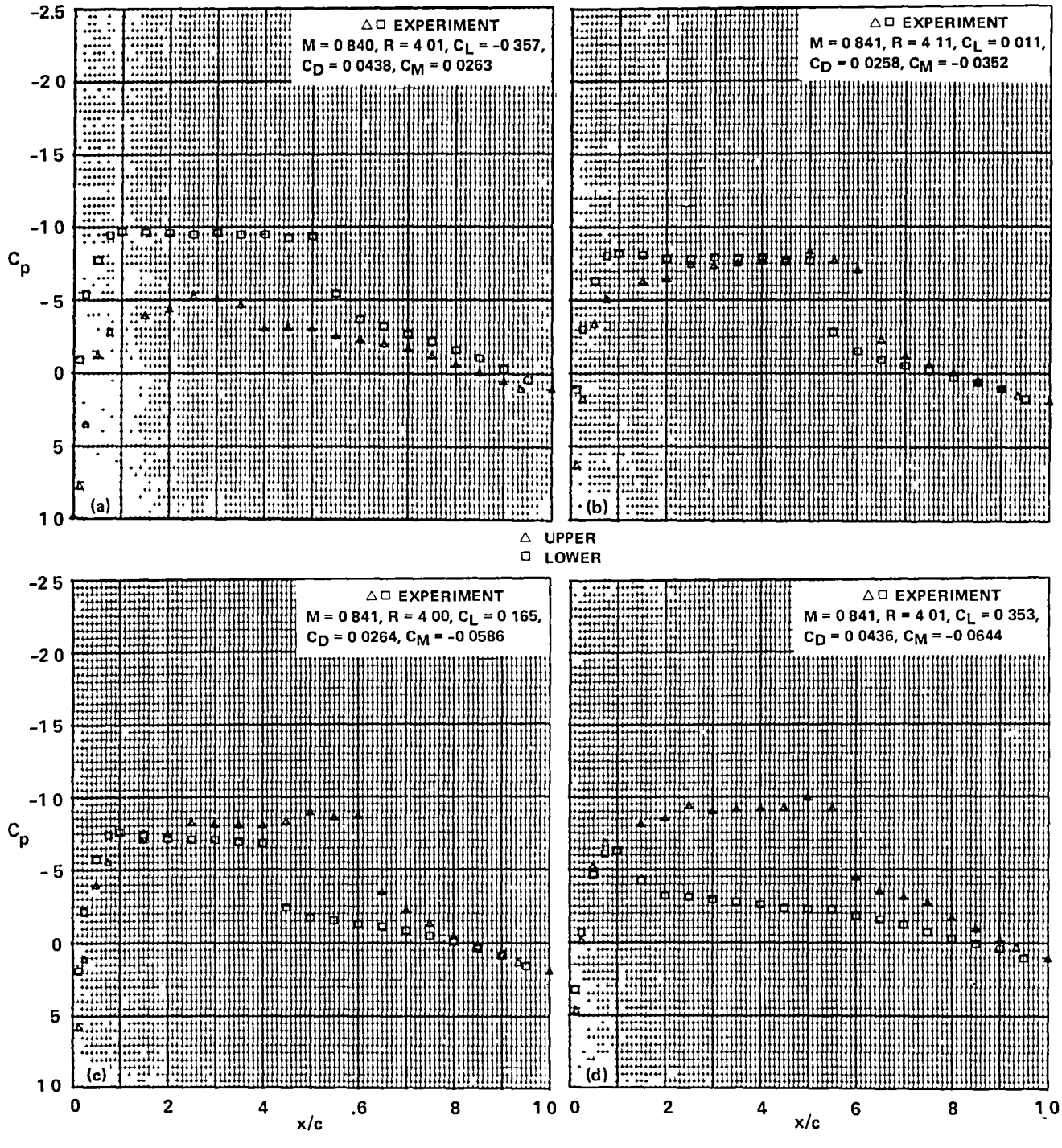

Figure 14.- Pressure distributions of the SC1095 airfoil, M_{set} = 0.84.

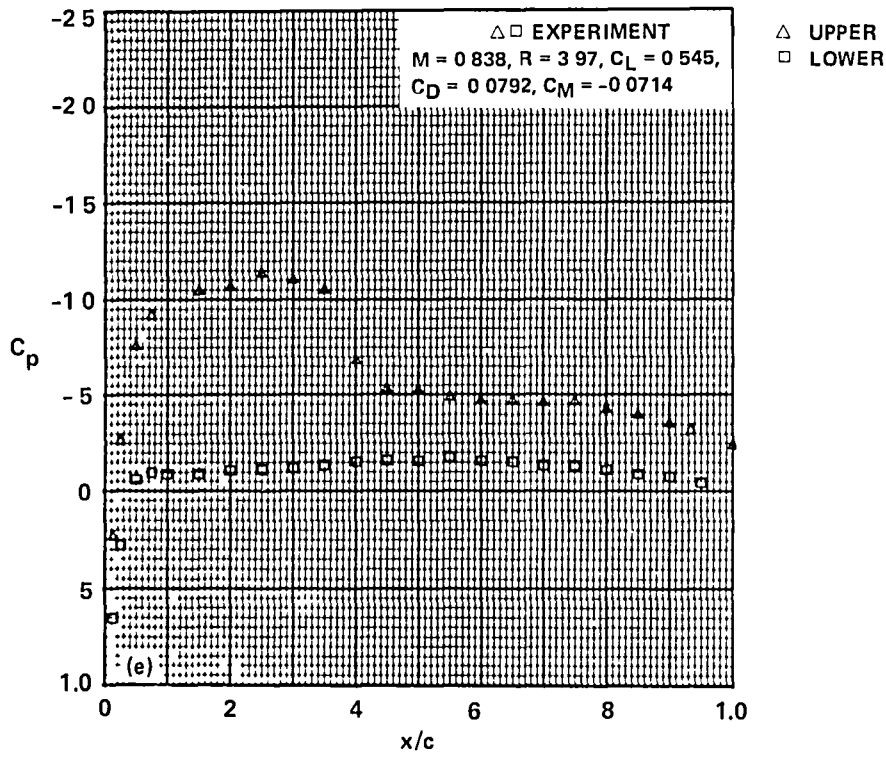

Figure 14.- Concluded.

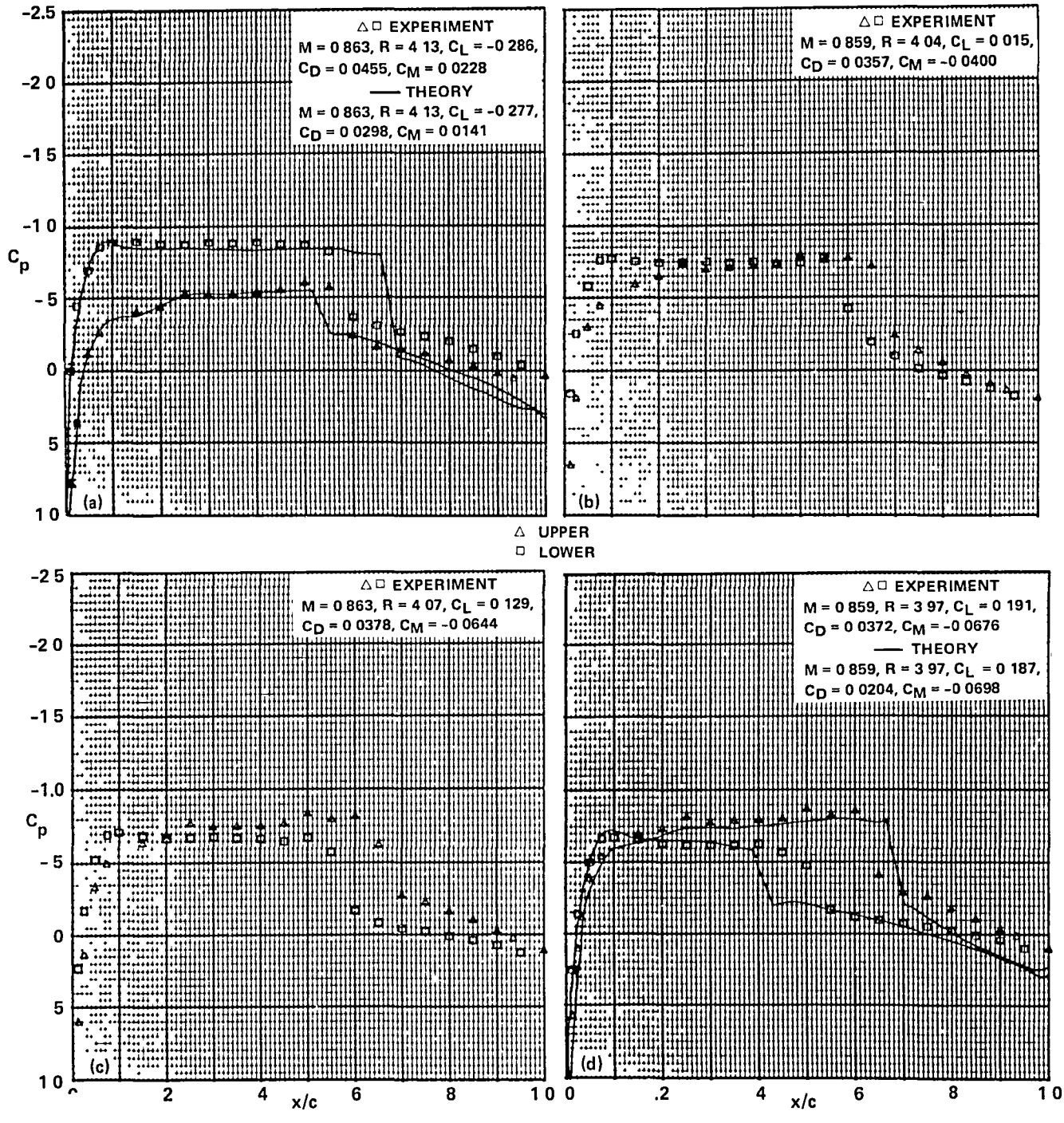

Figure 15.- Pressure distributions of the SC1095 airfoil, M_{set} = 0.86.

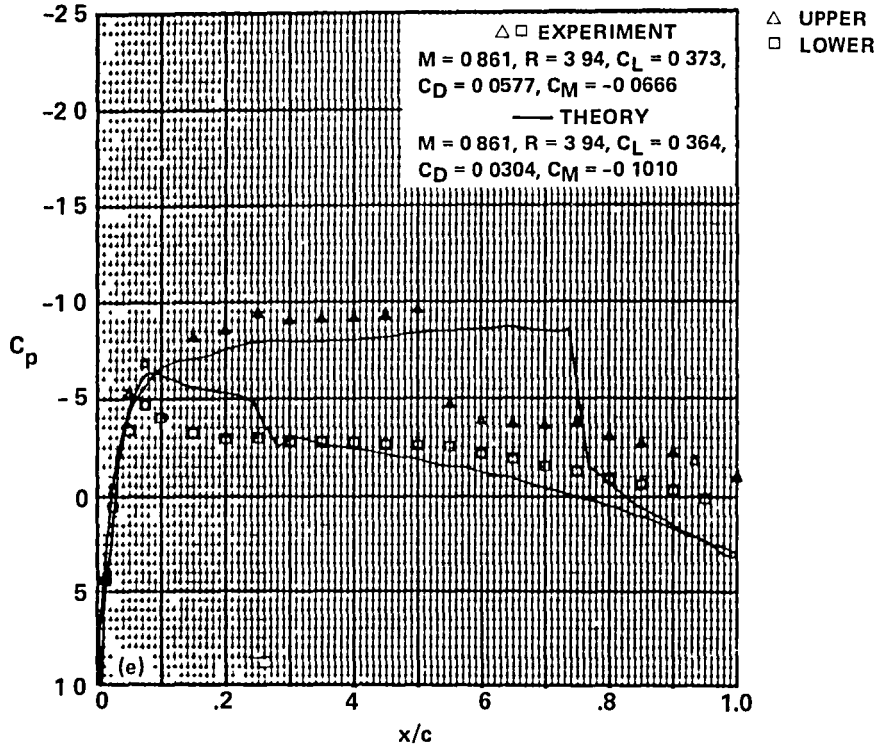

Figure 15.- Concluded.

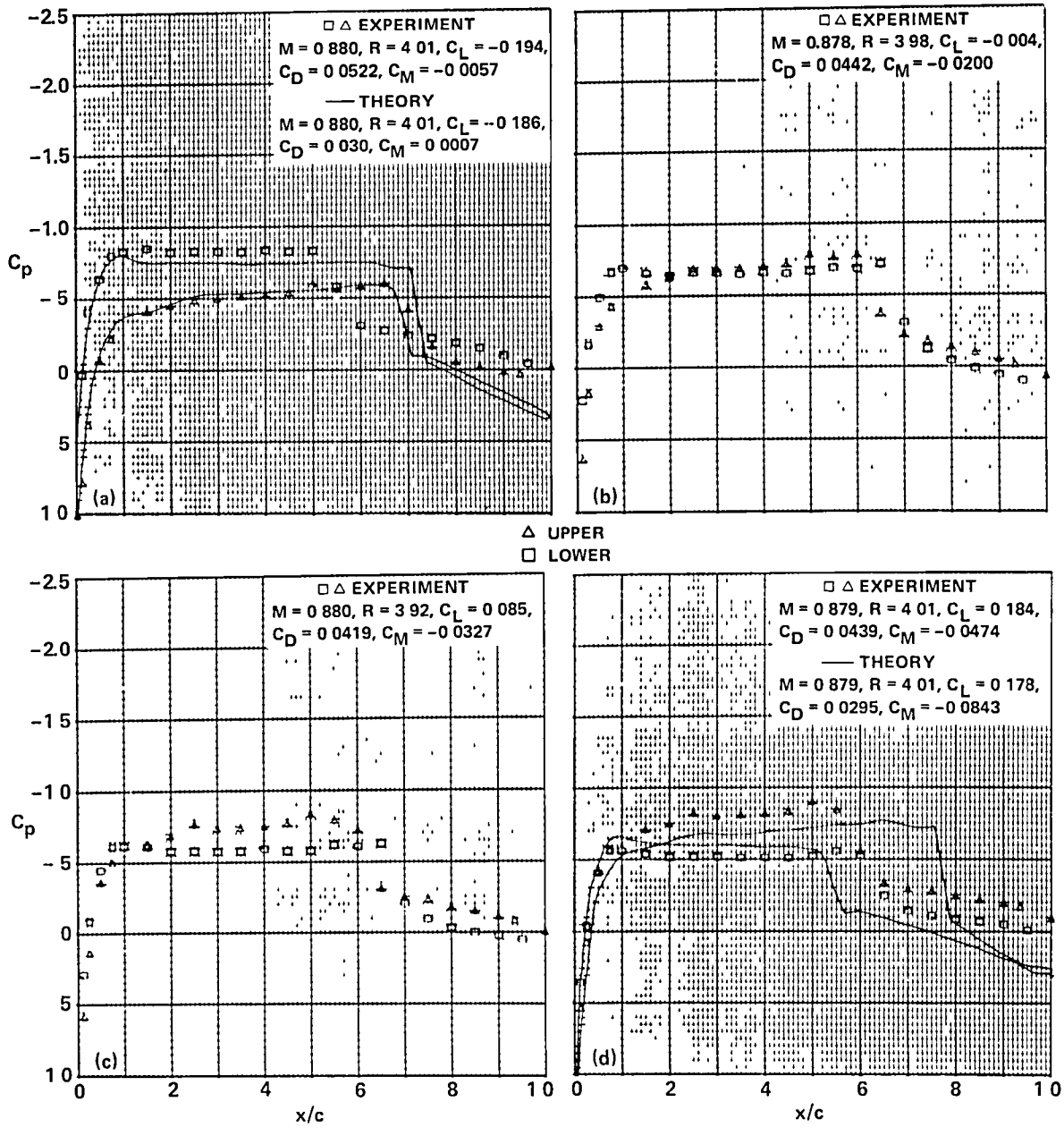

Figure 16.- Pressure distributions of the SC1095 airfoil, M_{set} = 0.88.

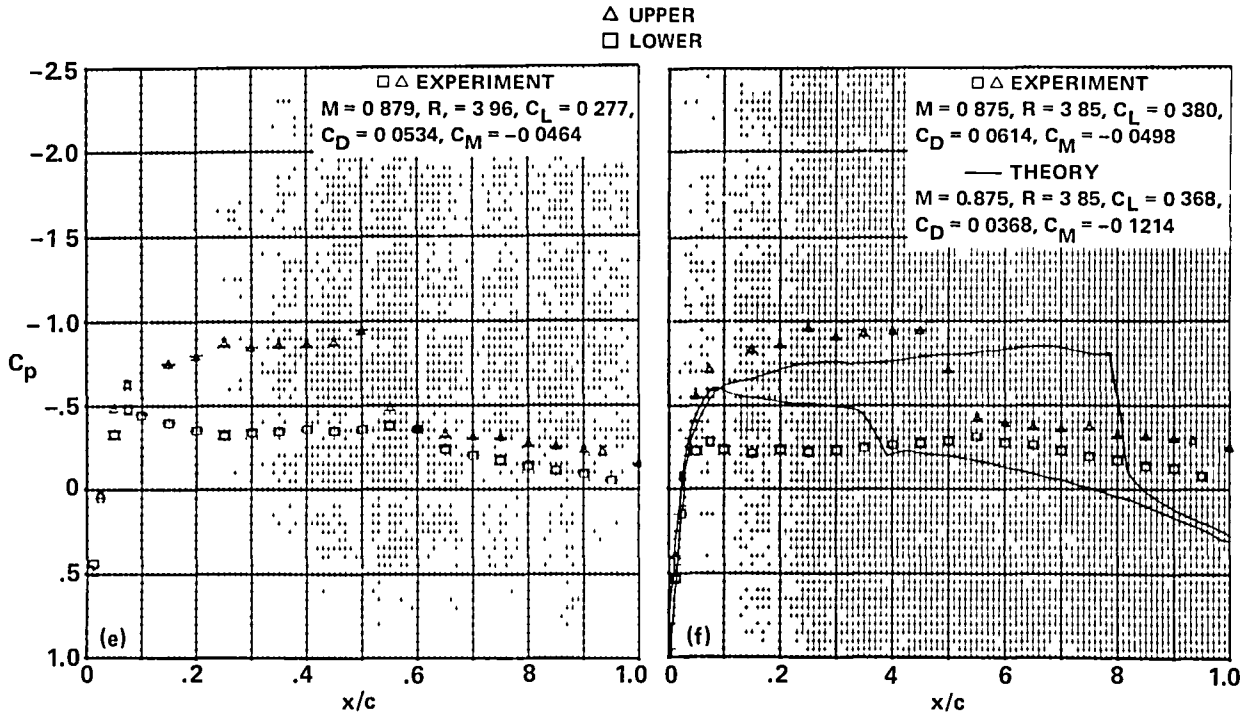

Figure 16.- Concluded.

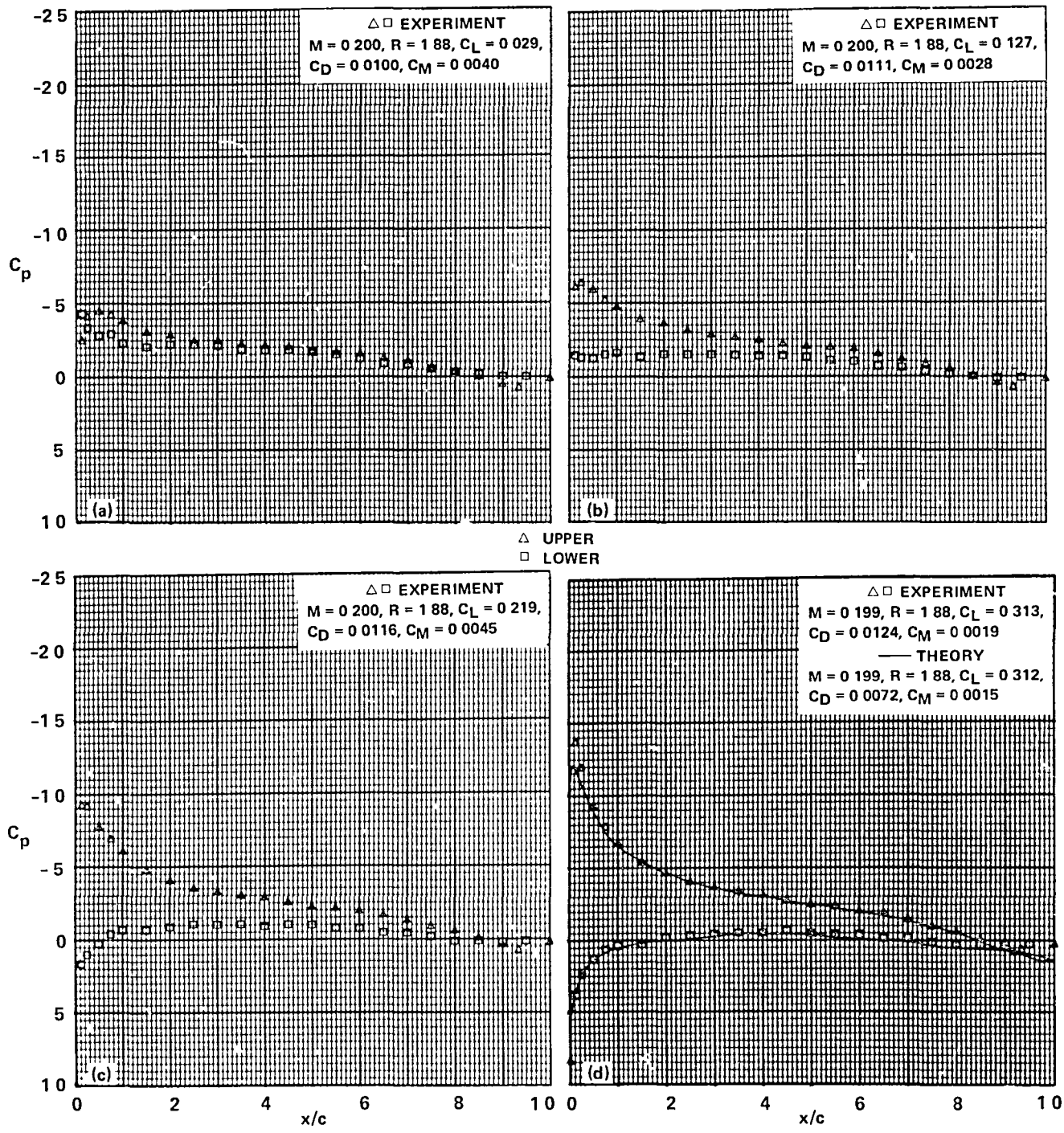

Figure 17.- Pressure distributions of the A-2 airfoil, M_{set} = 0.2.

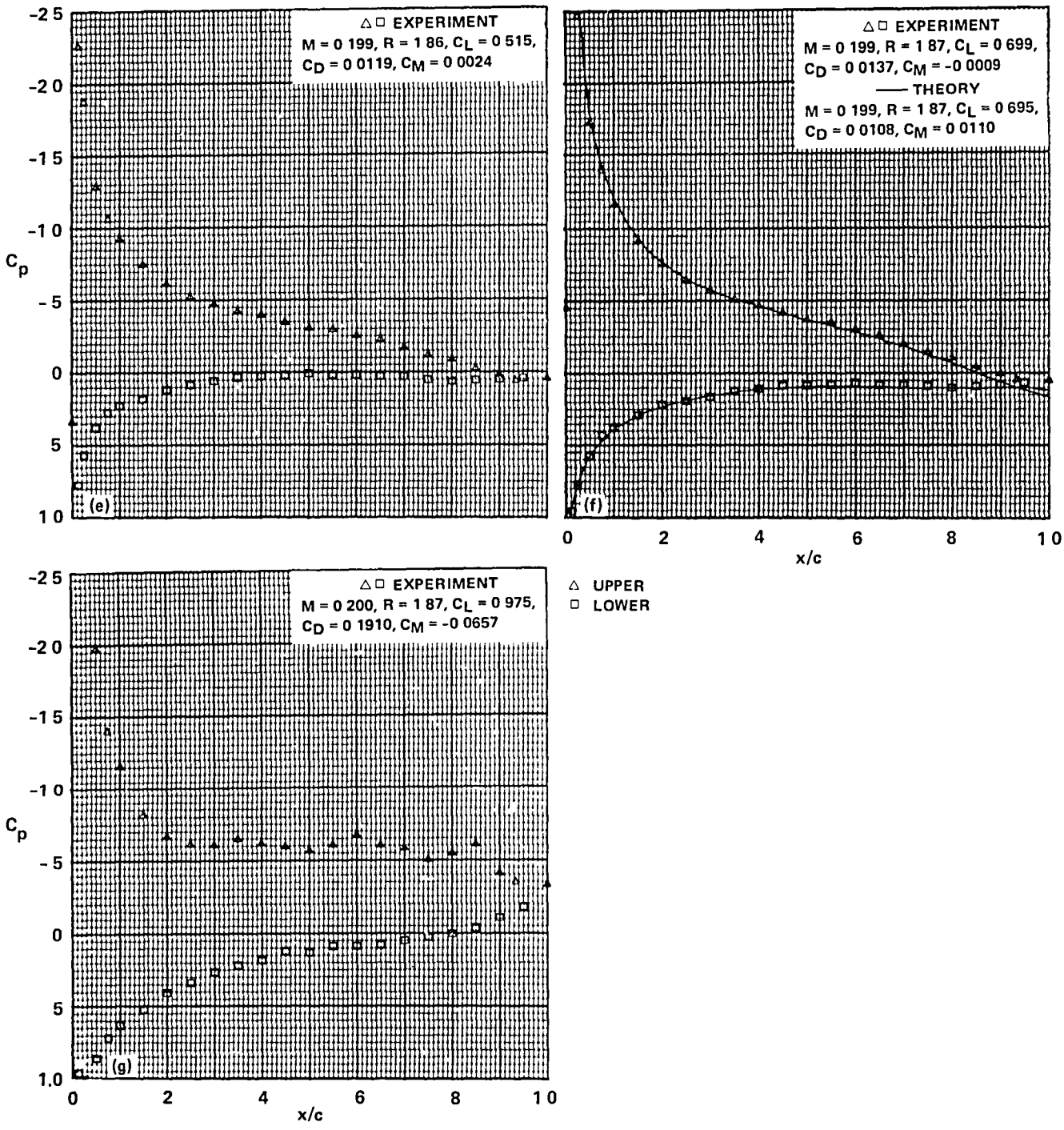

Figure 17.- Concluded.

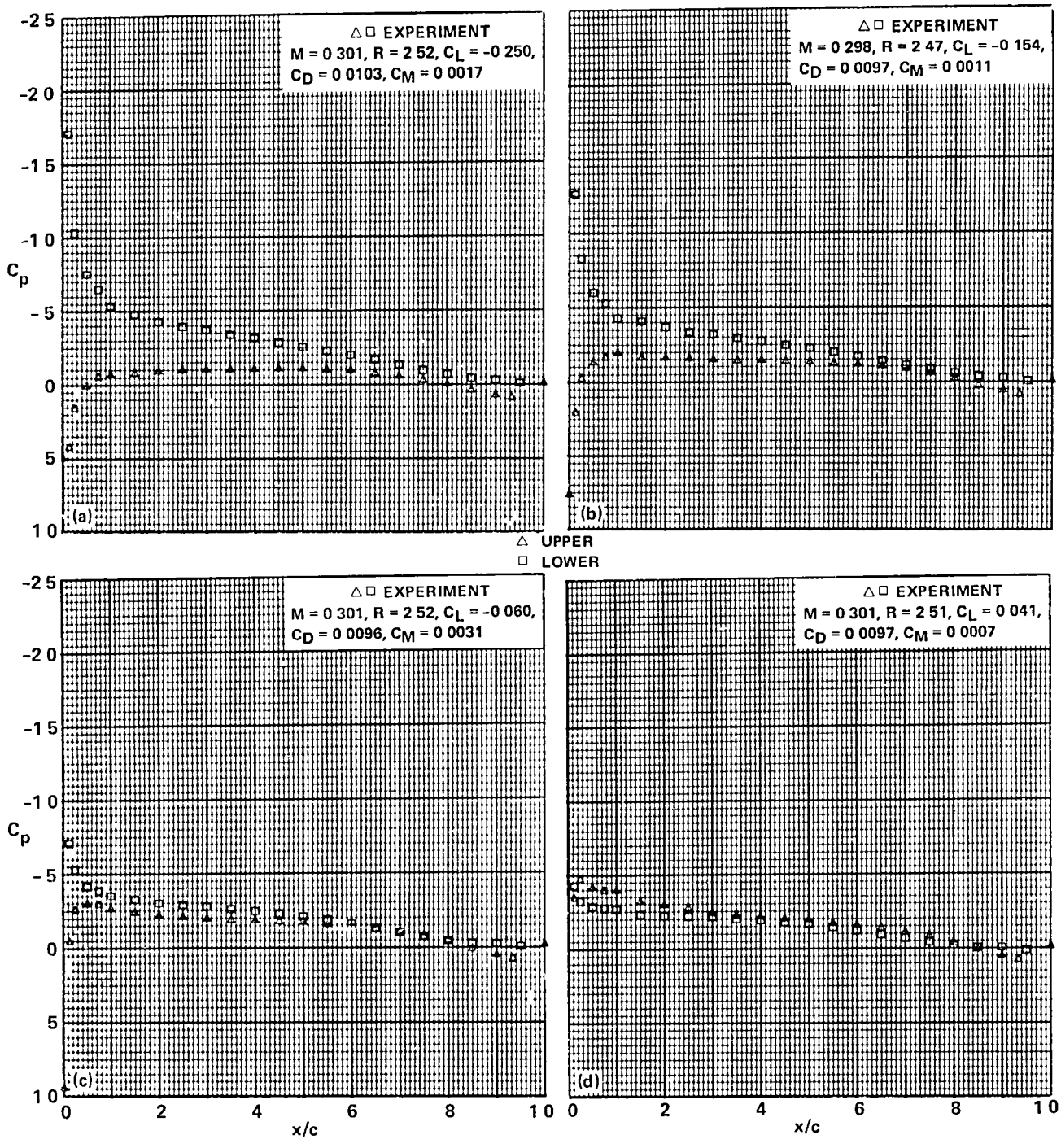

Figure 18.- Pressure distributions of the A-2 airfoil, M_{set} = 0.3.

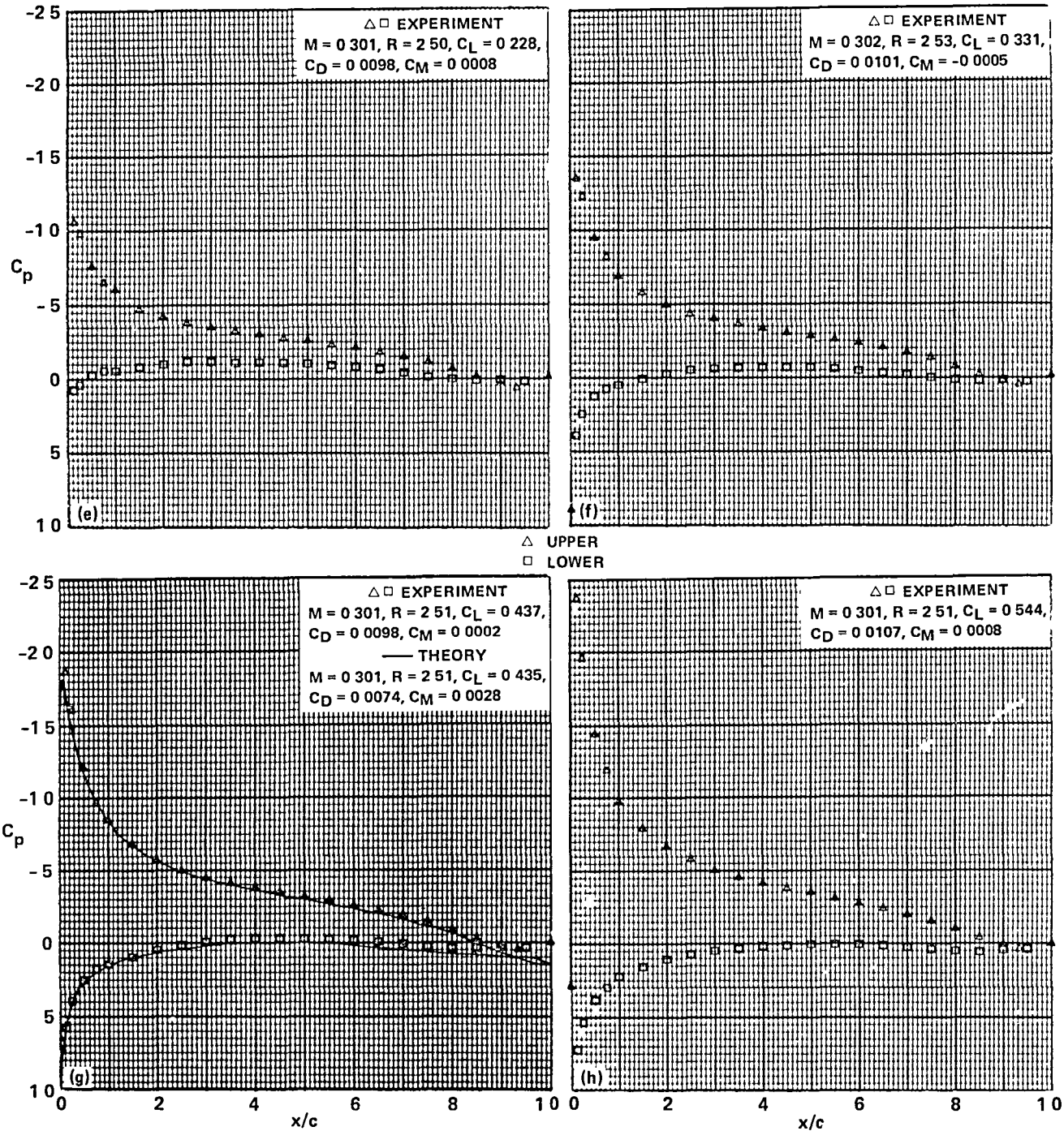

Figure 18.- Continued.

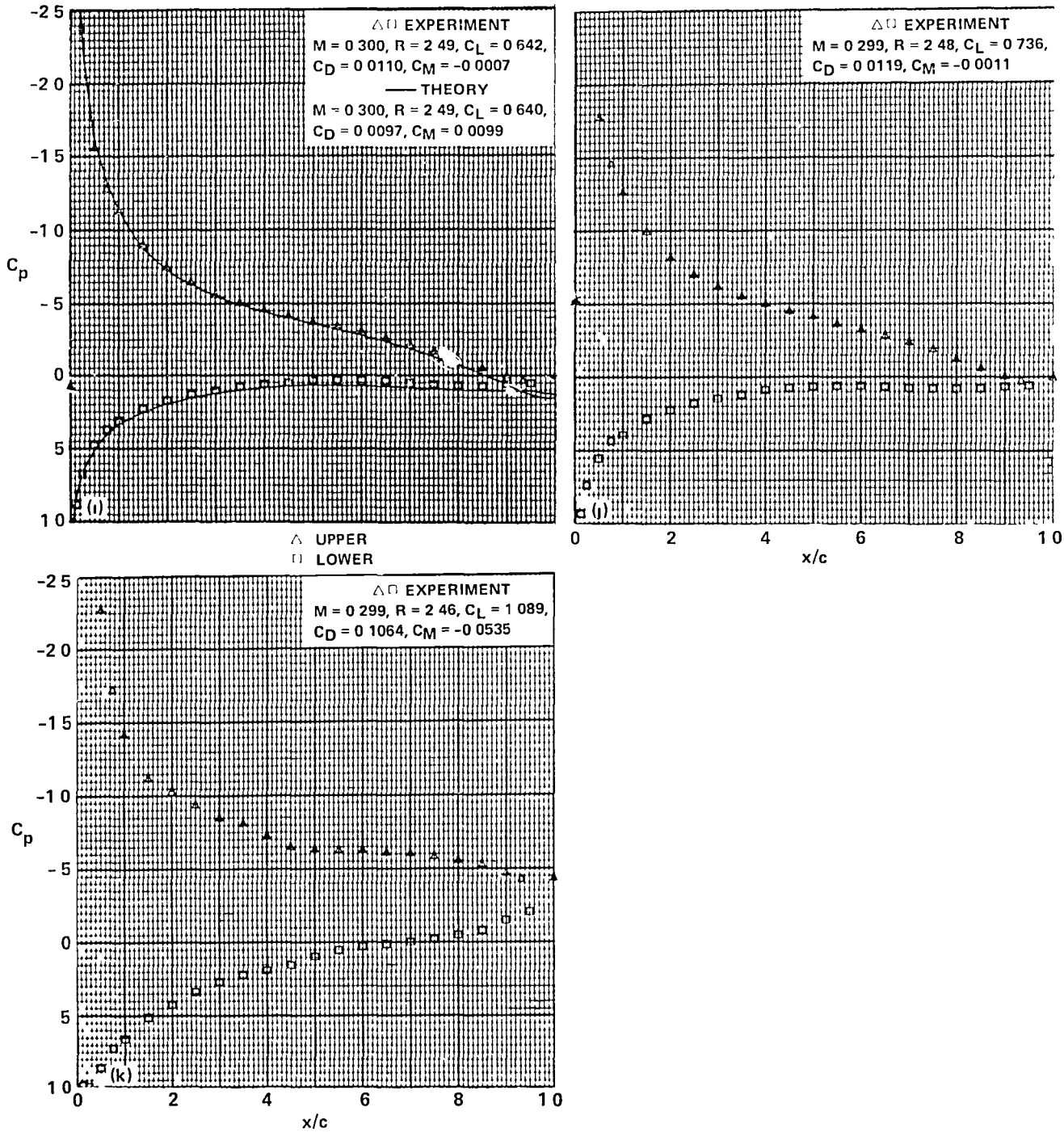

Figure 18.- Concluded.

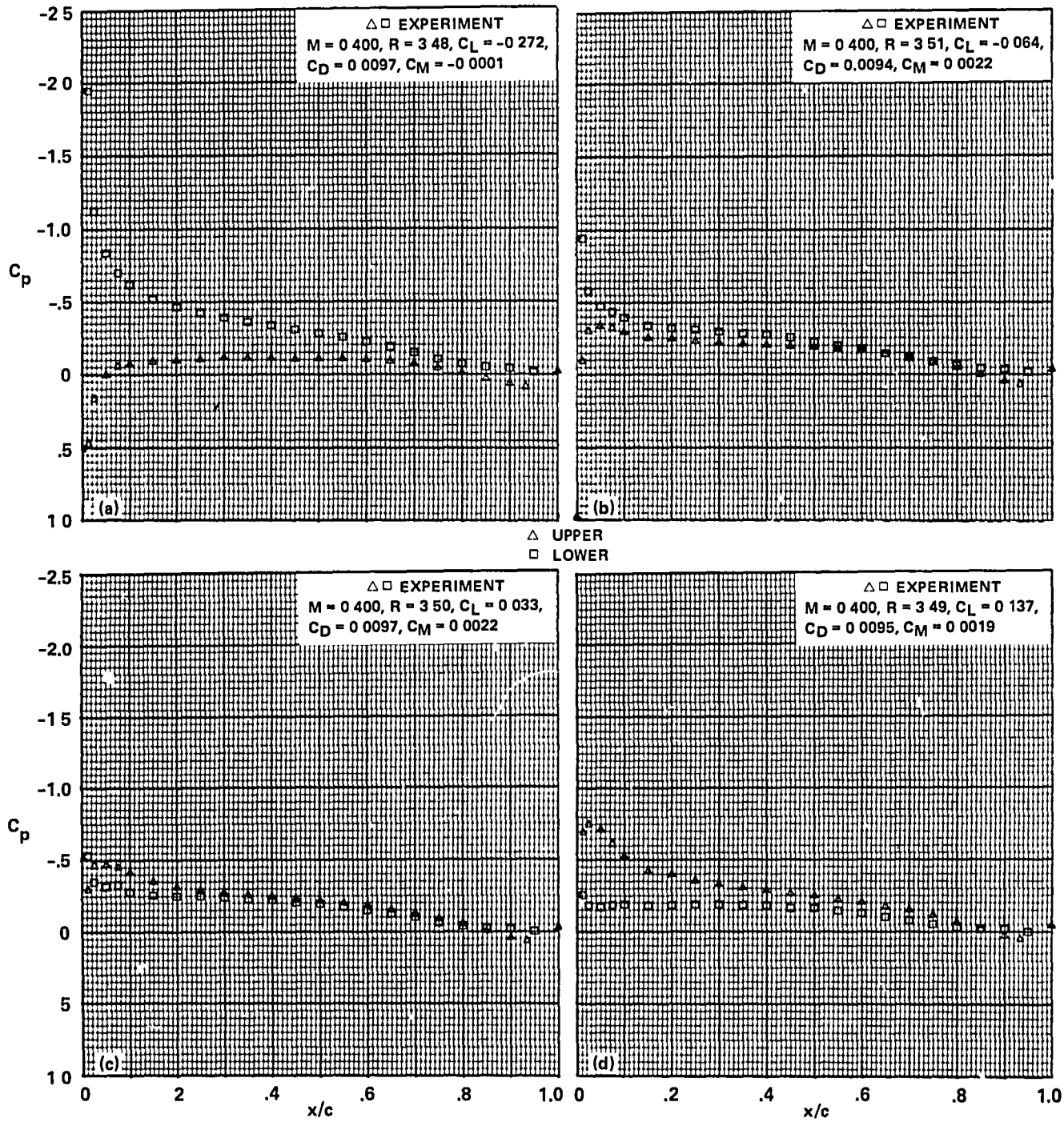

Figure 19.- Pressure distributions of the A-2 airfoil, M_{set} = 0.4.

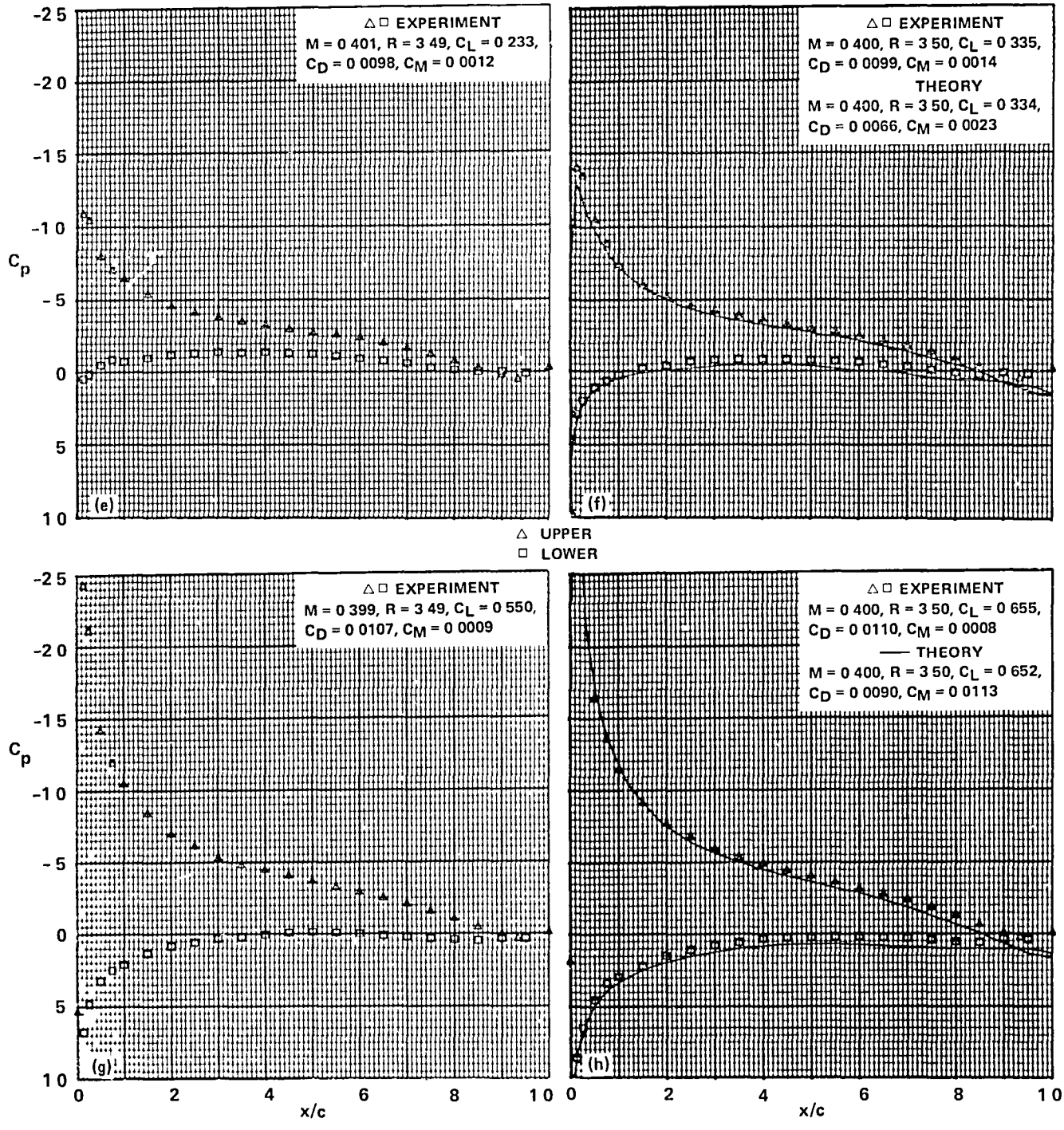

Figure 19.- Continued.

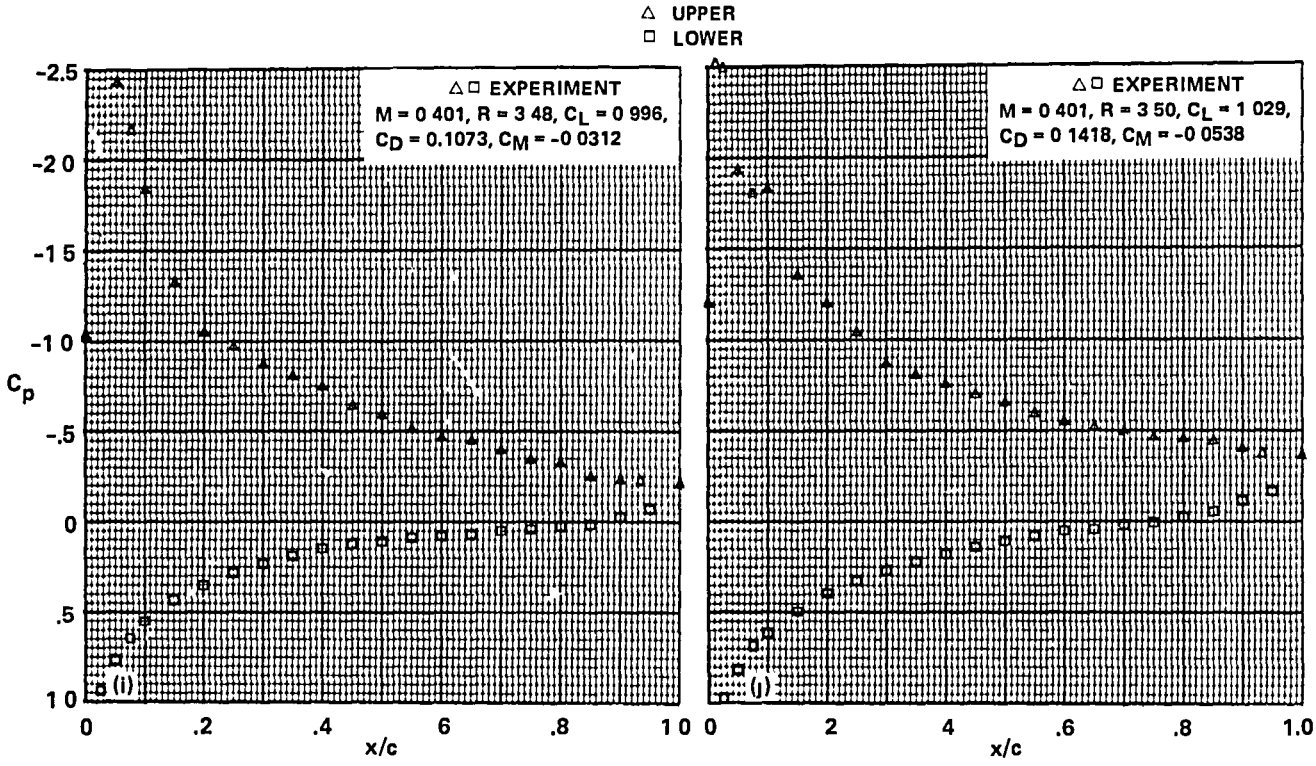

Figure 19.- Concluded.

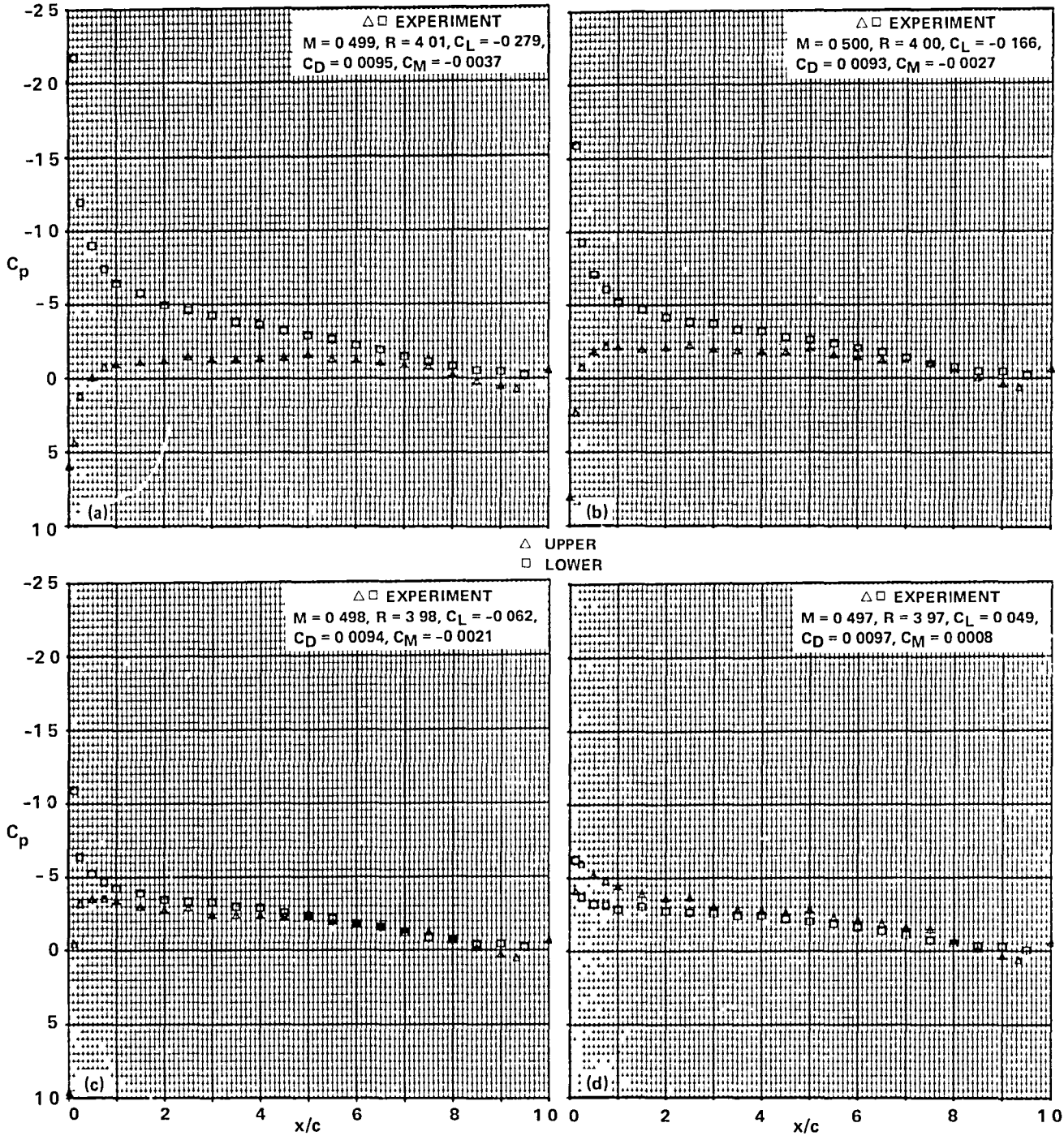

Figure 20.- Pressure distributions of the A-2 airfoil, M_{set} = 0.5.

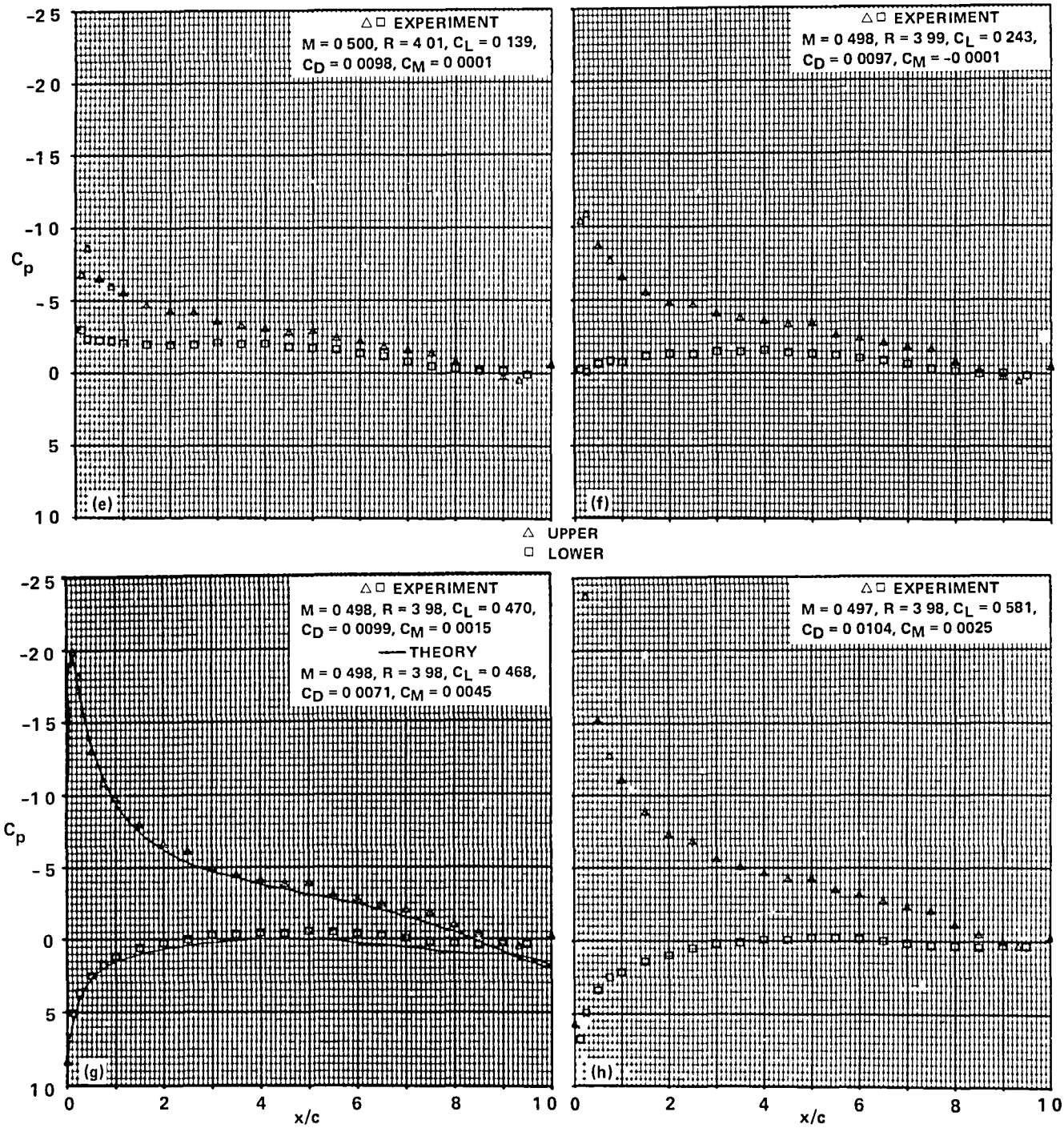

Figure 20.- Continued.

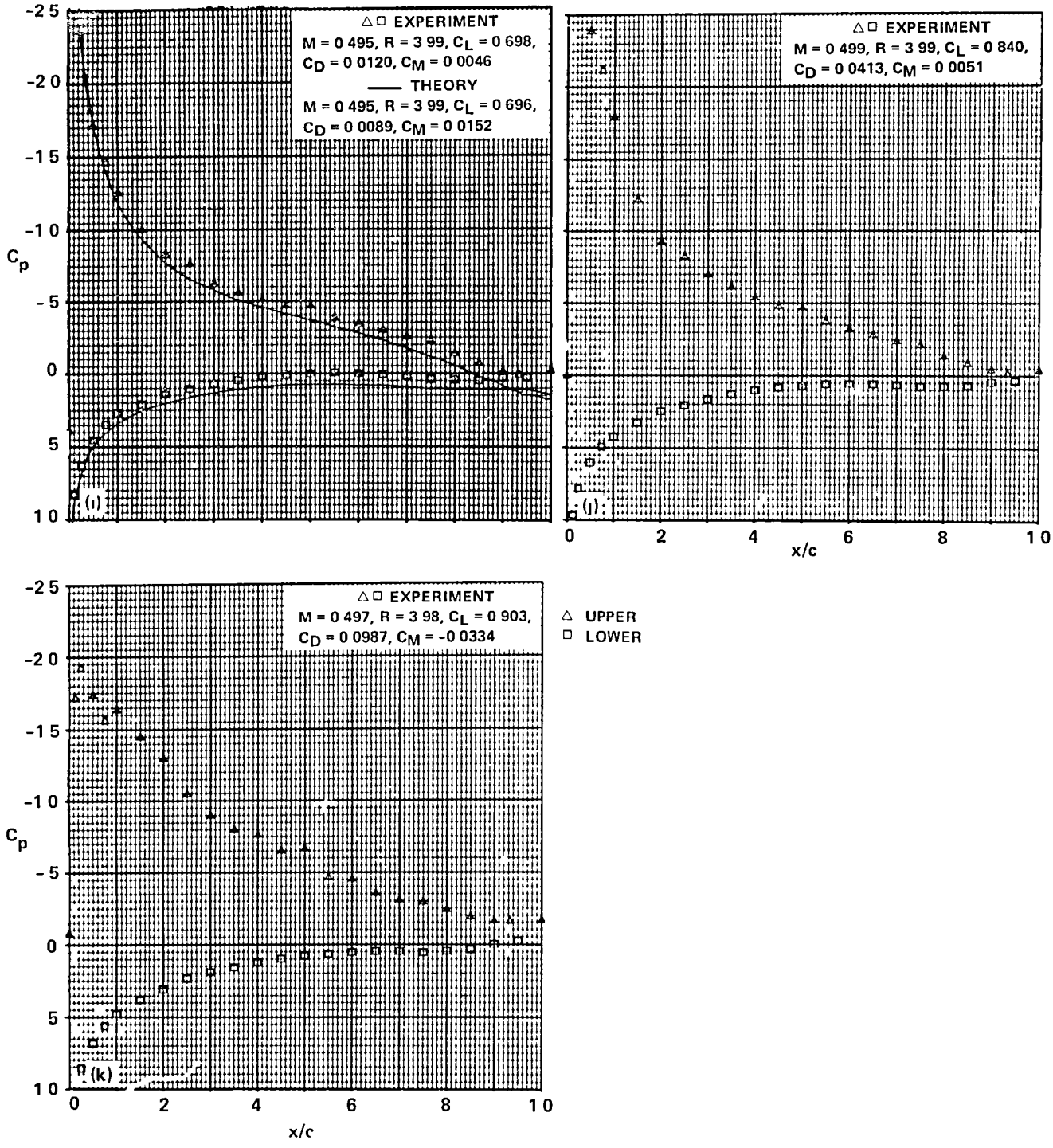

Figure 20.- Concluded.

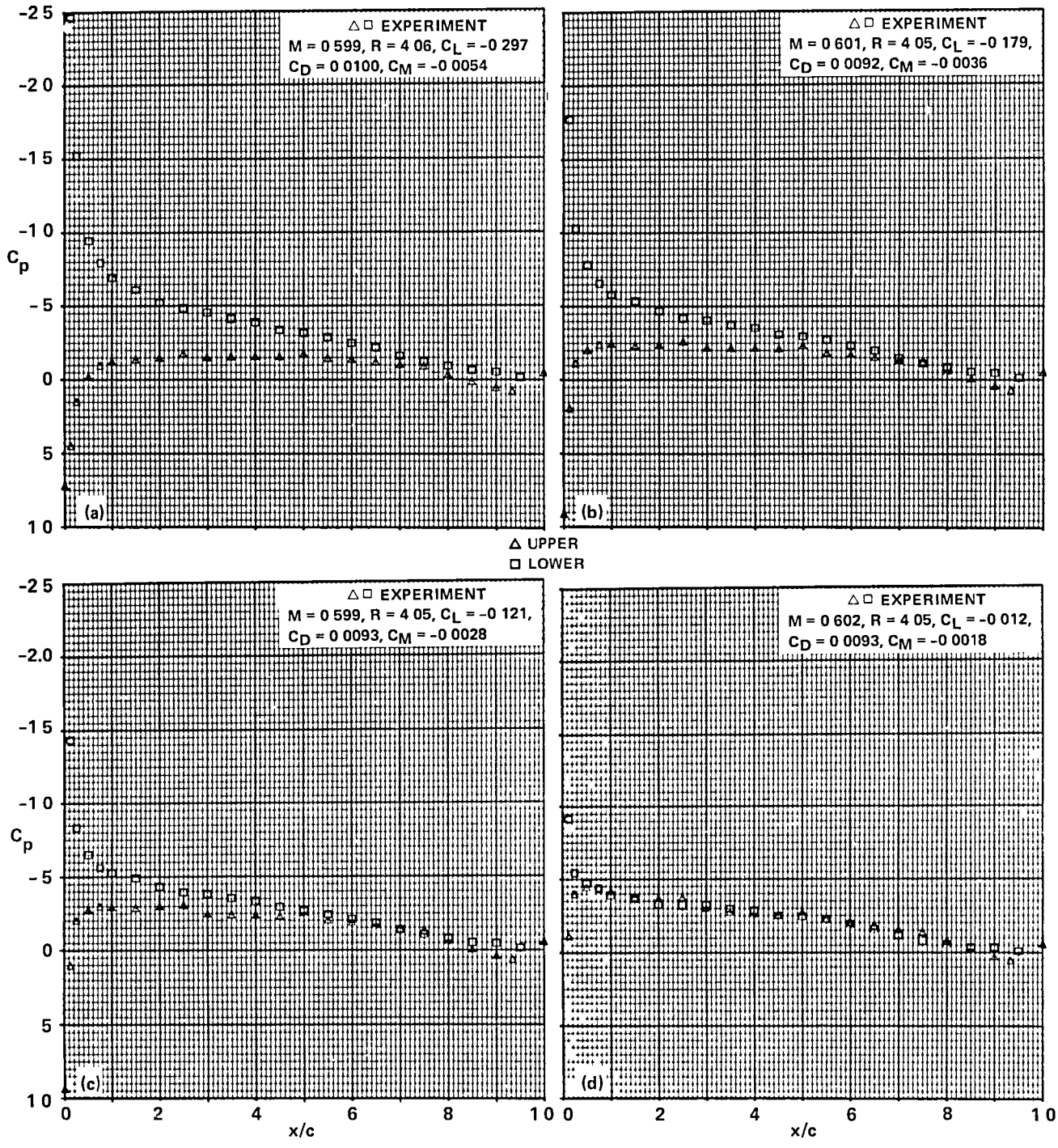

Figure 21.- Pressure distributions of the A-2 airfoil, M_{set} = 0.6.

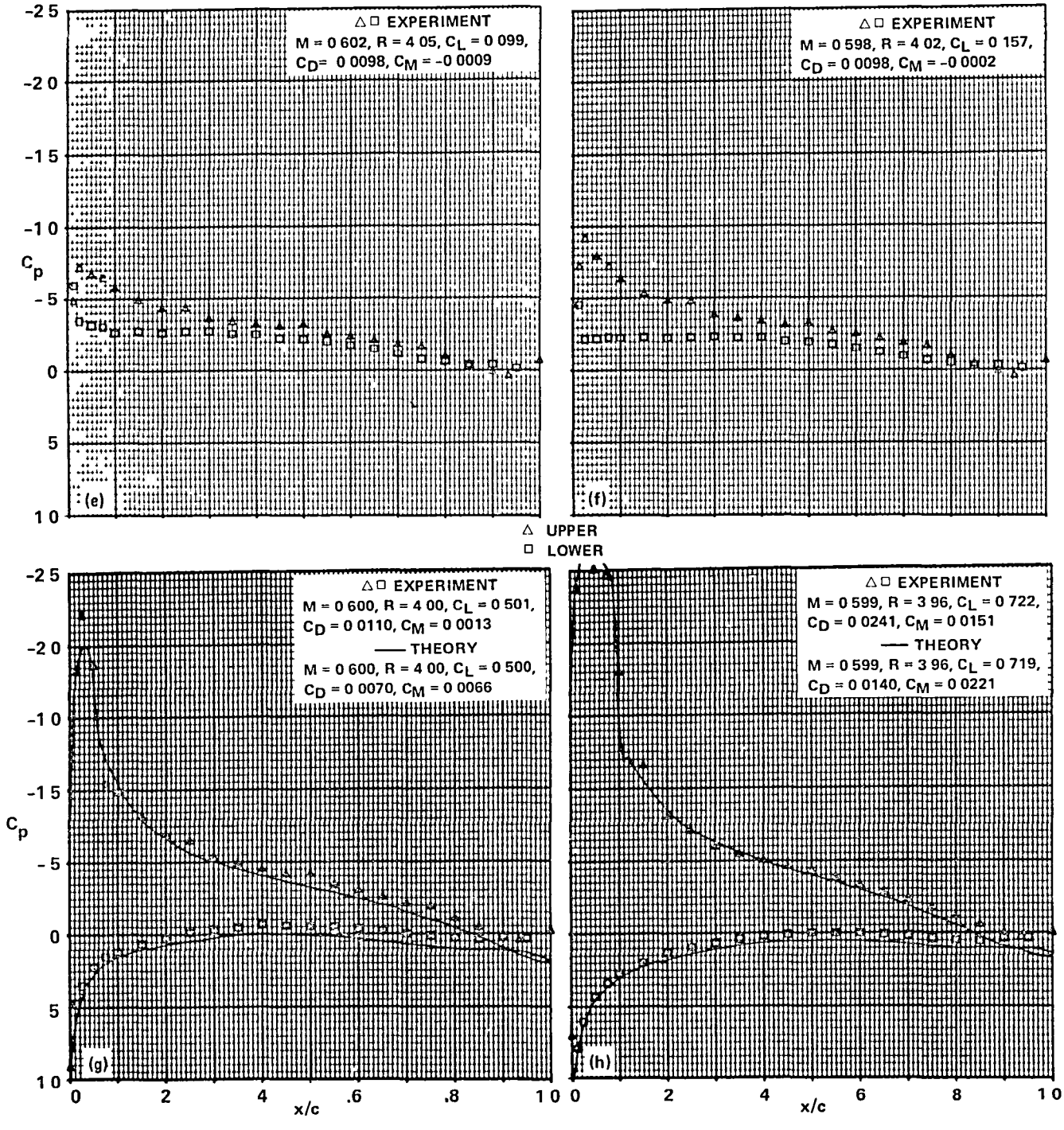

Figure 21.- Continued.

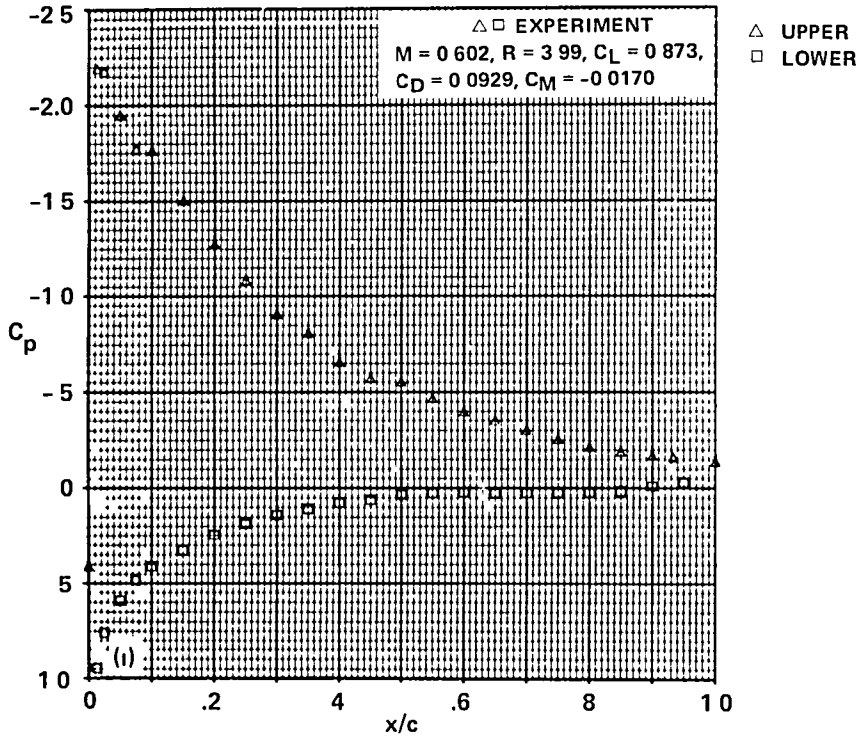

Figure 21.- Concluded.

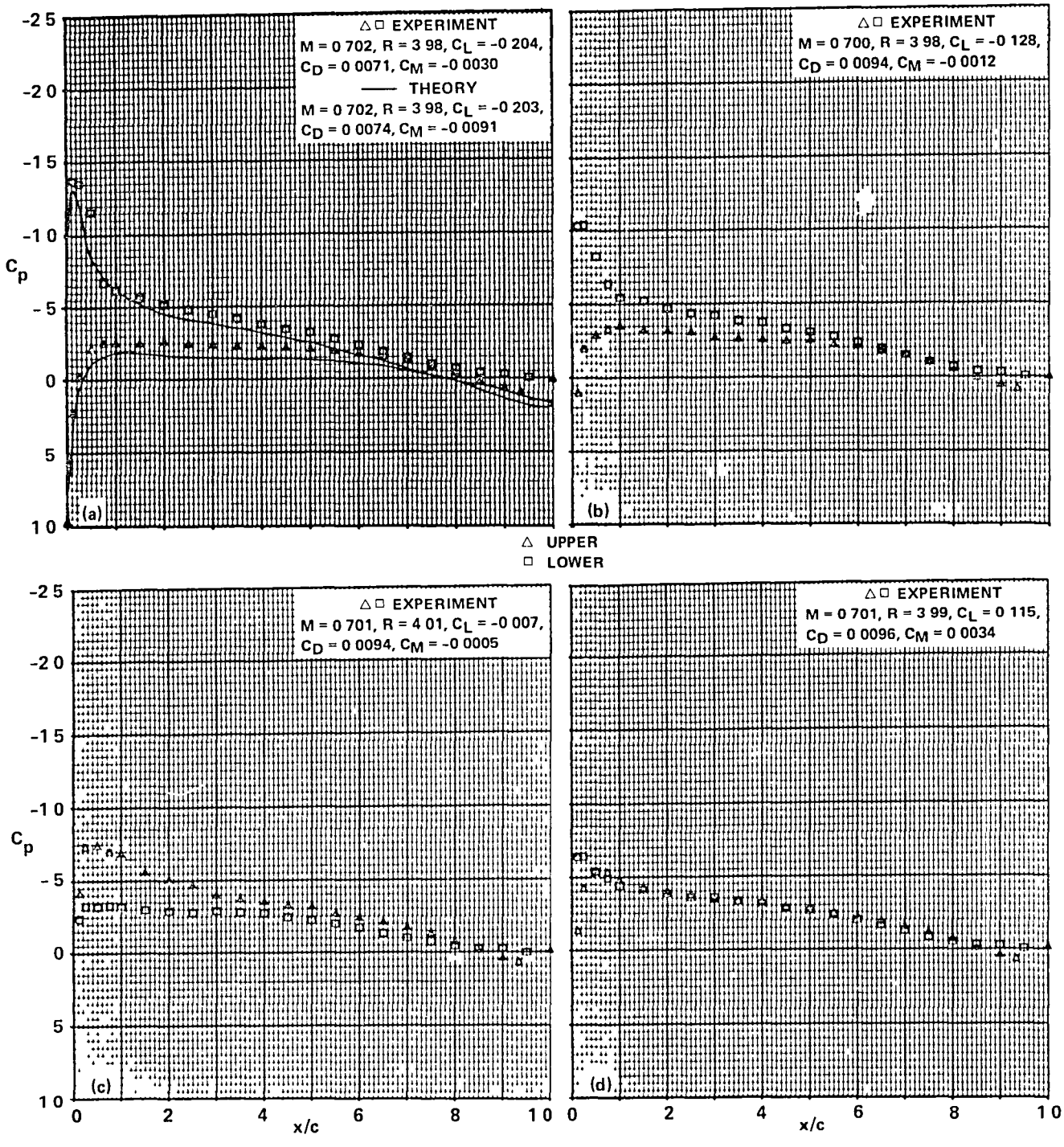

Figure 22.- Pressure distributions for the A-2 airfoil, M_{set} = 0.7.

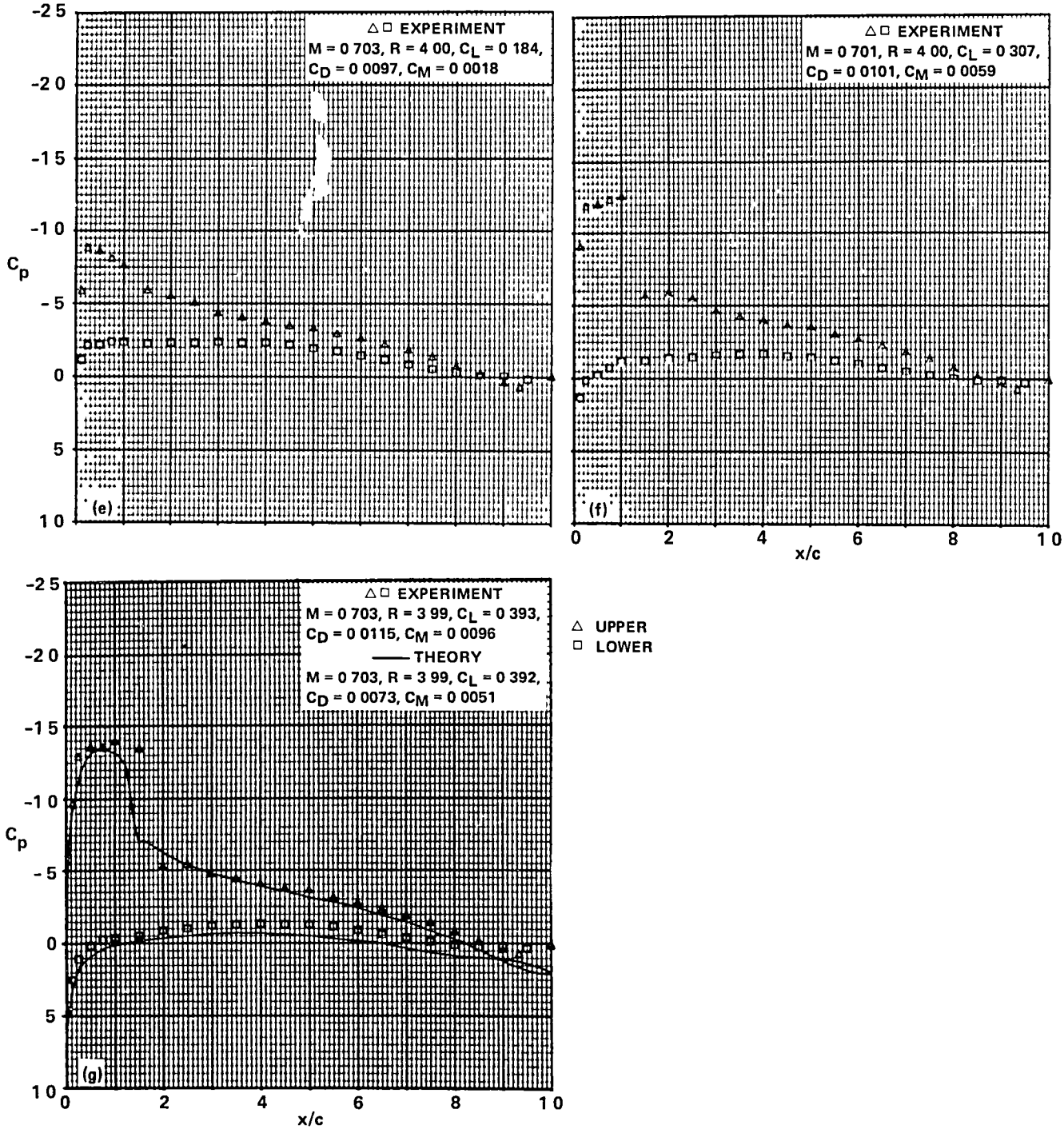

Figure 22.- Concluded.

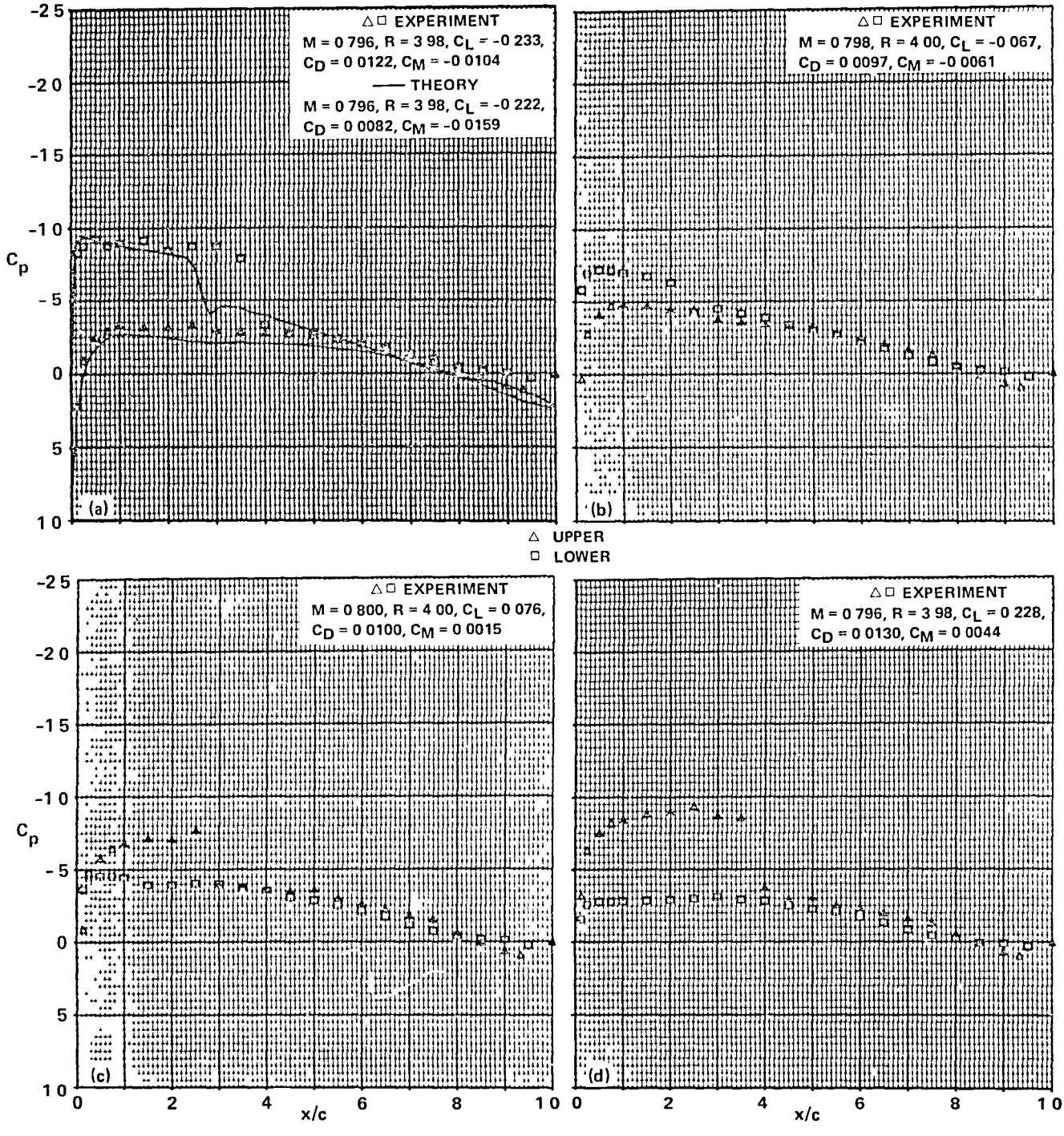

Figure 23.- Pressure distributions of the A-2 airfoil, M_{set} = 0.8.

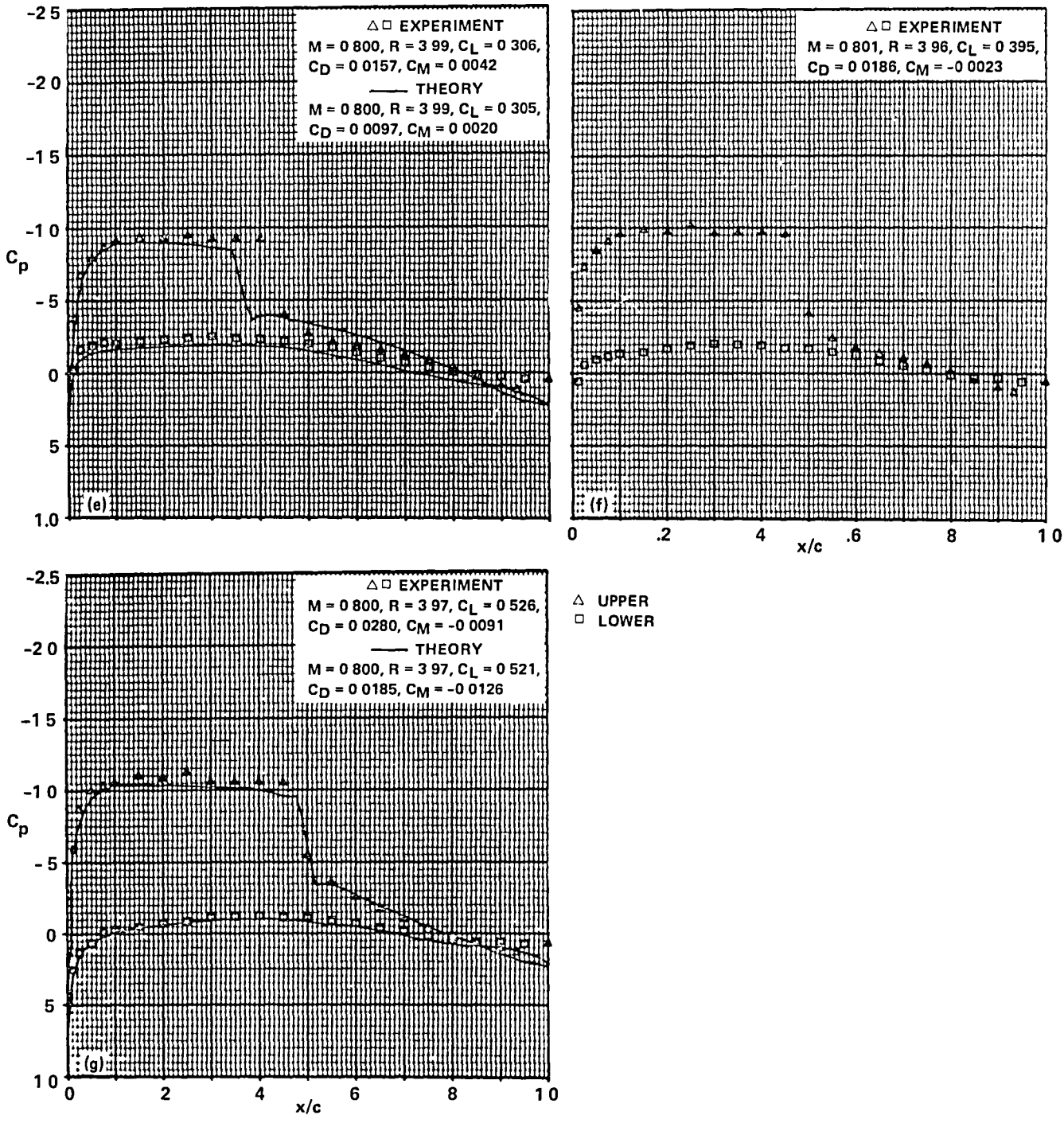

Figure 23.- Concluded.

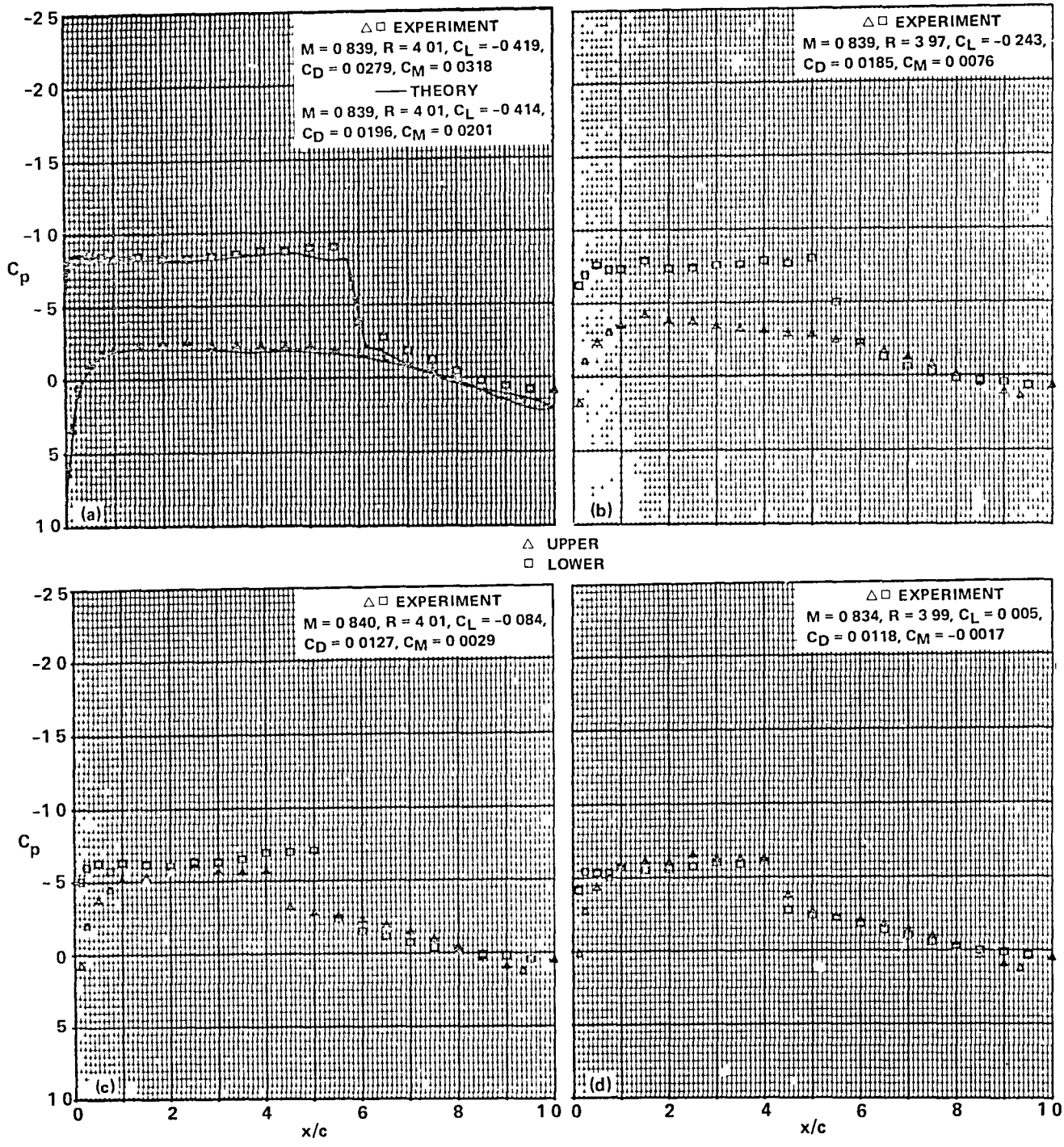

Figure 24.- Pressure distributions of the A-2 airfoil, M_{set} = 0.84.

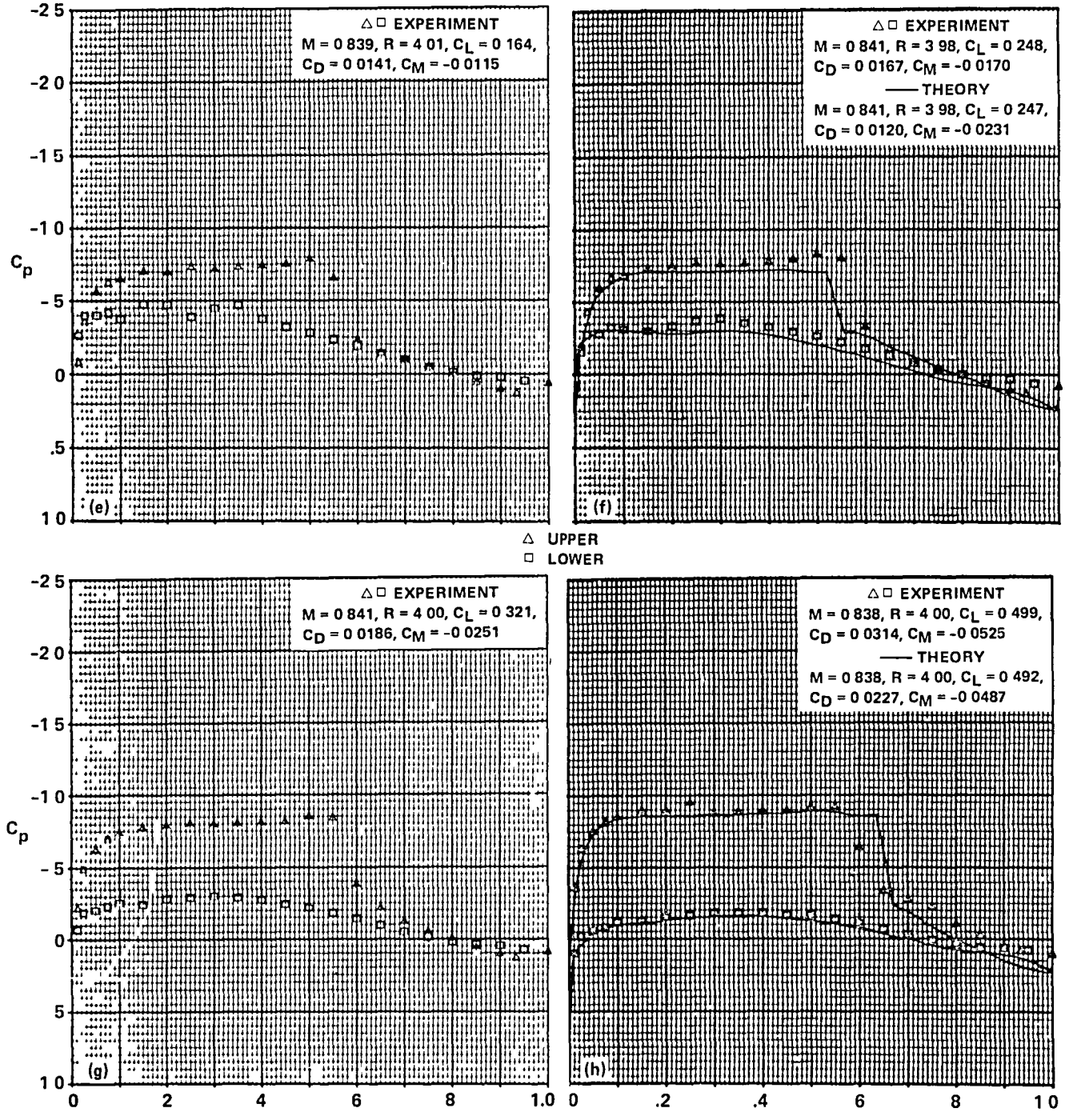

Figure 24.- Concluded.

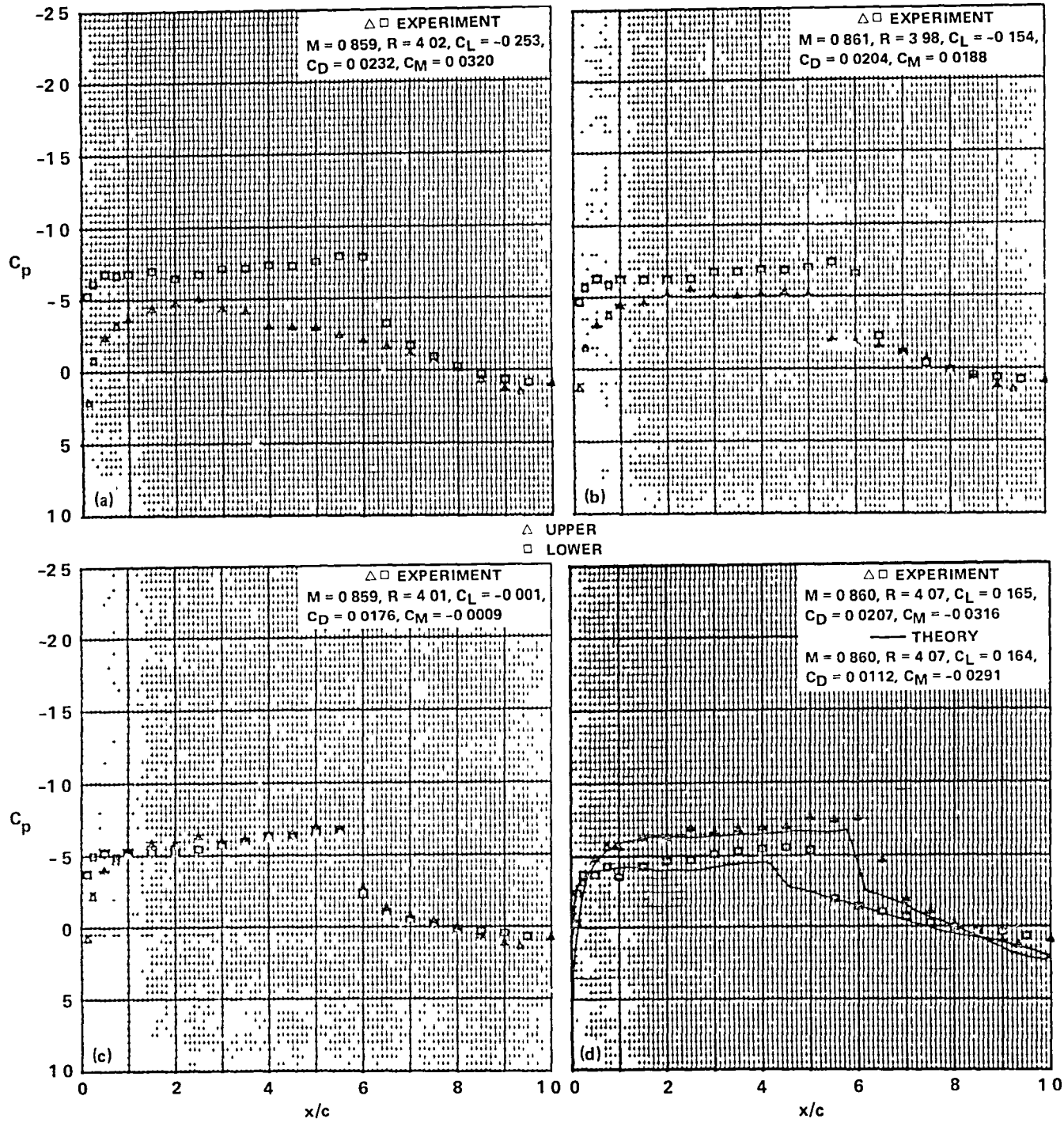

Figure 25.- Pressure distributions of the A-2 airfoil, M_{set} = 0.86.

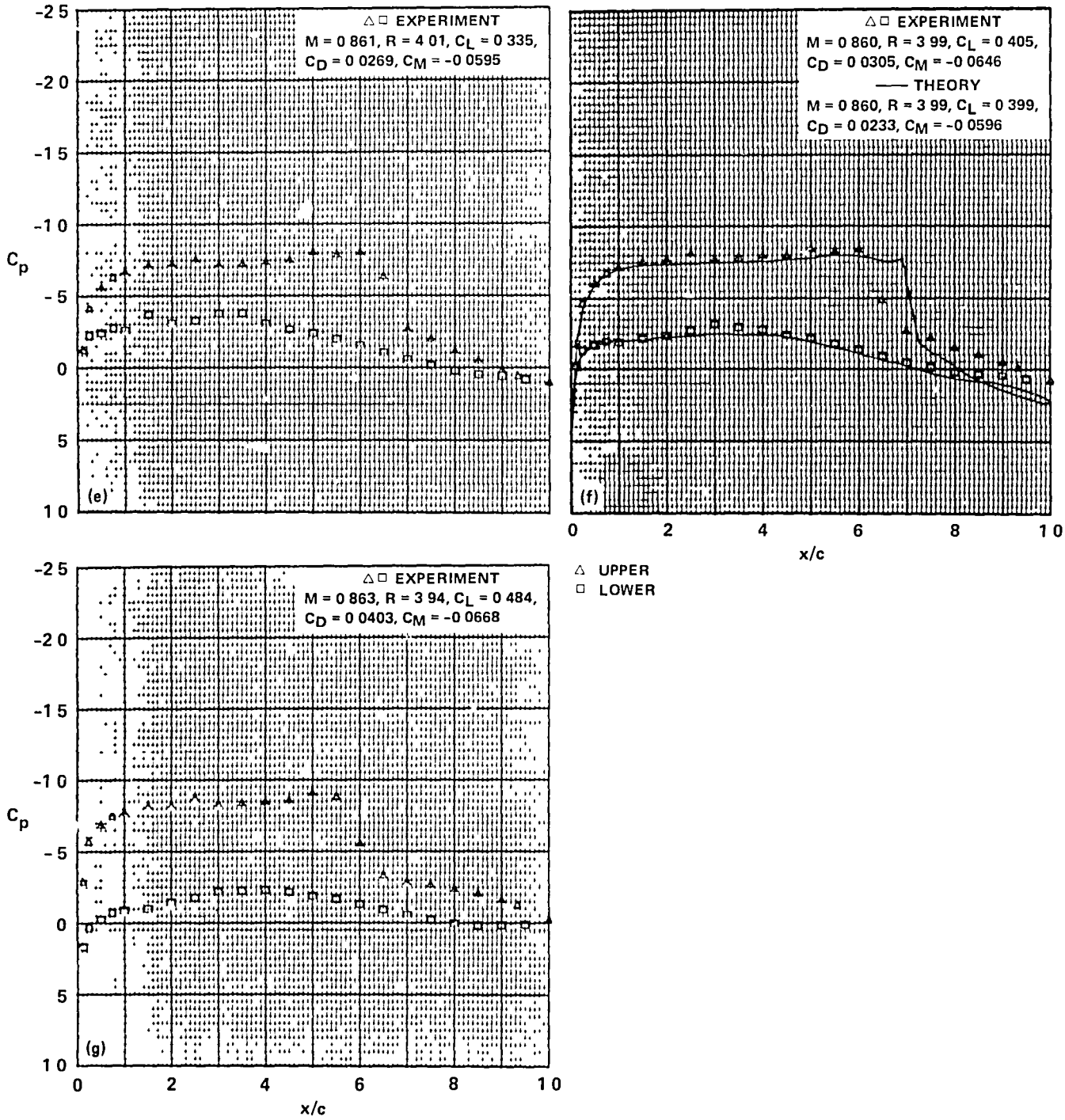

Figure 25.- Concluded.

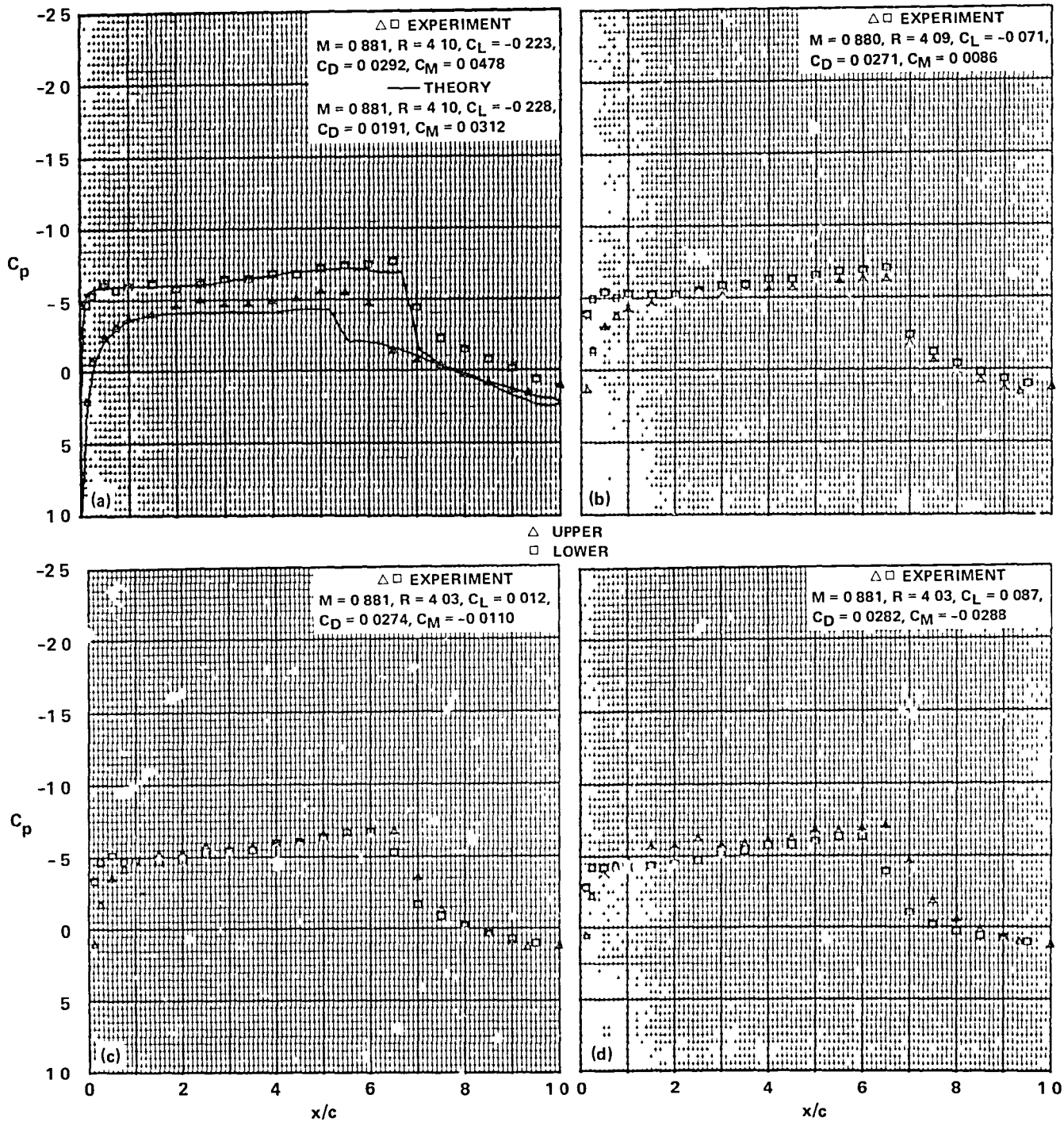

Figure 26.- Pressure distributions of the A-2 airfoil, M_{set} = 0.88.

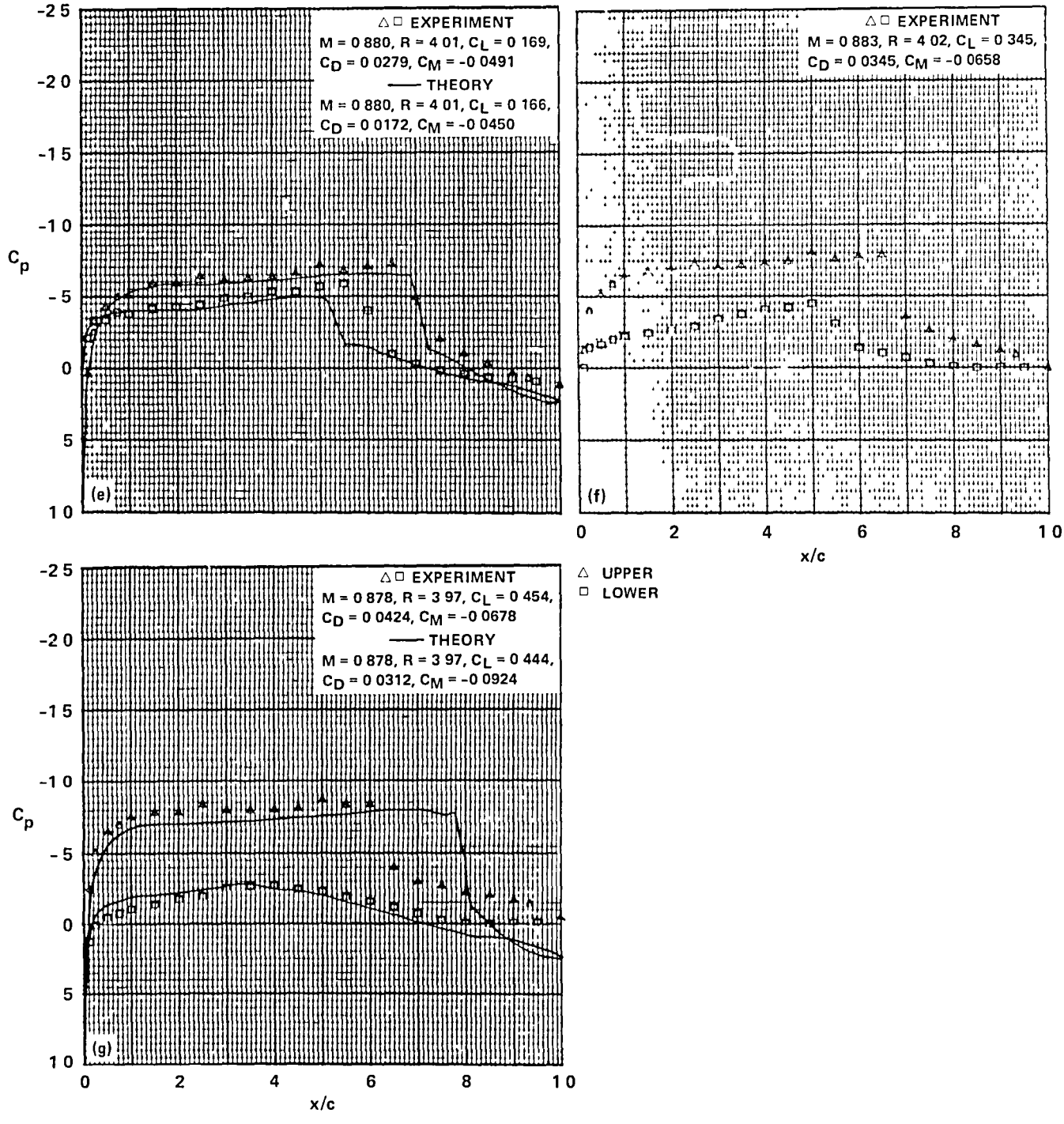

Figure 26.- Concluded.

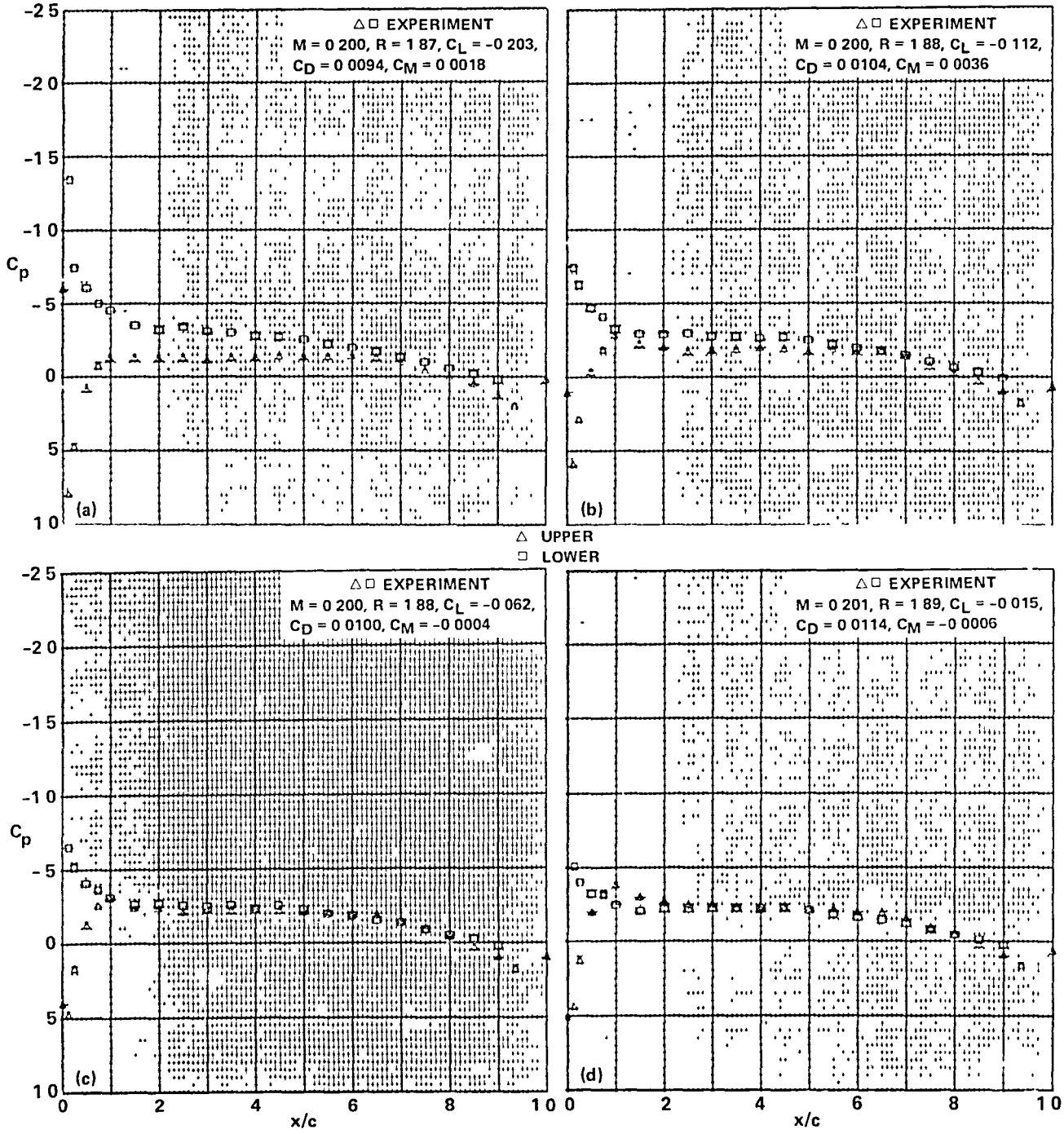

Figure 27.- Pressure distributions of the SSC-A09 airfoil, M_{set} = 0.2.

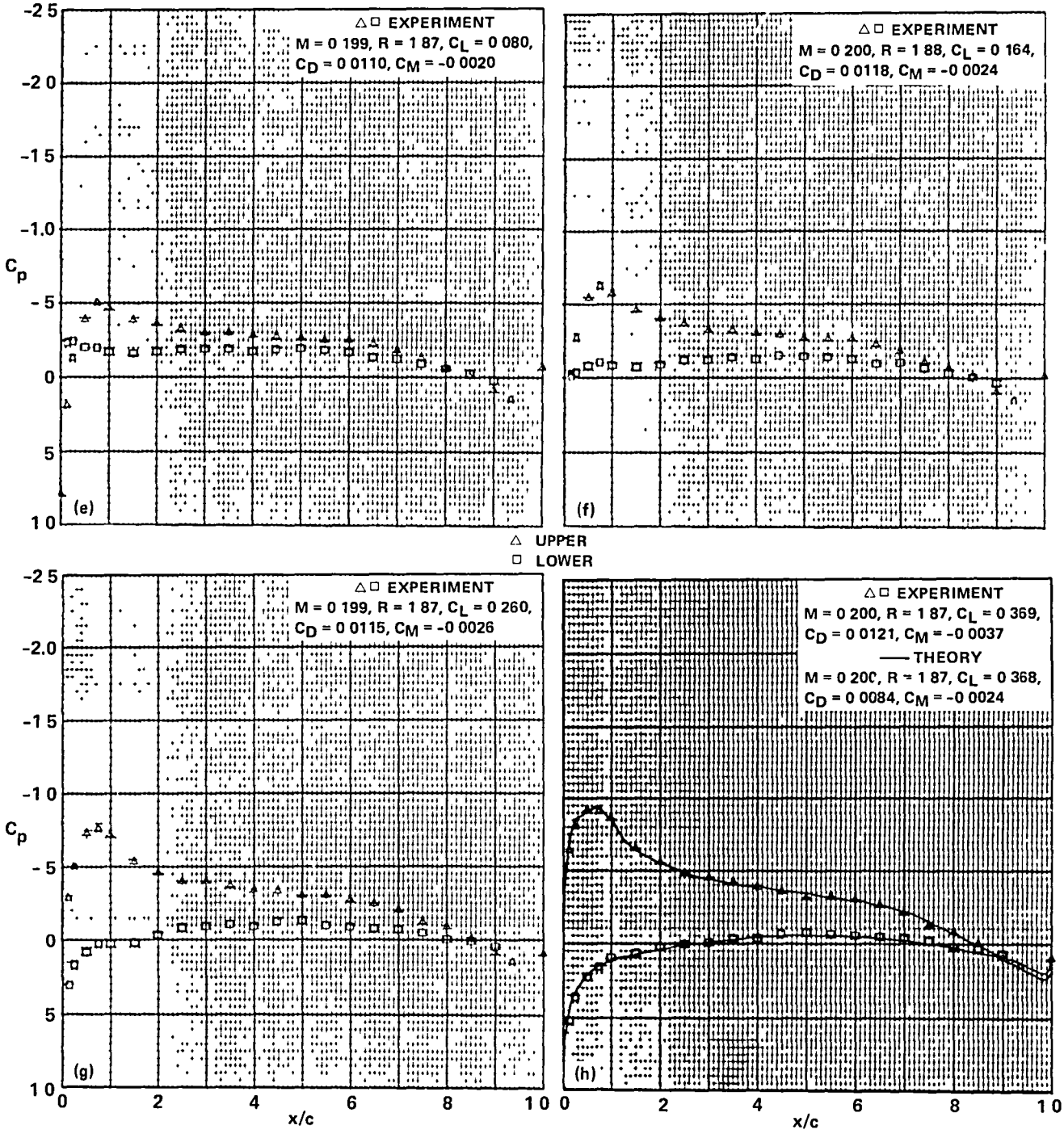

Figure 27.- Continued.

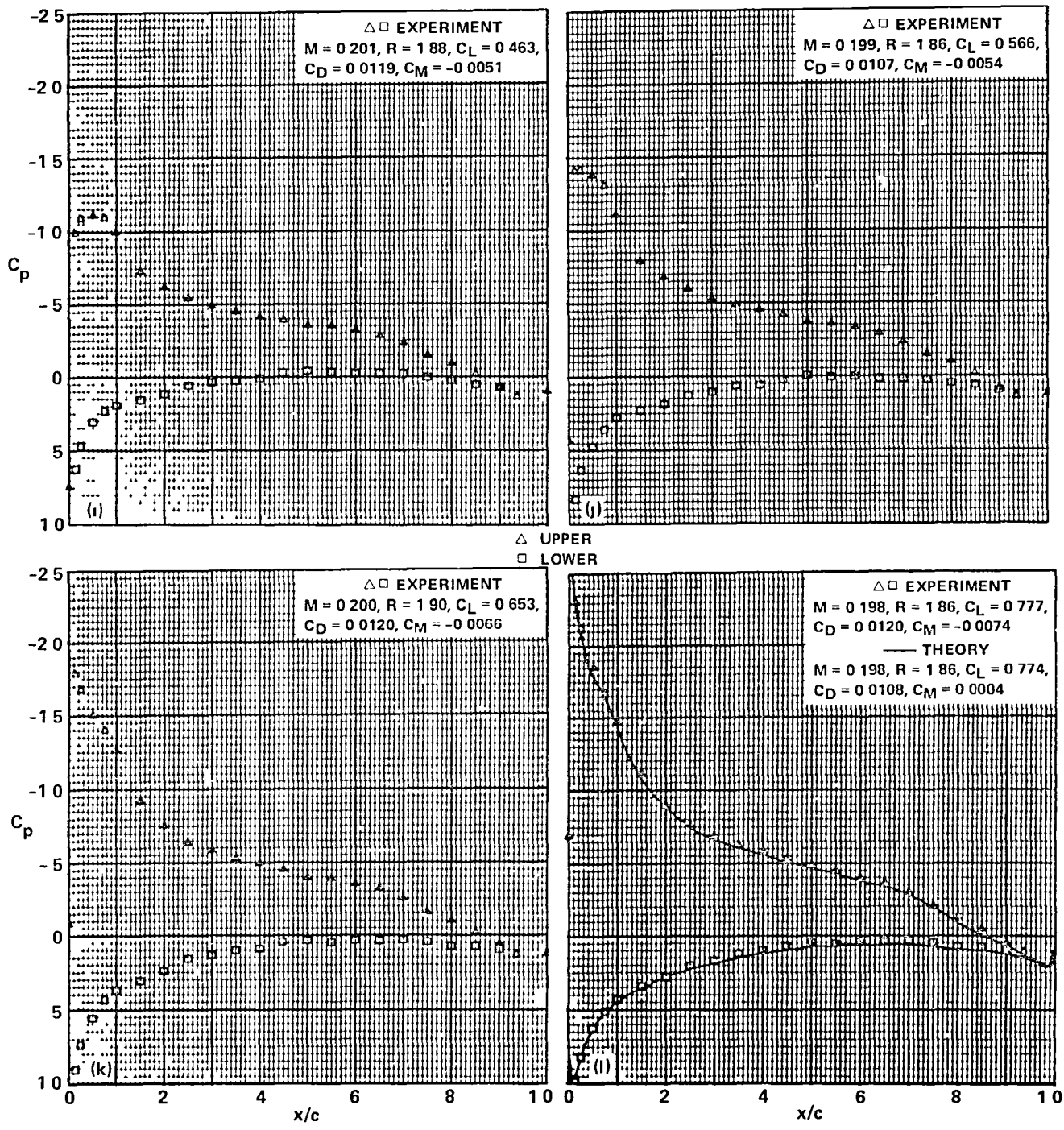

Figure 27.- Continued.

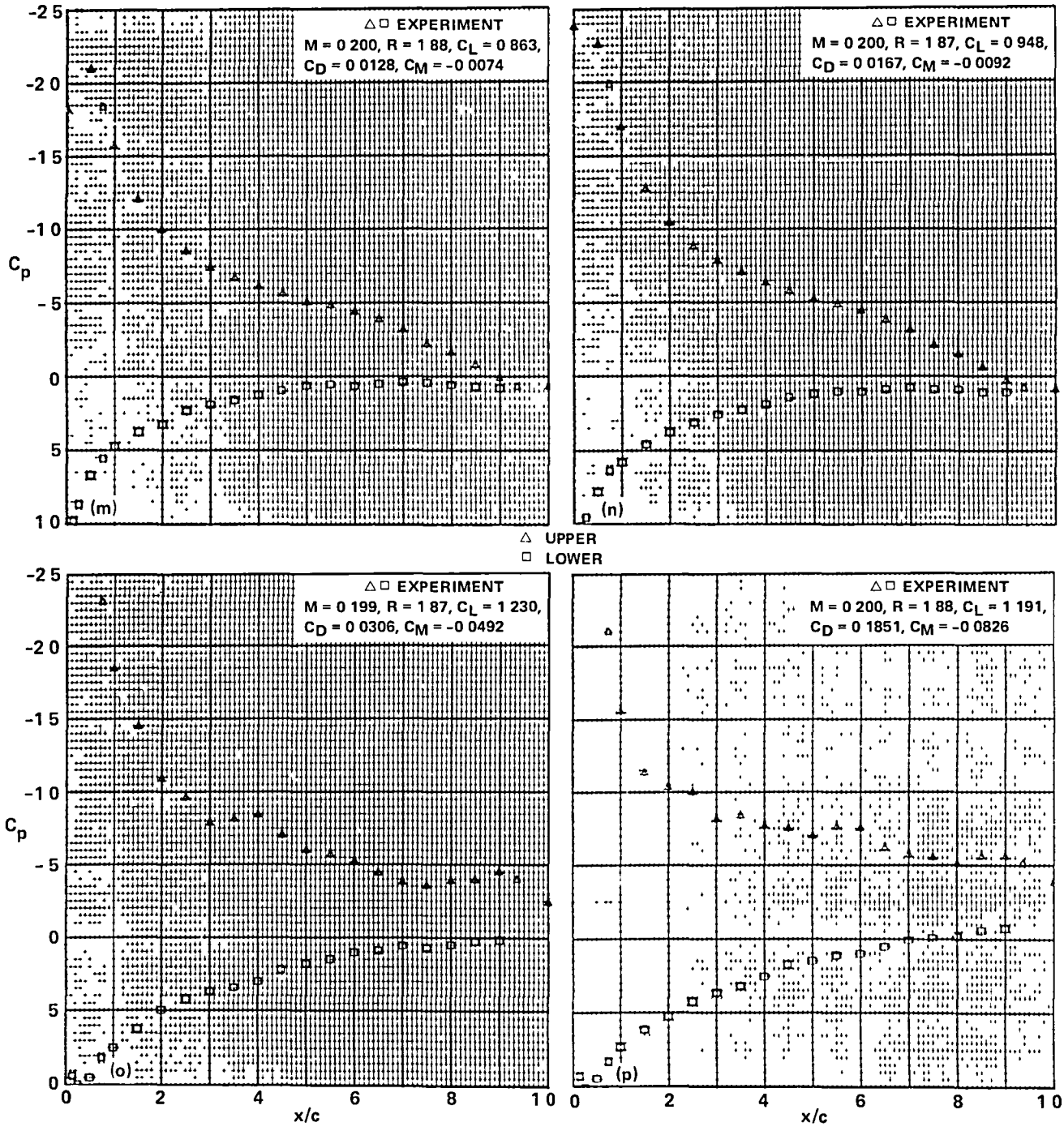

Figure 27.- Concluded.

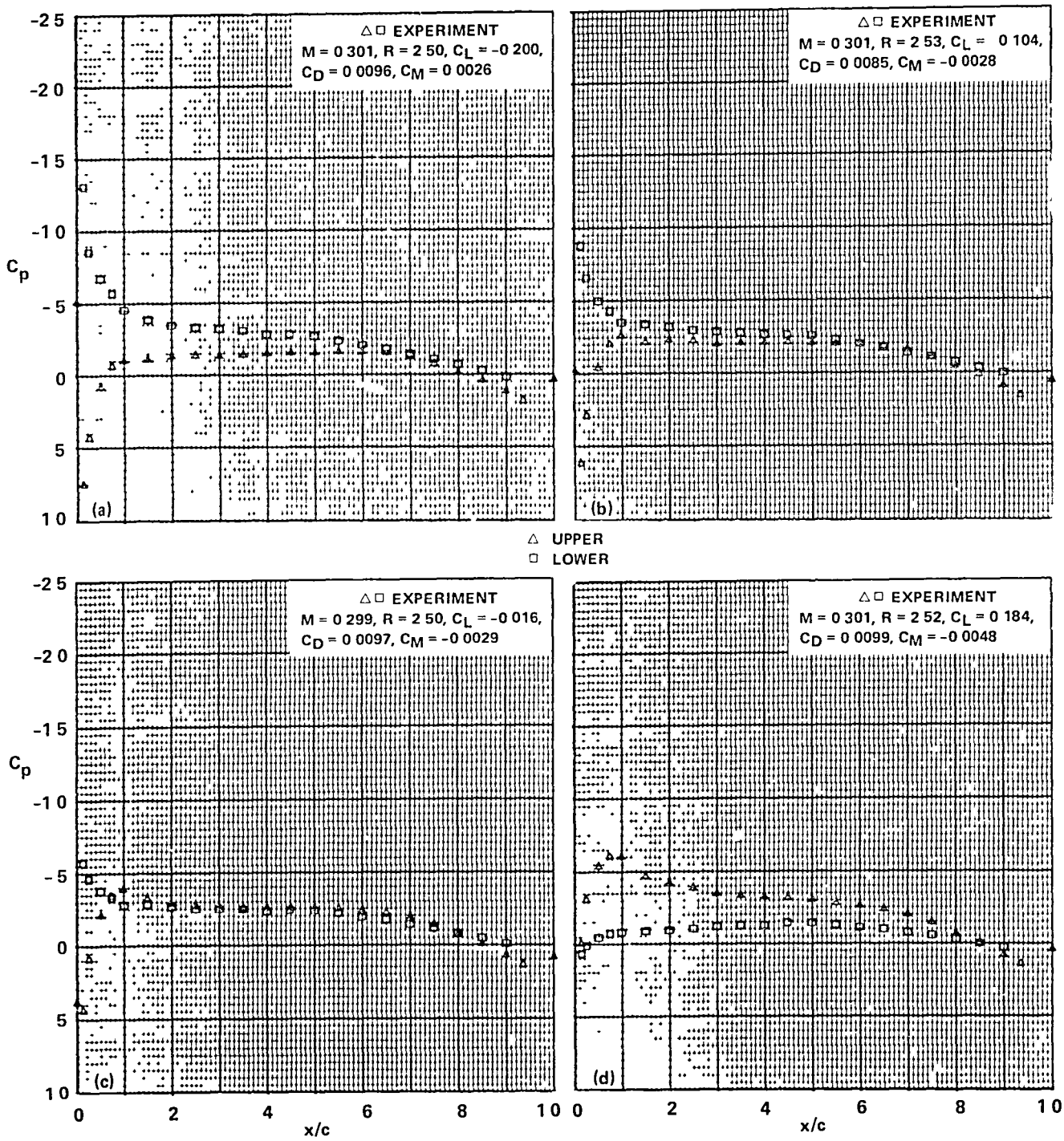

Figure 28.- Pressure distributions of the SSC-A09 airfoil, M_{set} = 0.3.

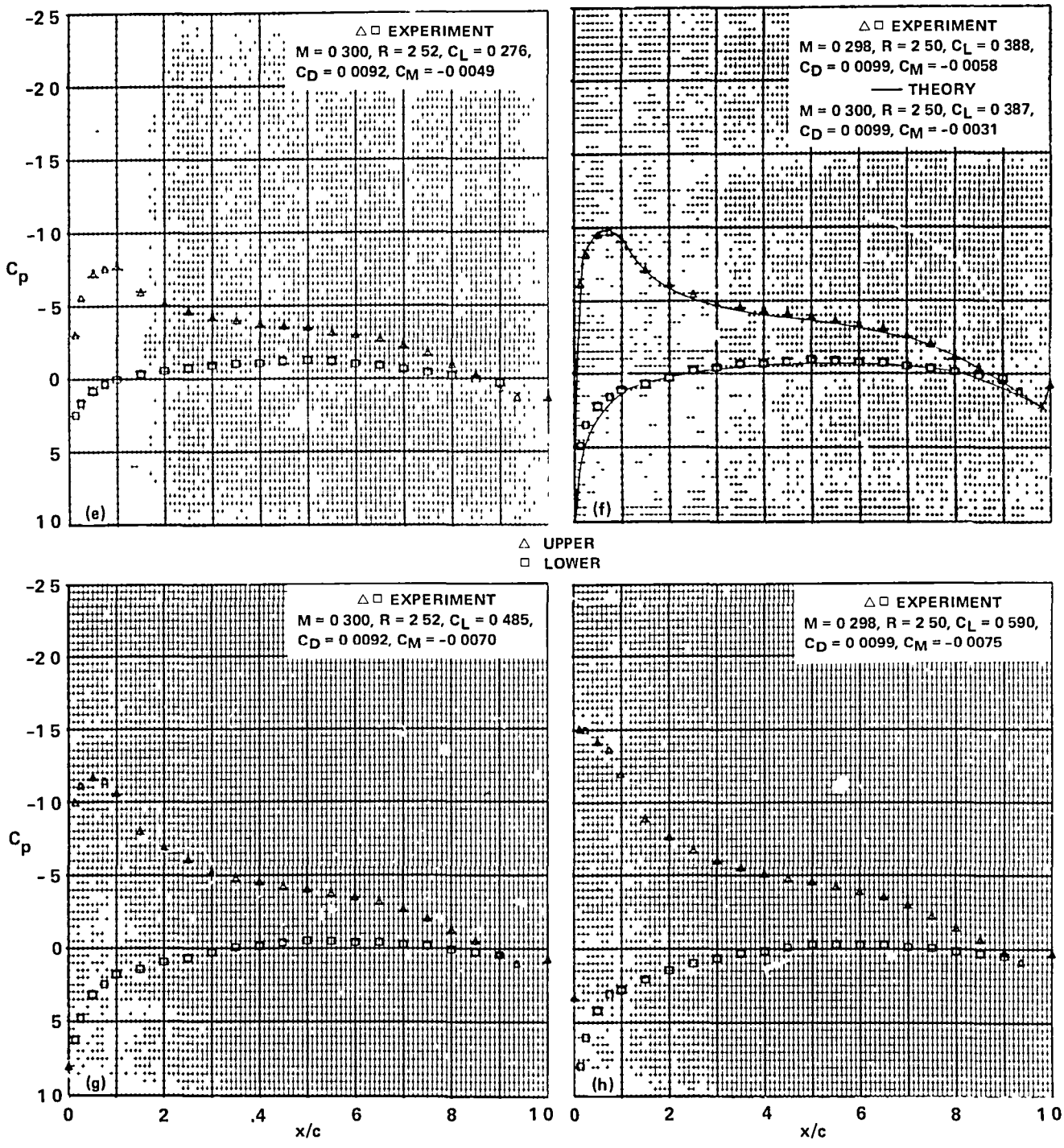

Figure 28.- Continued.

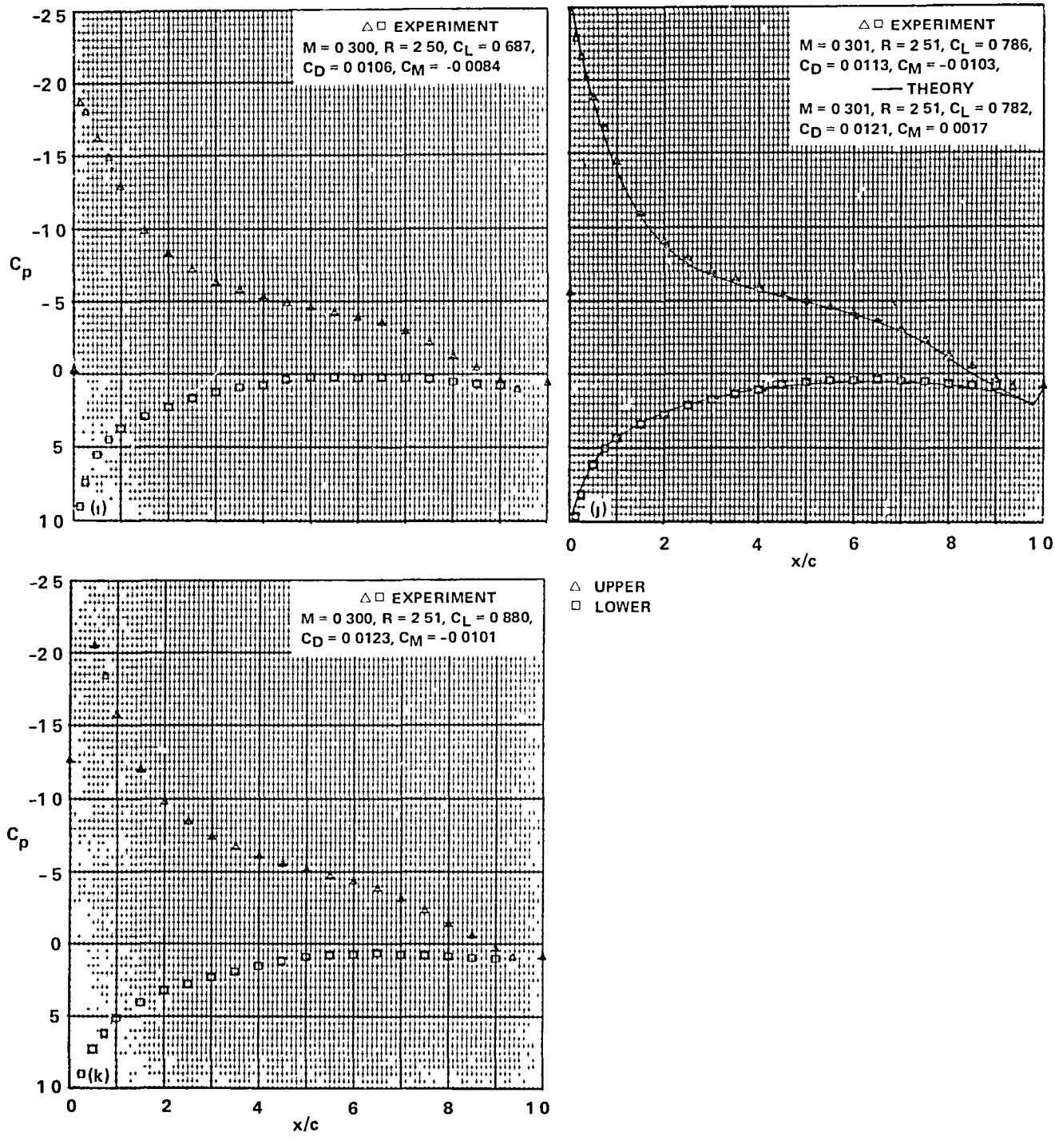

Figure 28.- Concluded.

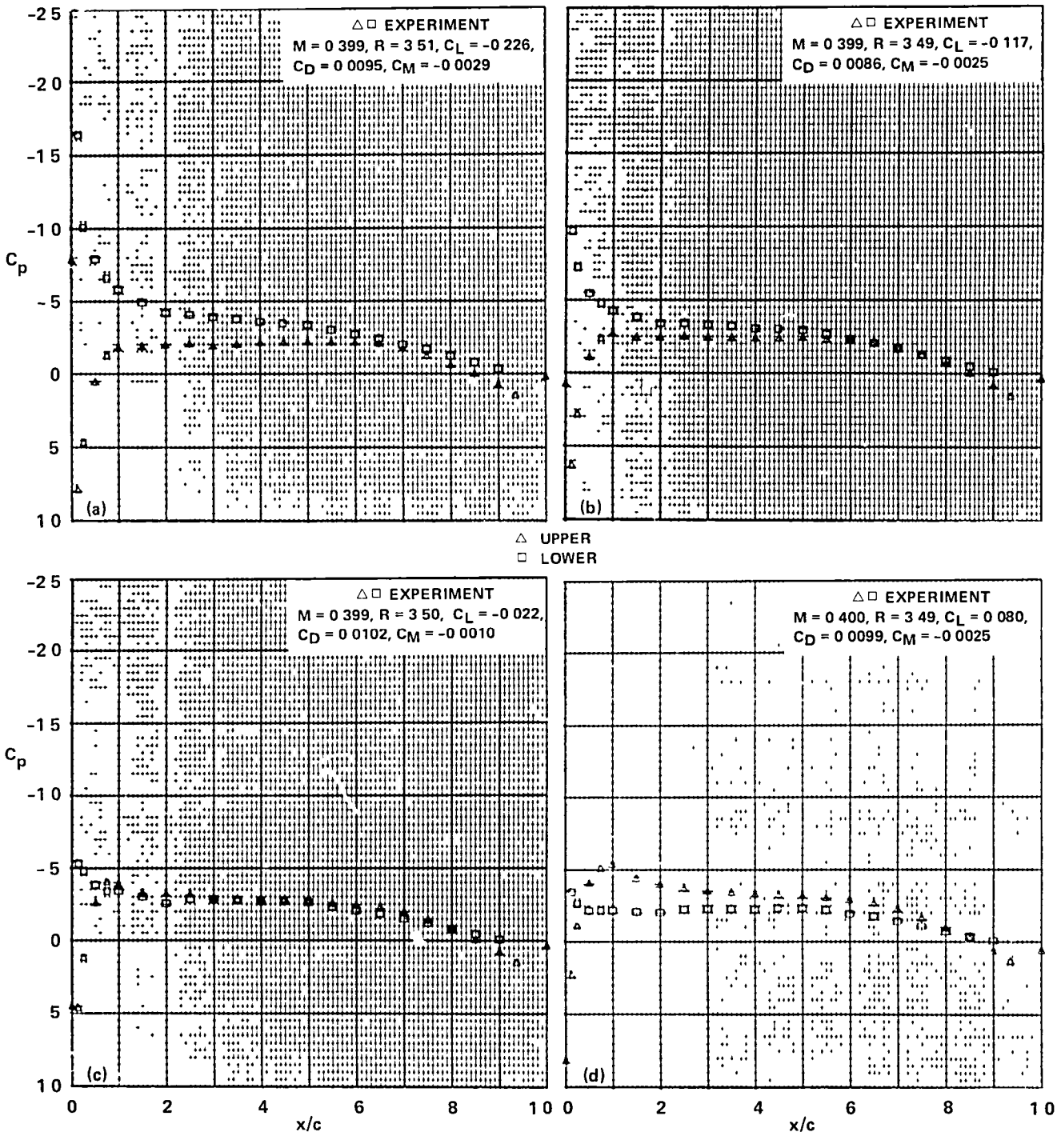

Figure 29.- Pressure distributions of the SSC-A09 airfoil, M_{set} = 0.4.

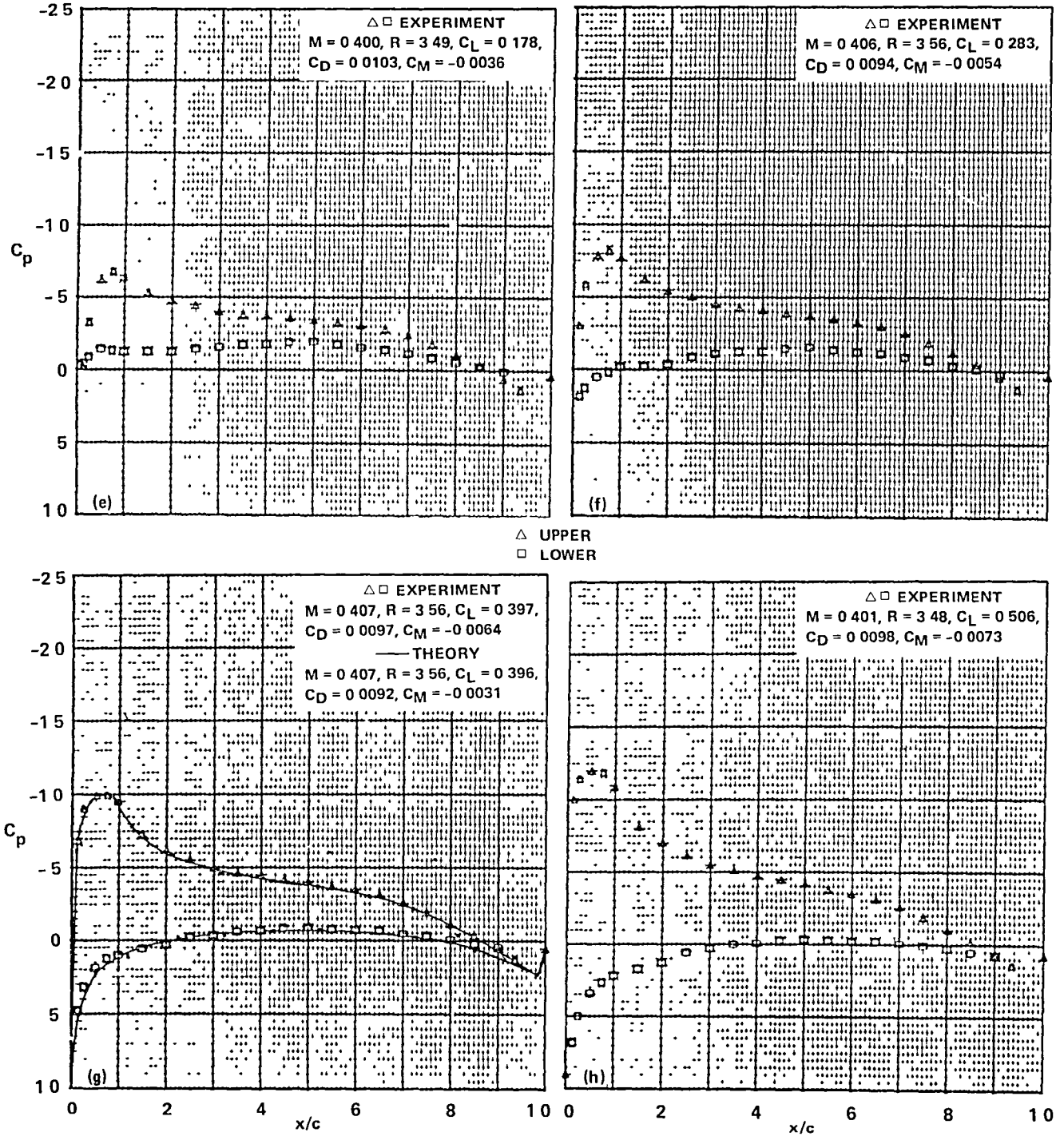

Figure 29.- Continued.

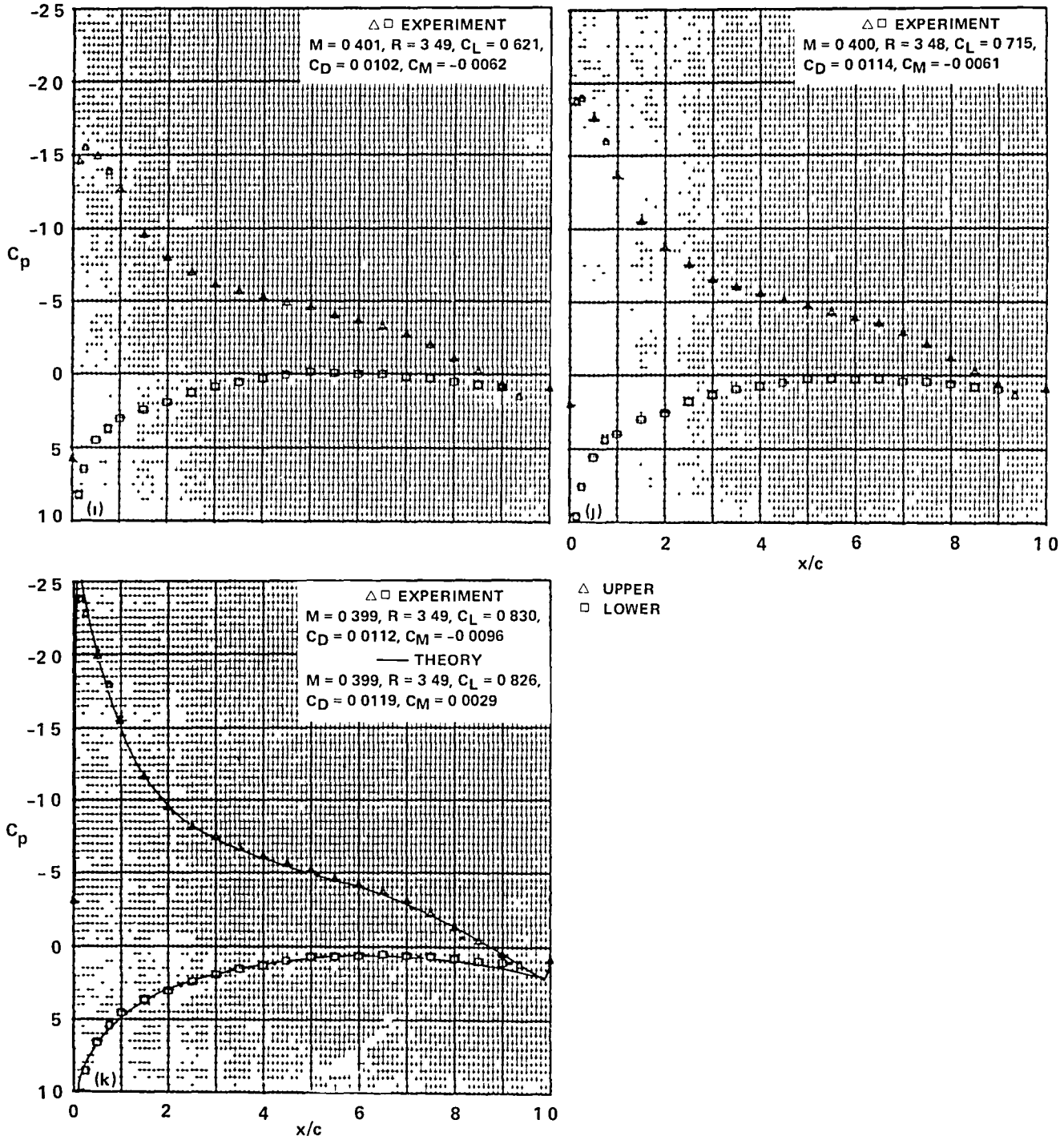

Figure 29.- Concluded.

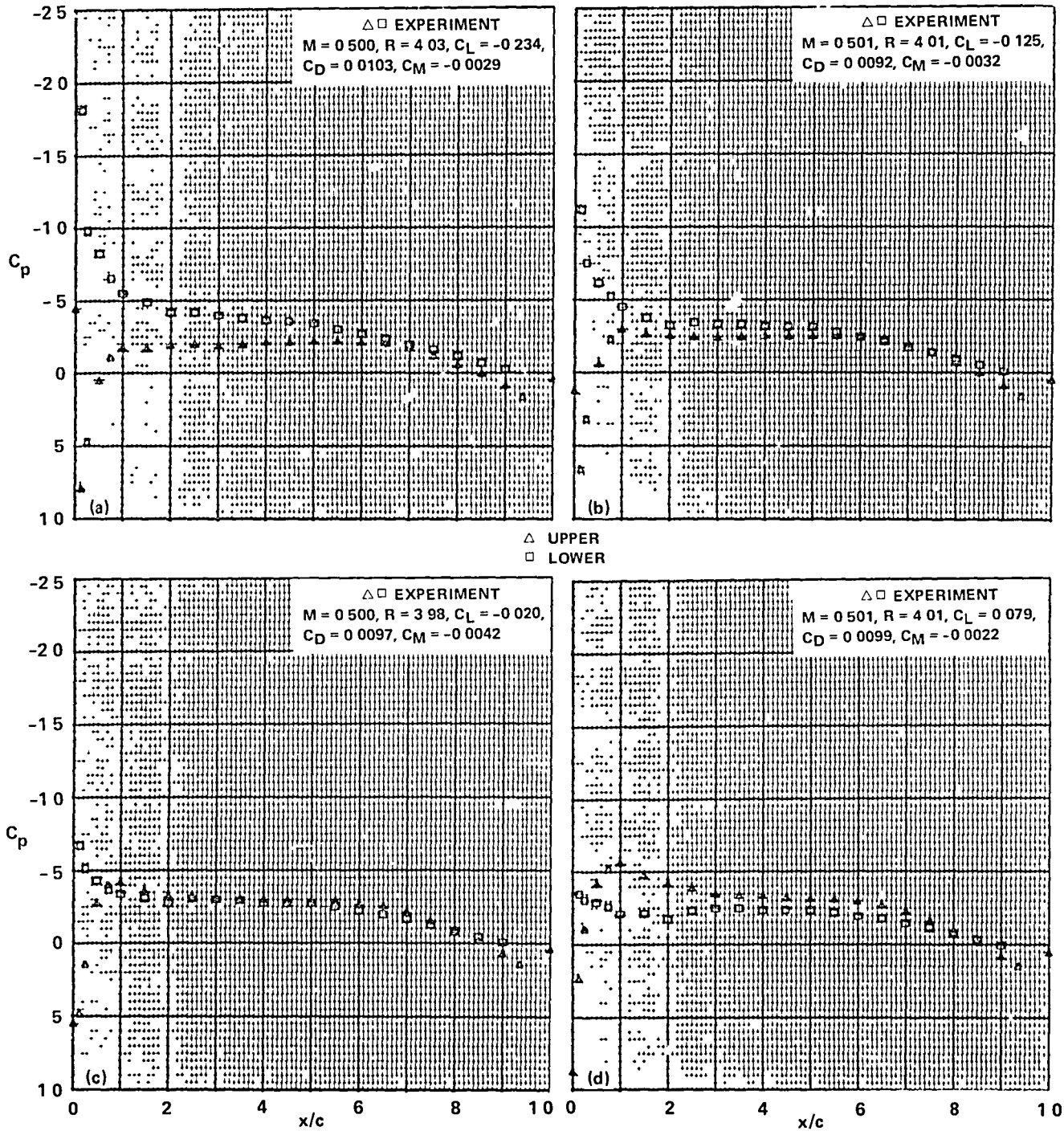

Figure 30.- Pressure distributions of the SSC-A09 airfoil, M_{set} = 0.5.

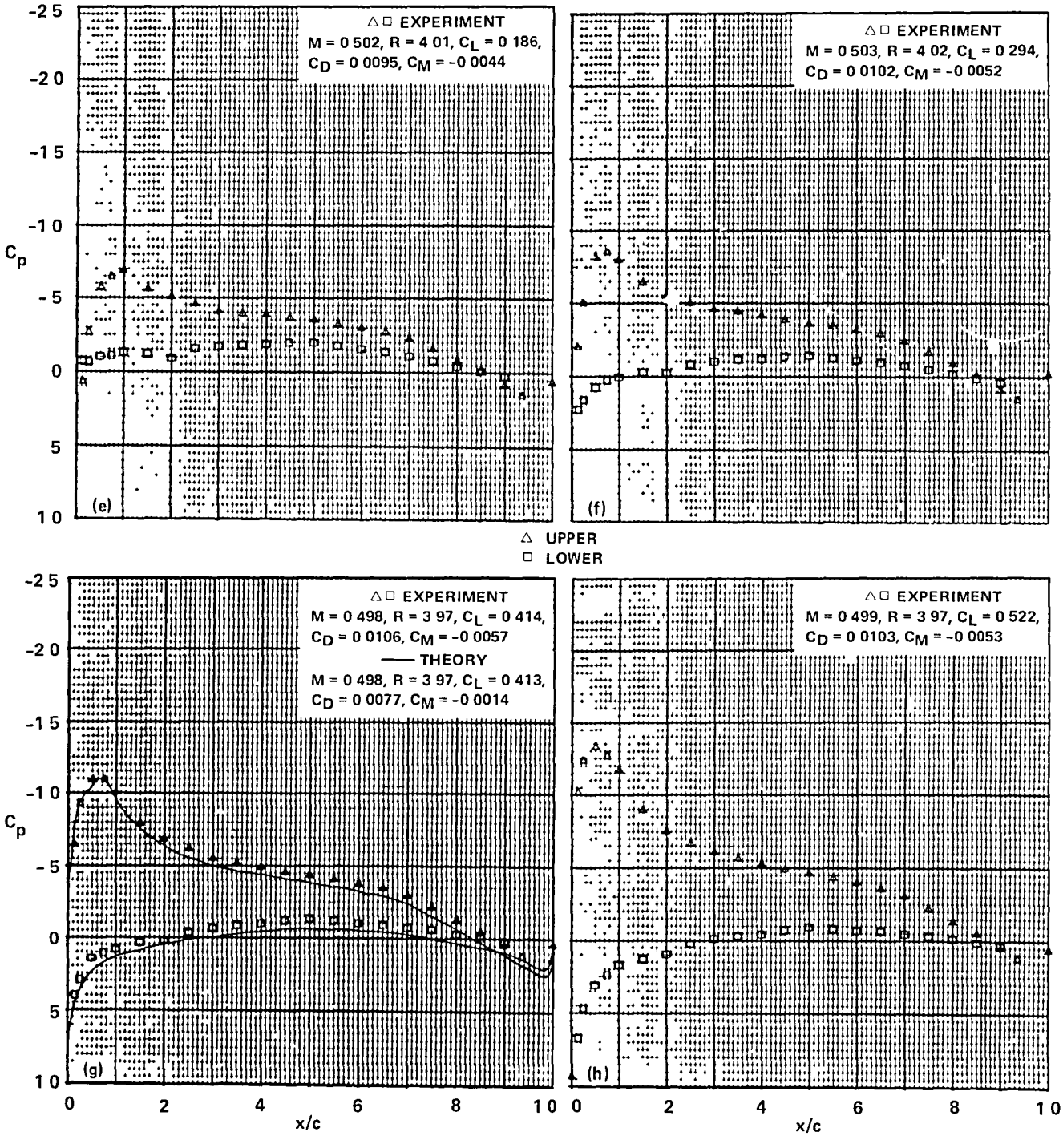

Figure 30.- Continued.

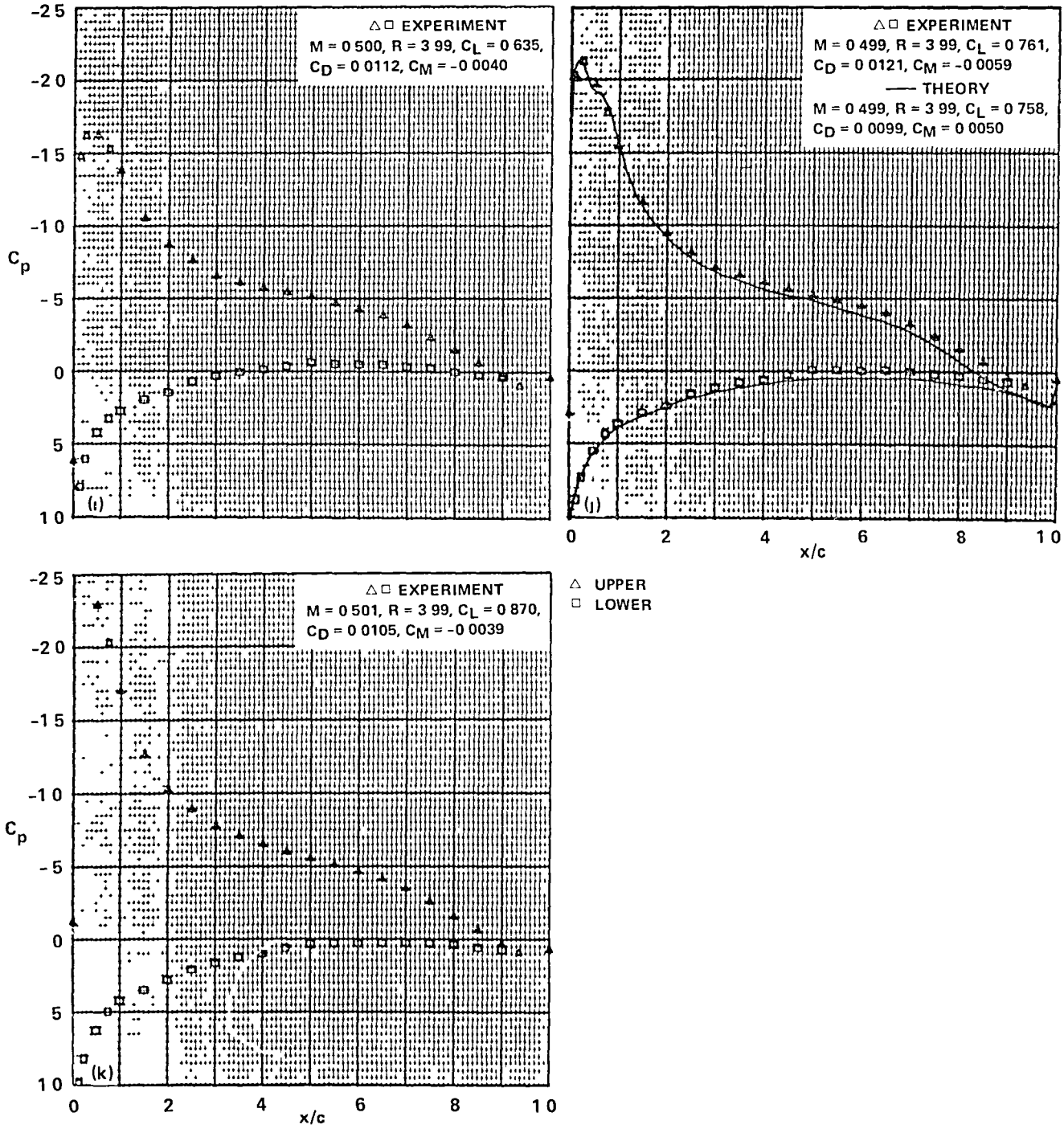

Figure 30.- Concluded.

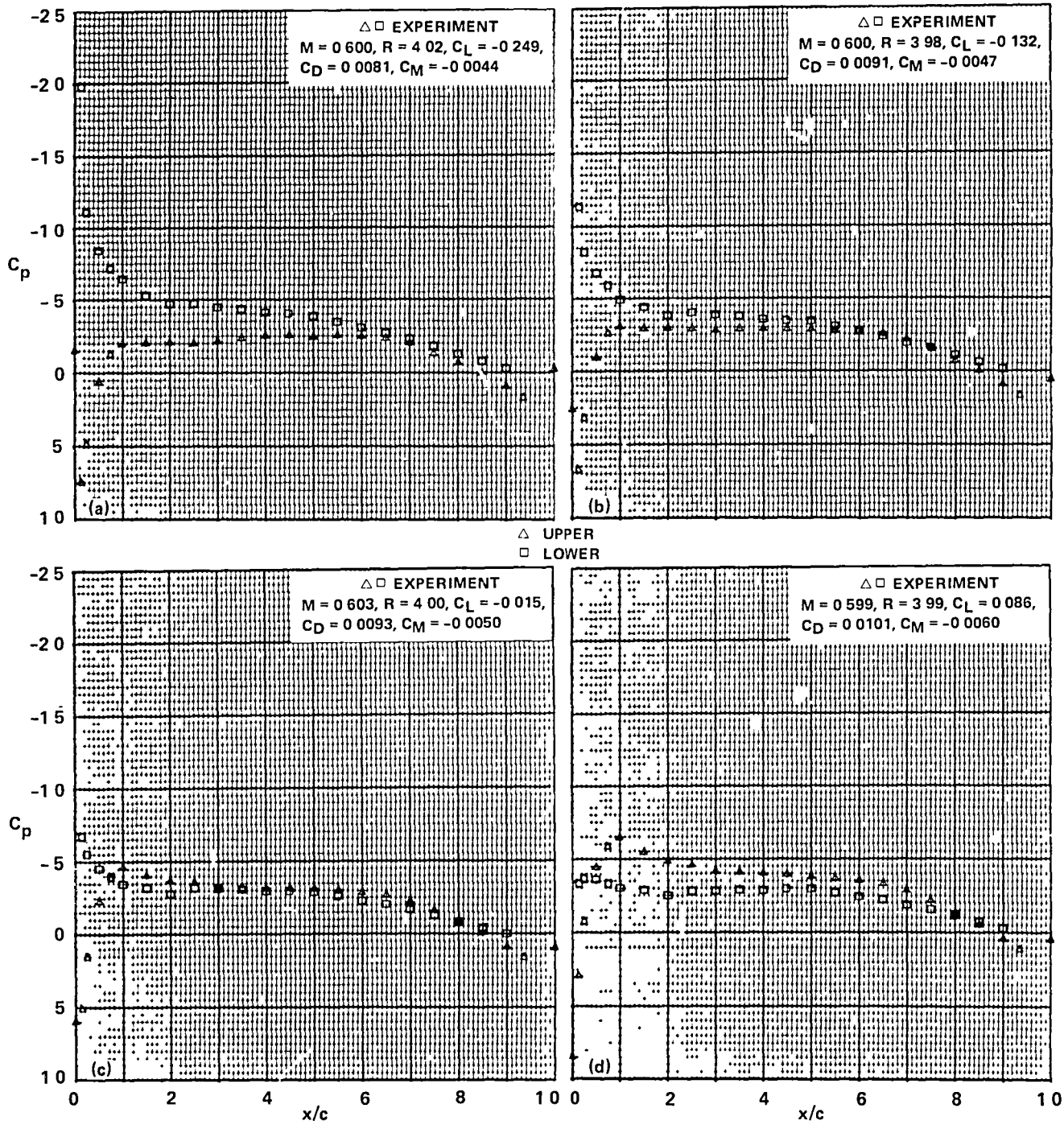

Figure 31.- Pressure distributions of the SSC-A09 airfoil, M_{set} = 0.6.

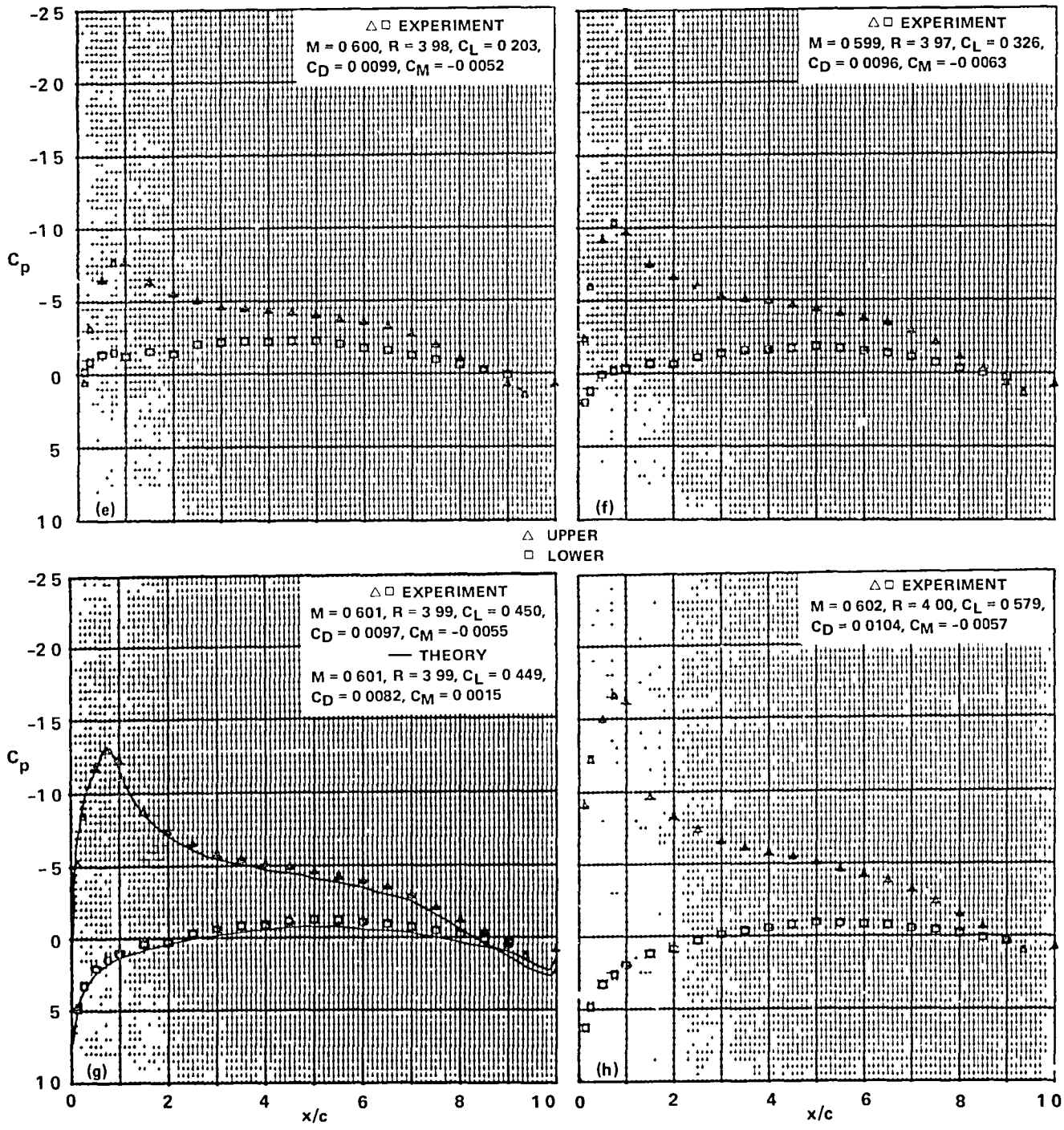

Figure 31.- Continued.

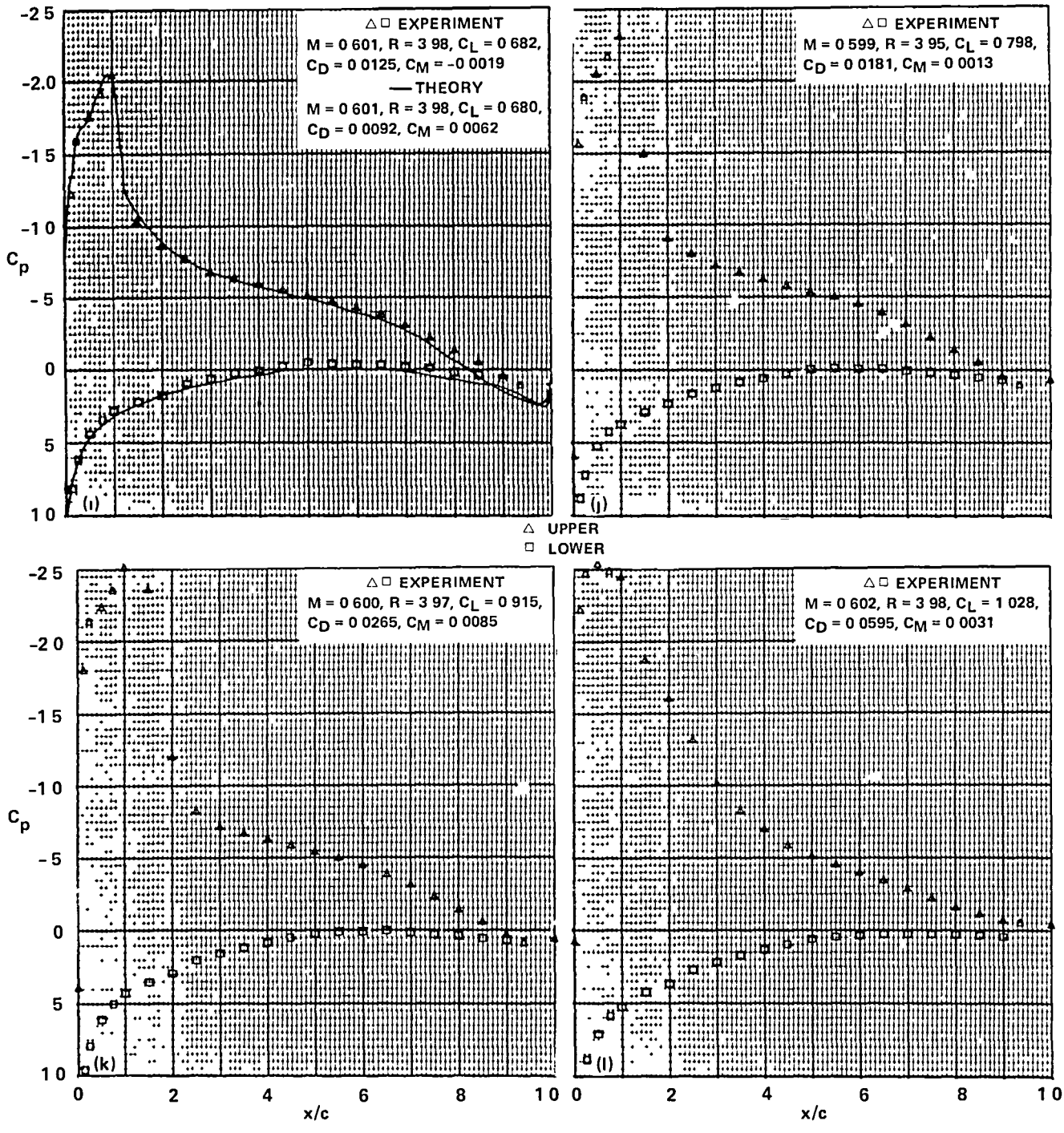

Figure 31.- Continued.

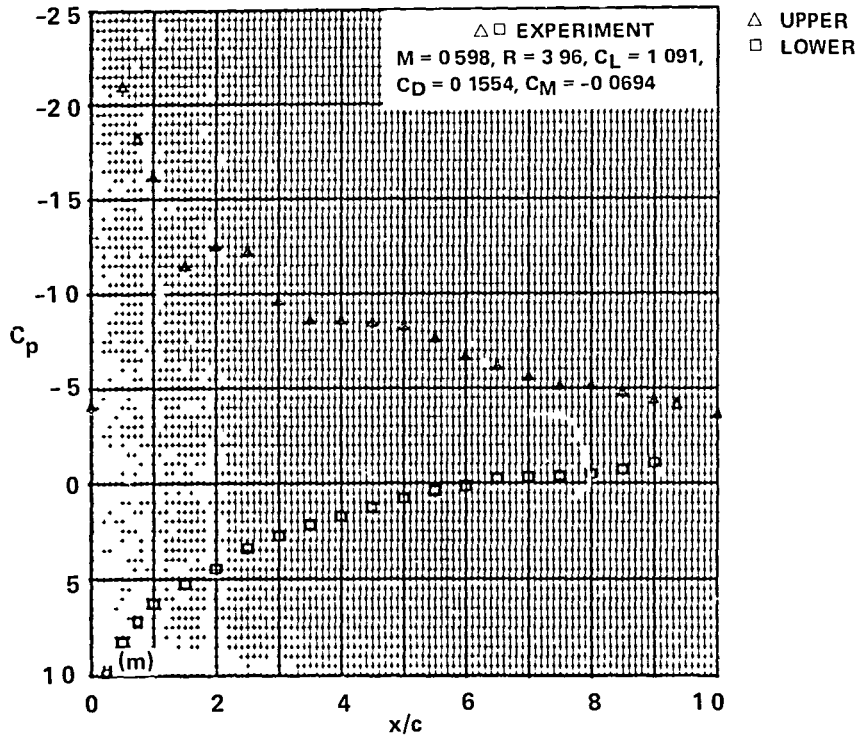

Figure 31.- Concluded.

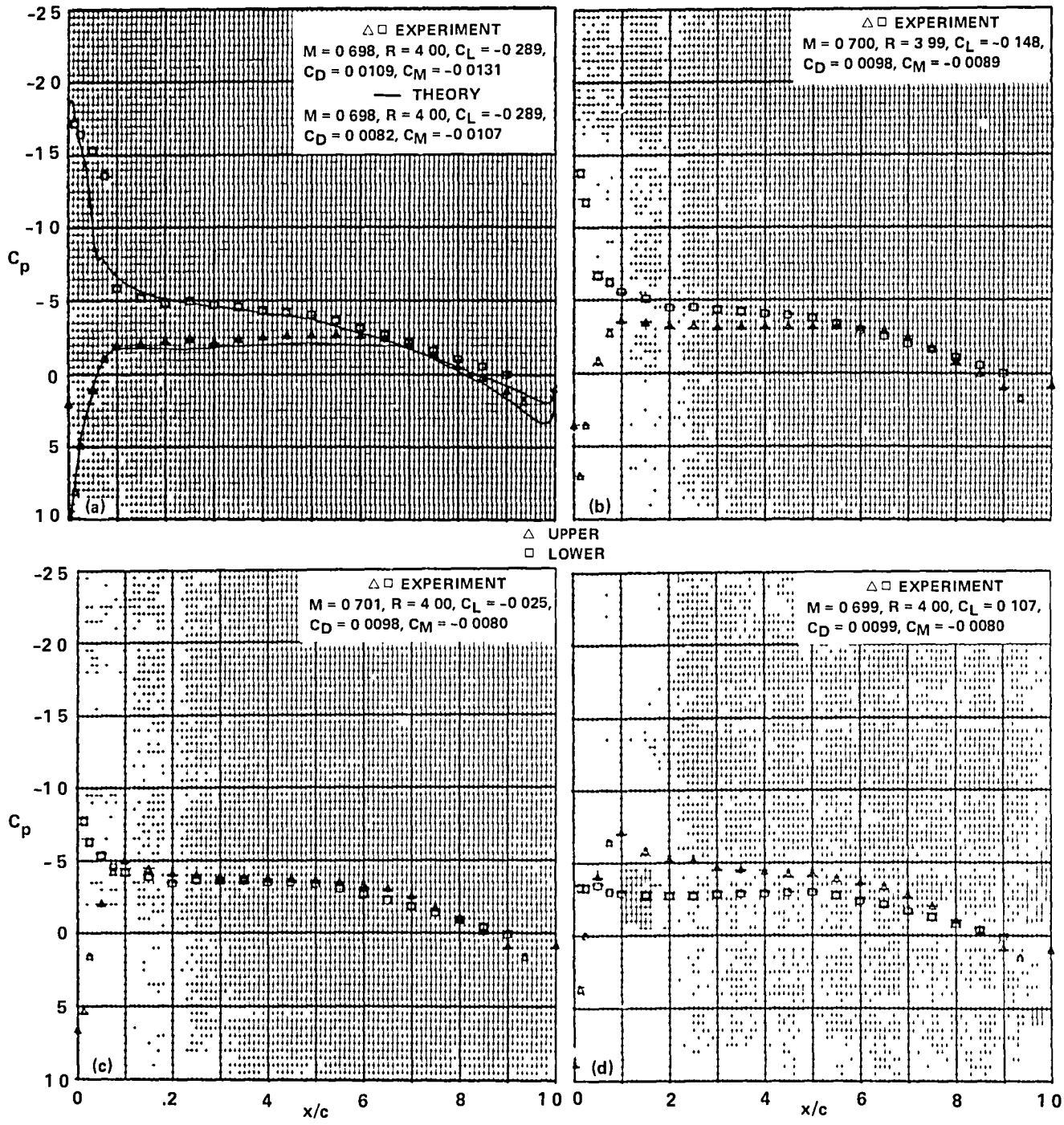

Figure 32.- Pressure distributions of the SSC-A09 airfoil, M_{set} = 0.70.

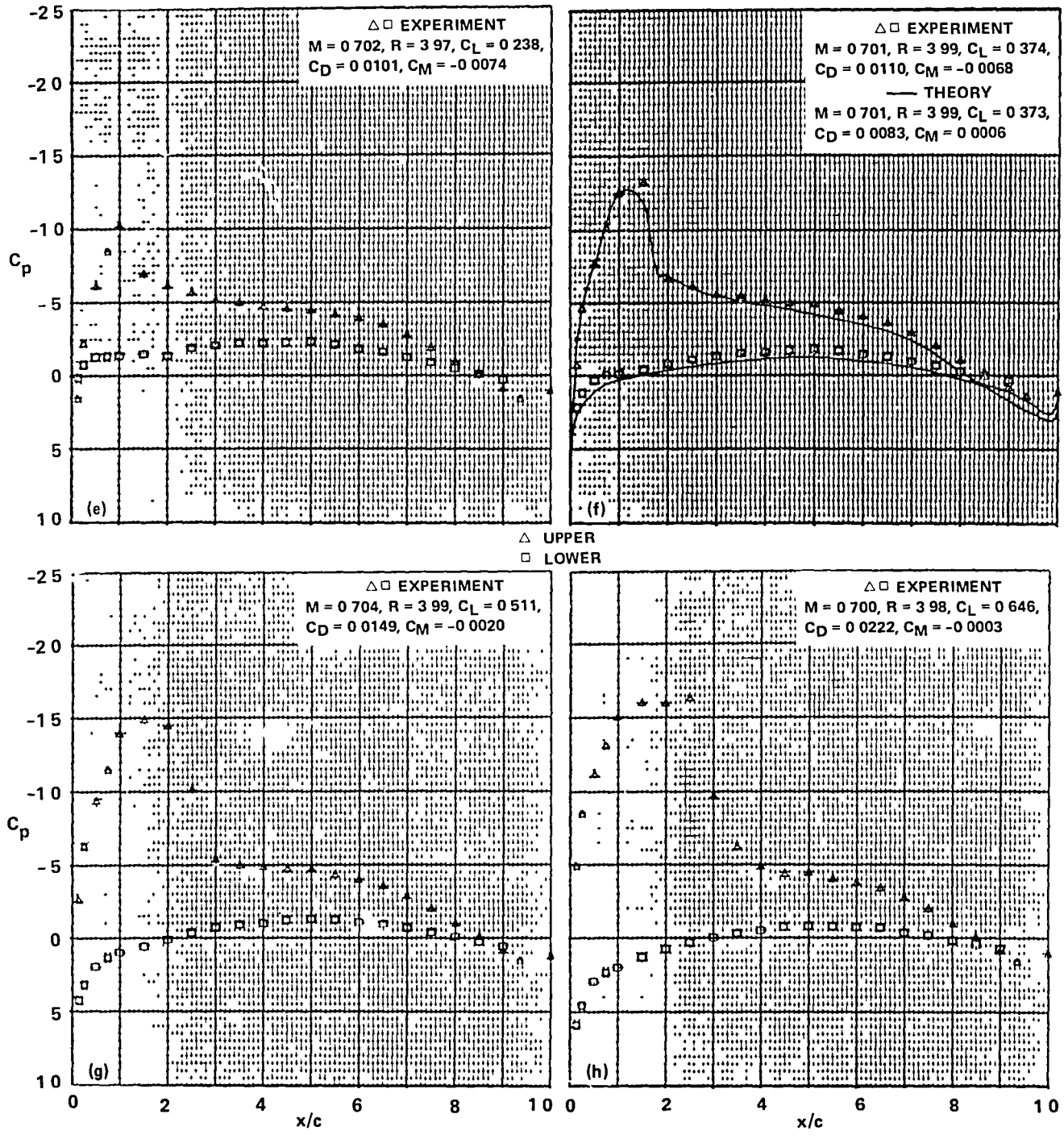

Figure 32.- Continued.

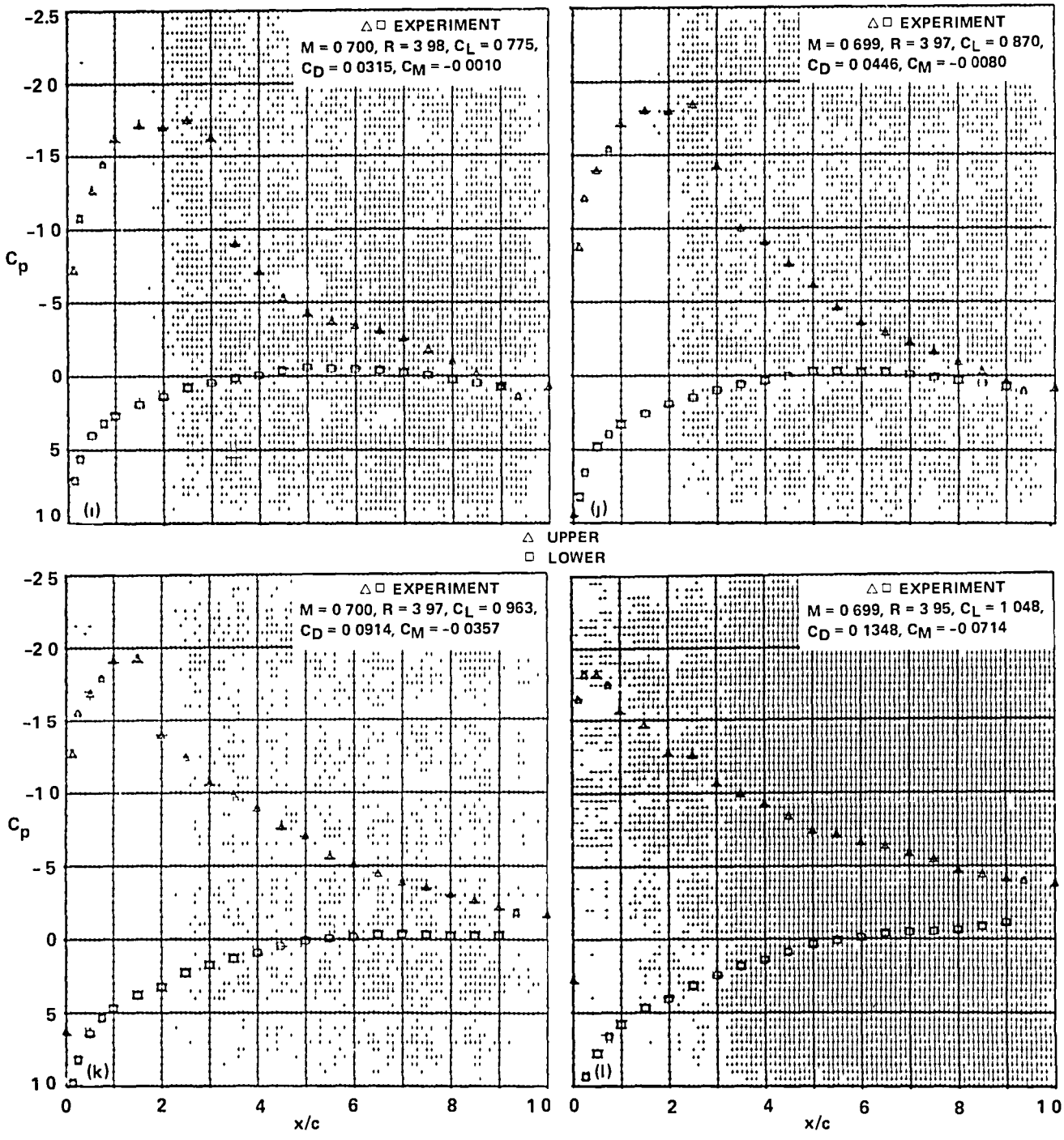

Figure 32.- Concluded.

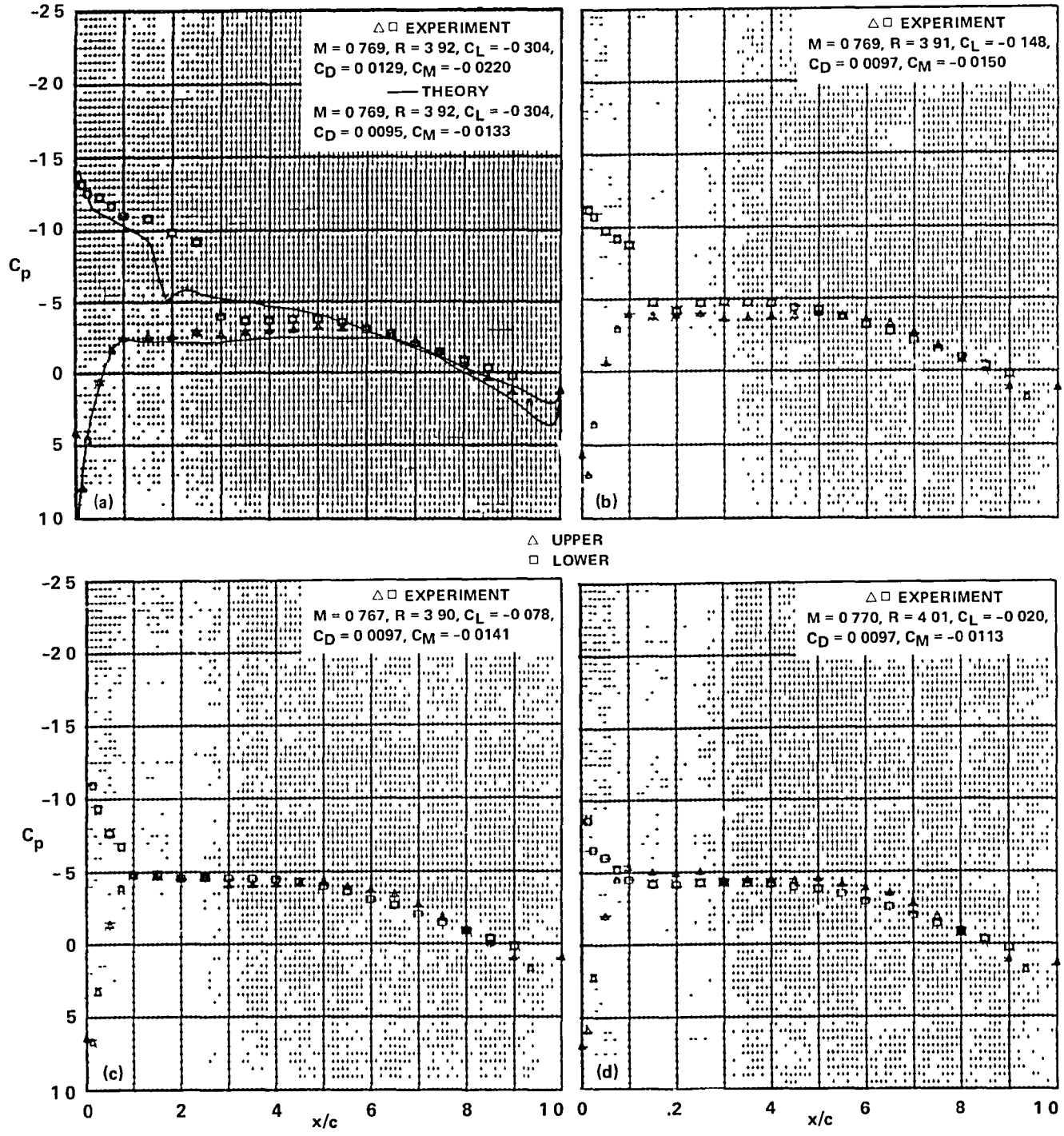

Figure 33.- Pressure distributions of the SSC-A09 airfoil, M_{set} = 0.77.

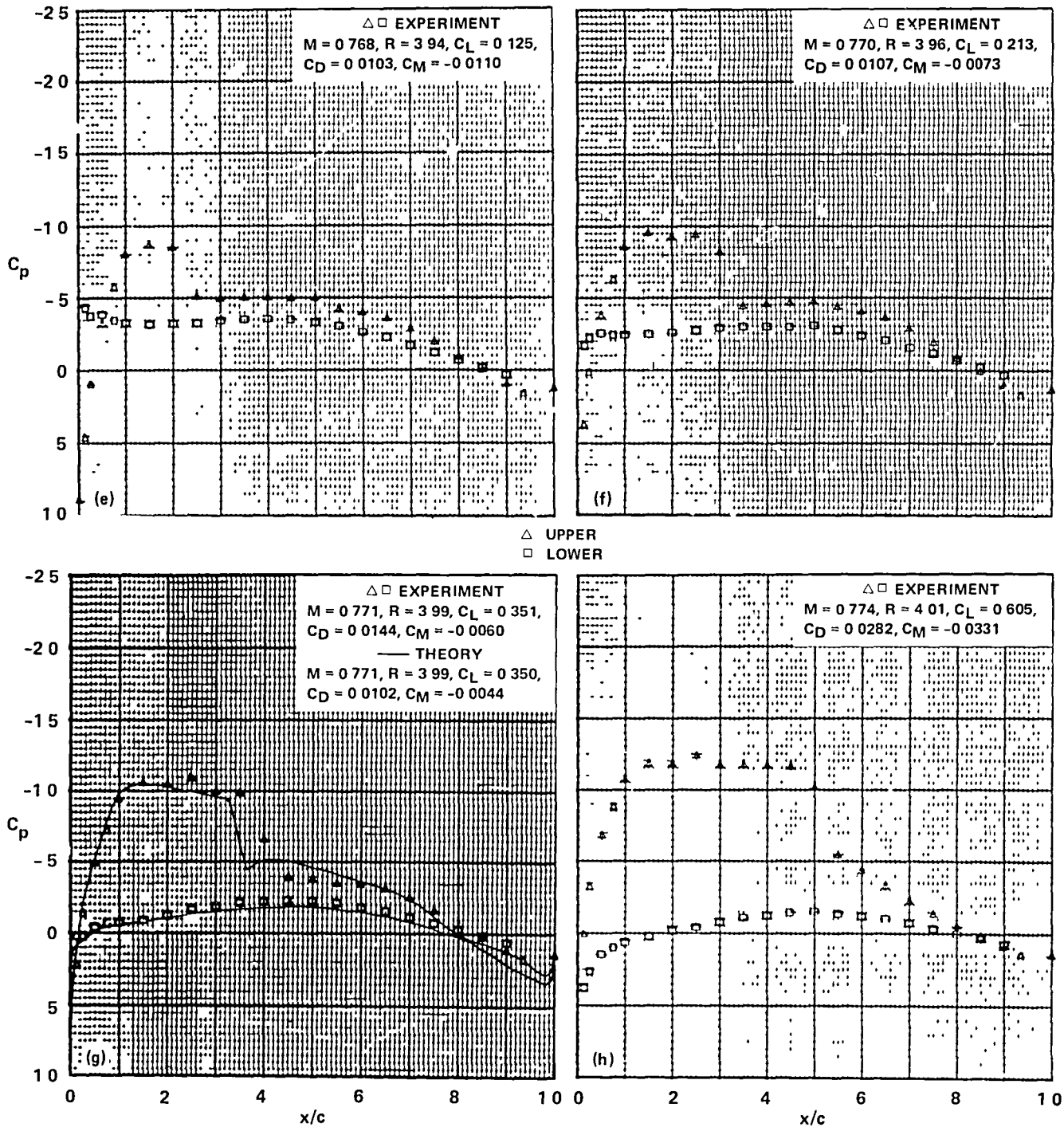

Figure 33.- Continued.

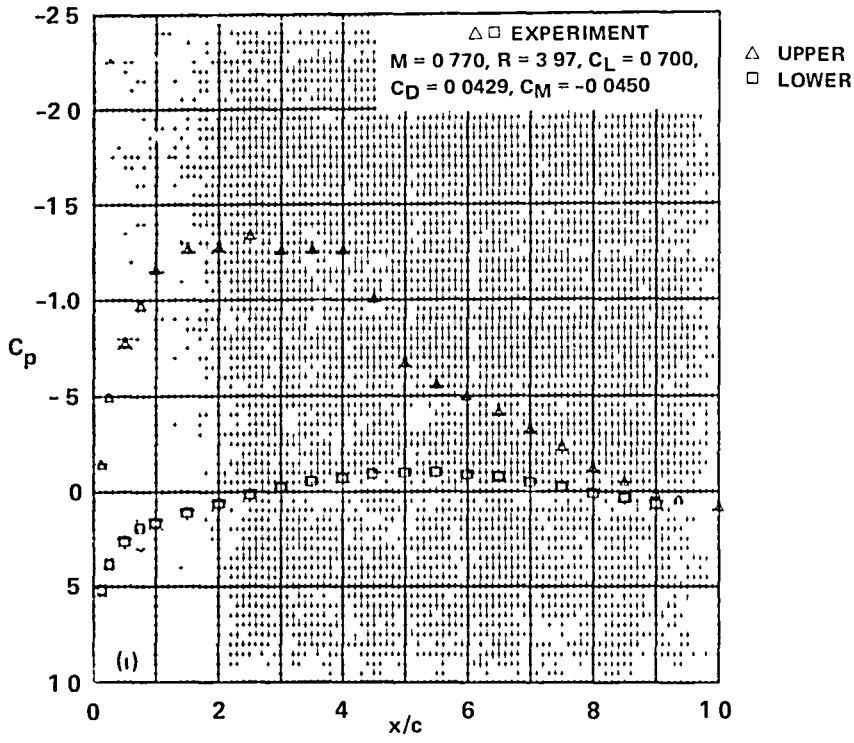

Figure 33.- Concluded.

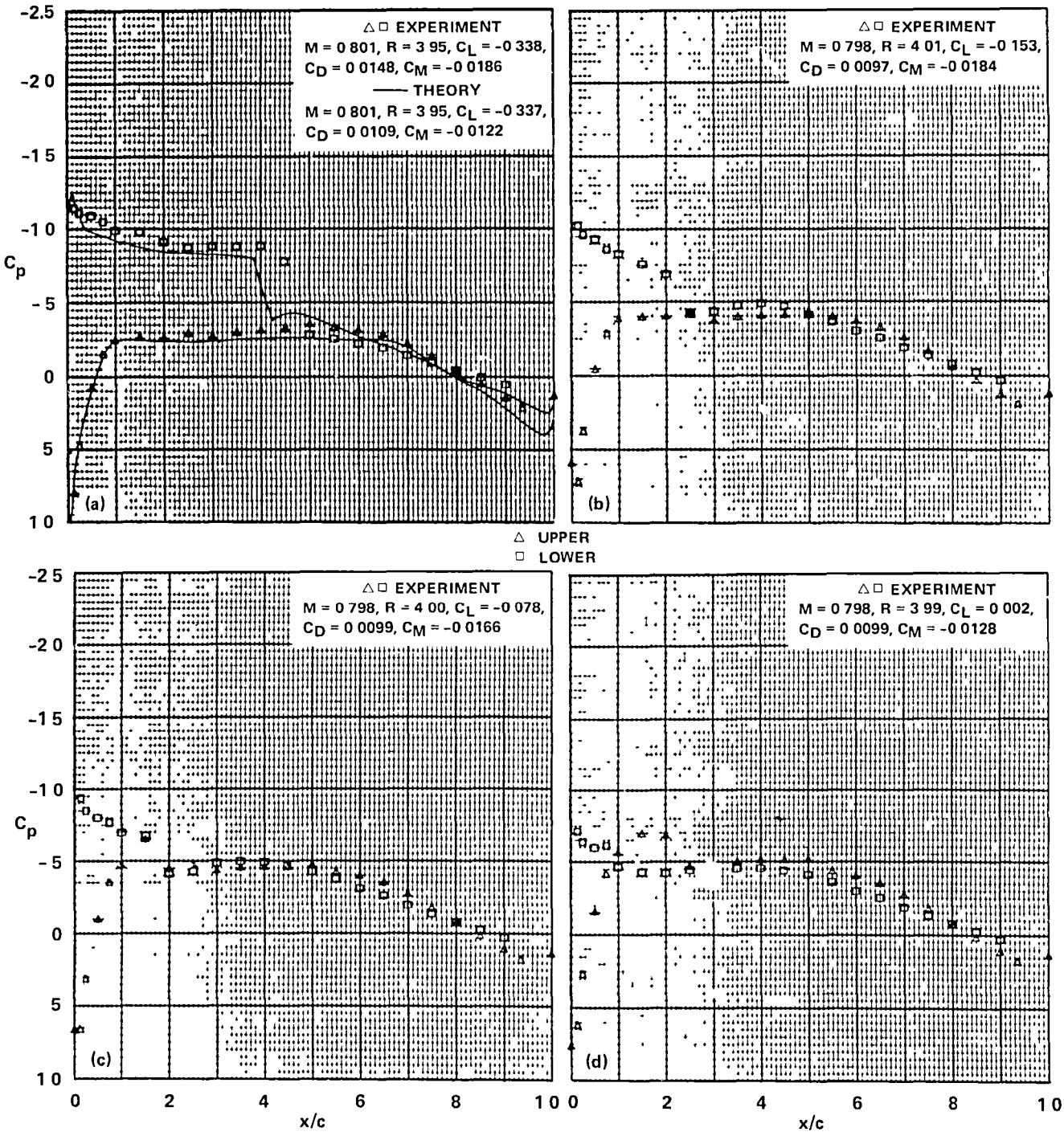

Figure 34.- Pressure distributions of the SSC-A09 airfoil, M_{set} = 0.80.

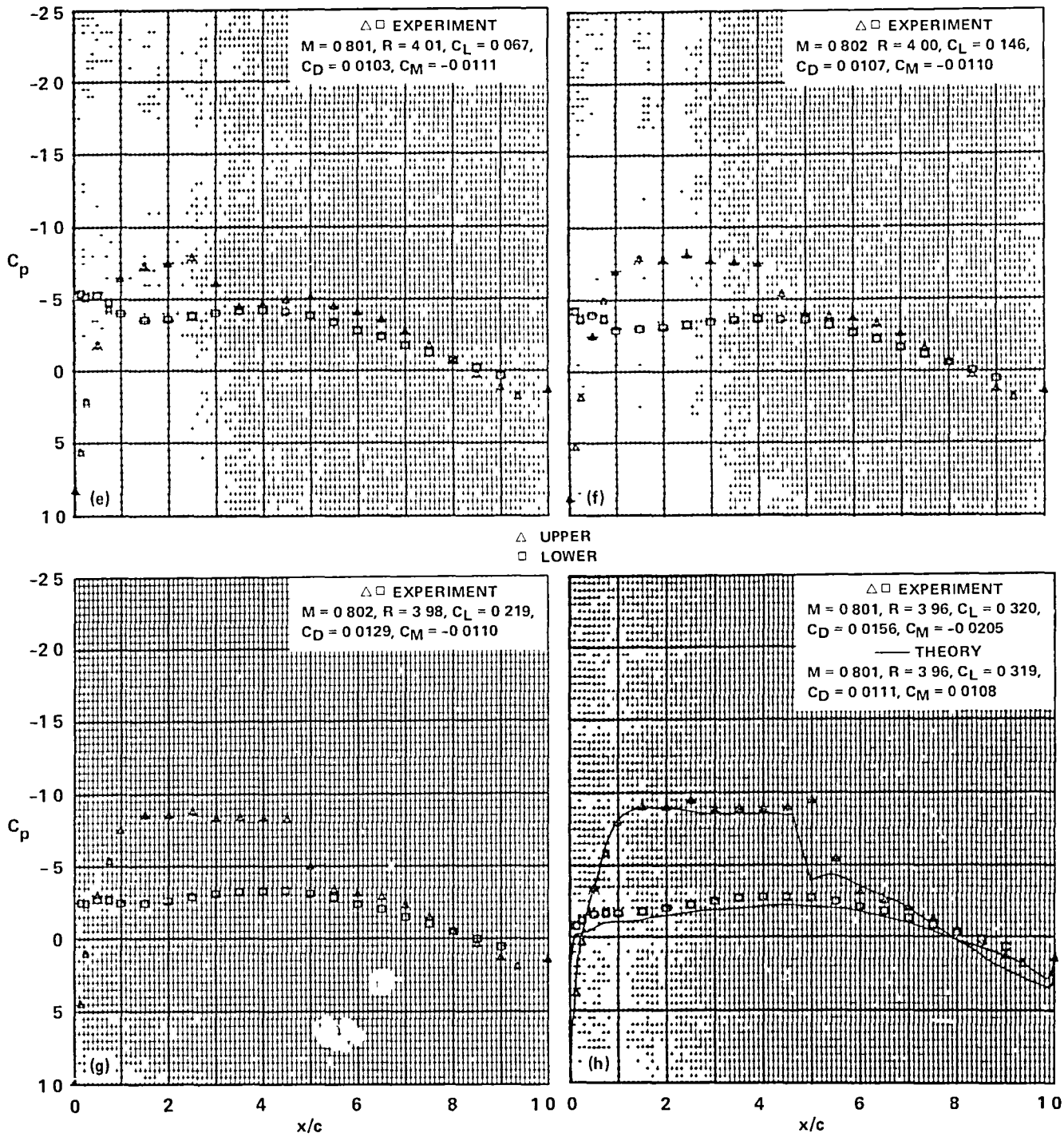

Figure 34.- Continued.

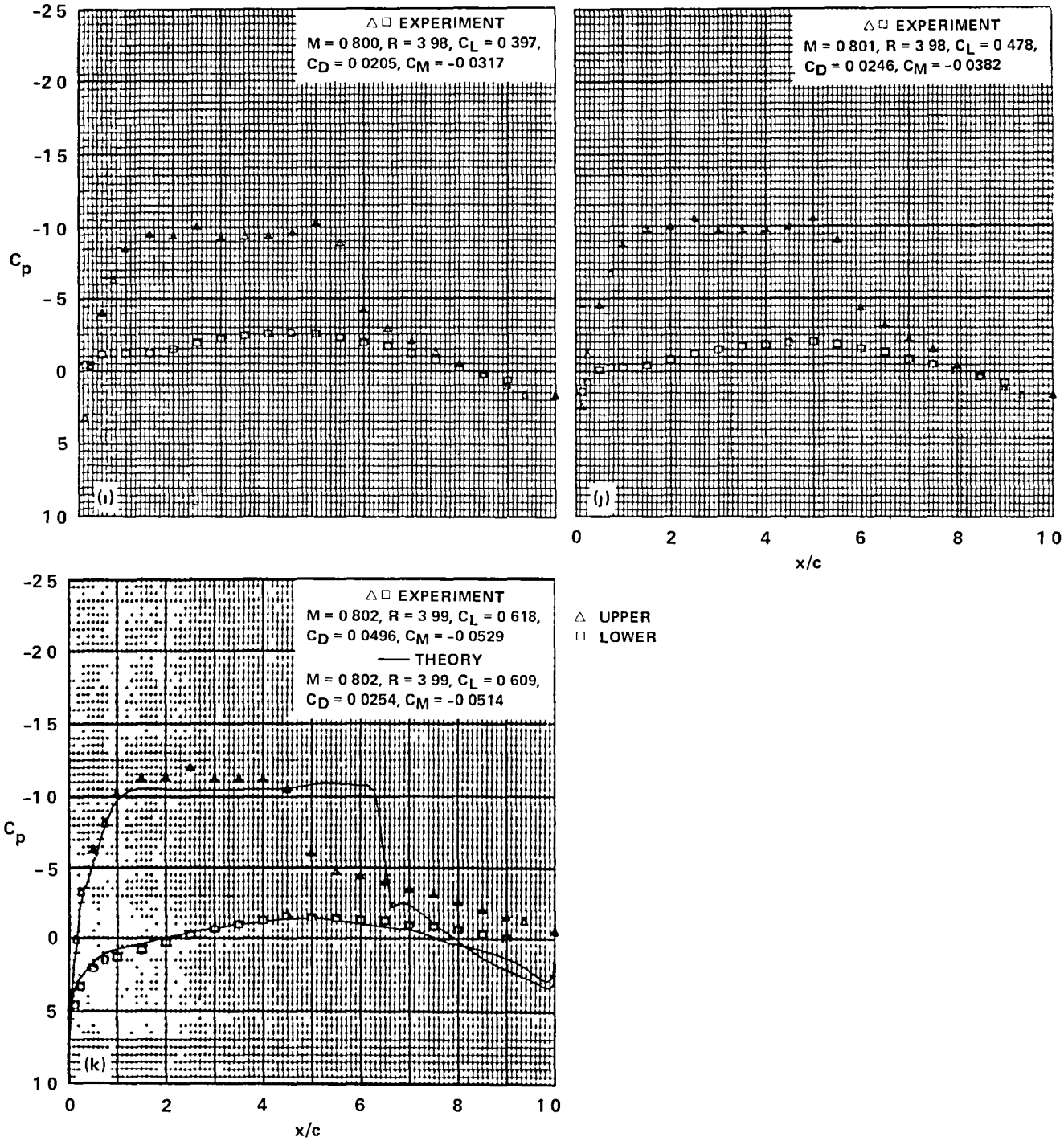

Figure 34.- Concluded.

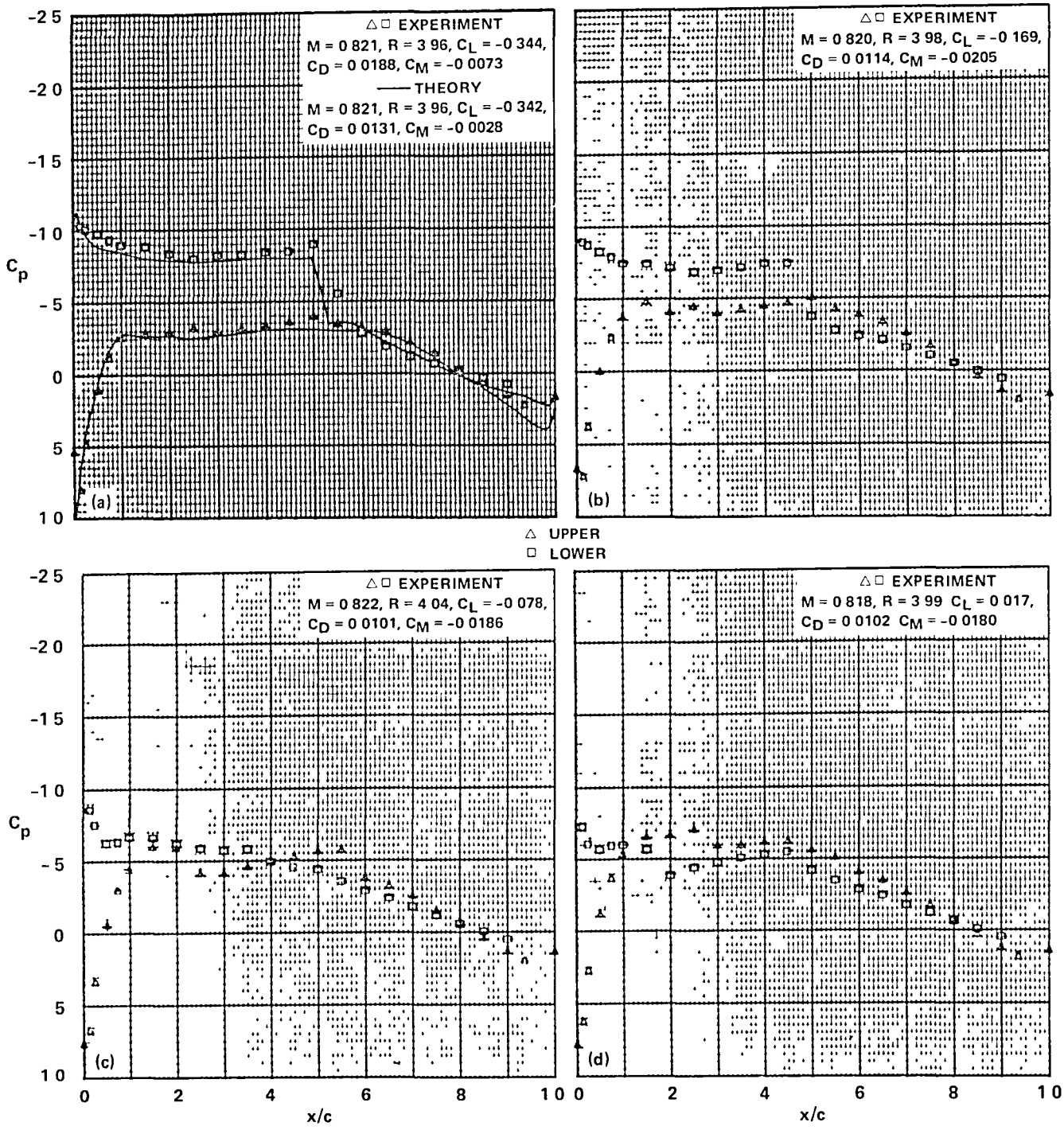

Figure 35.- Pressure distributions of the SSC-A09 airfoil, M_{set} = 0.82.

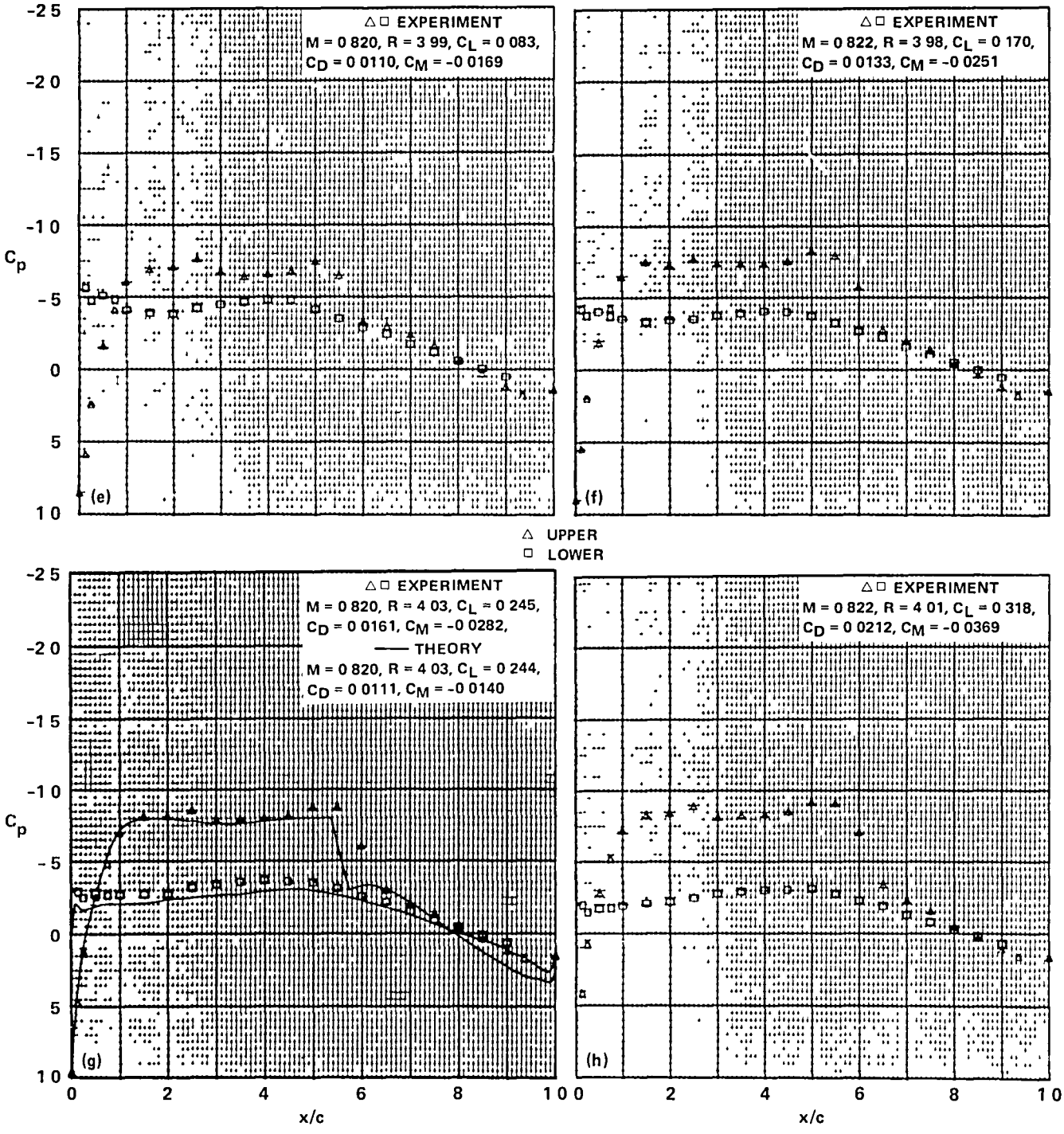

Figure 35.- Continued.

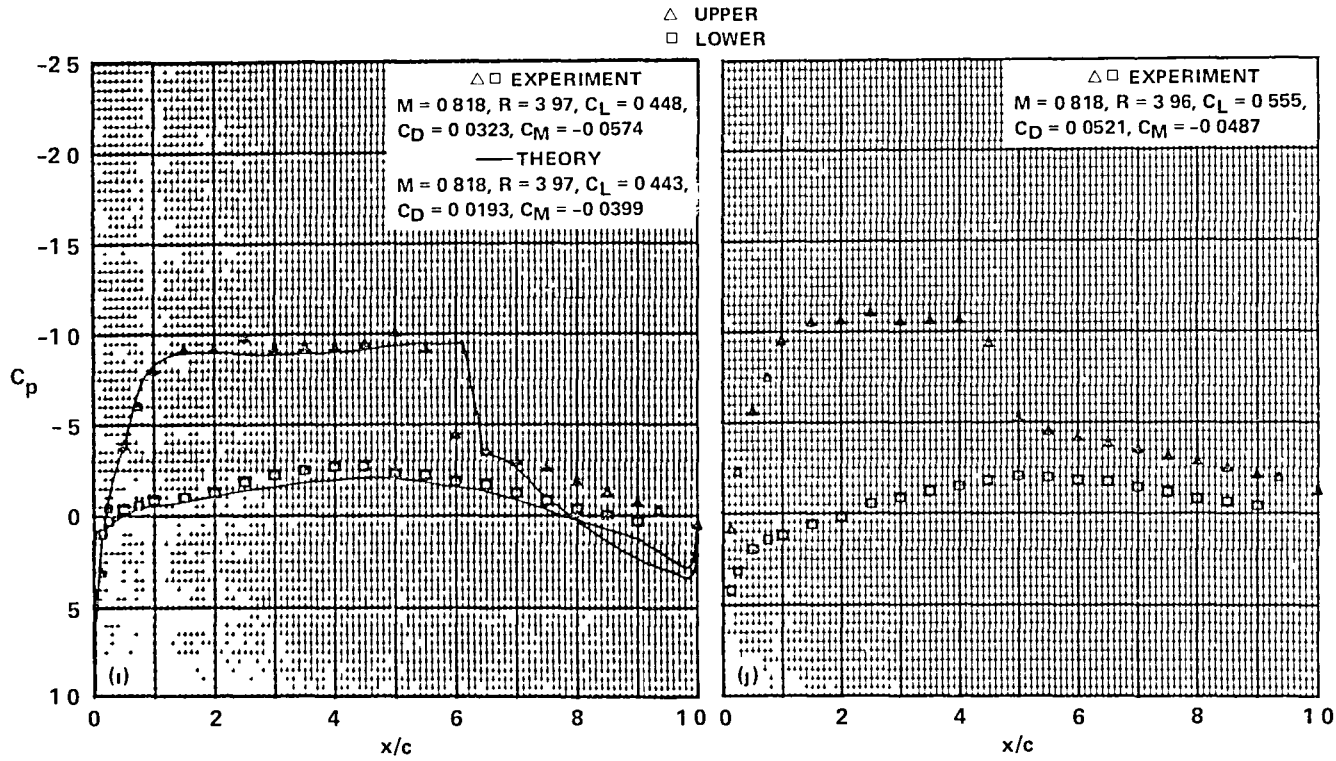

Figure 35.- Concluded.

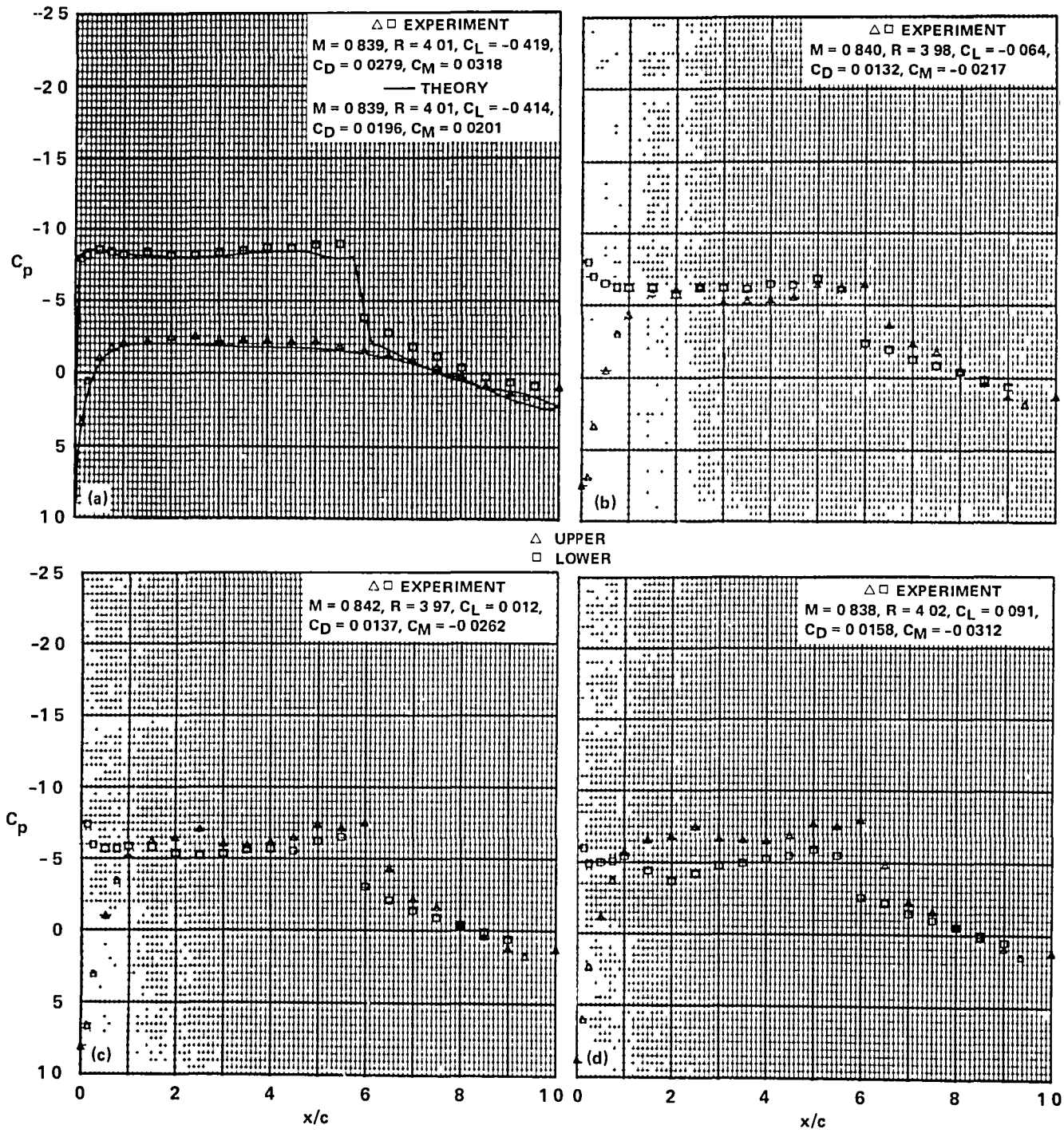

Figure 36.- Pressure distributions of the SSC-A09 airfoil, M_{set} = 0.84.

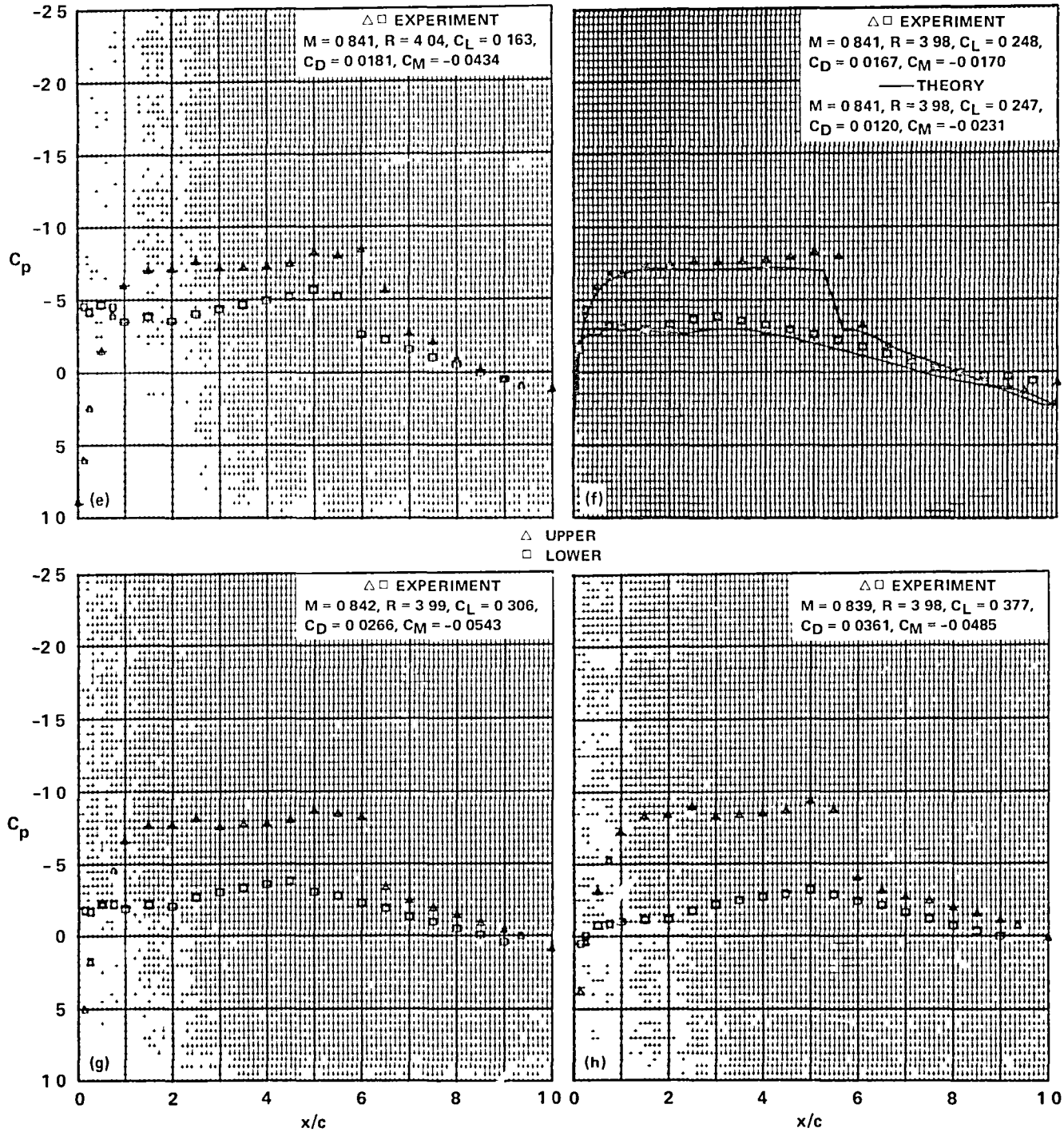

Figure 36.- Continued.

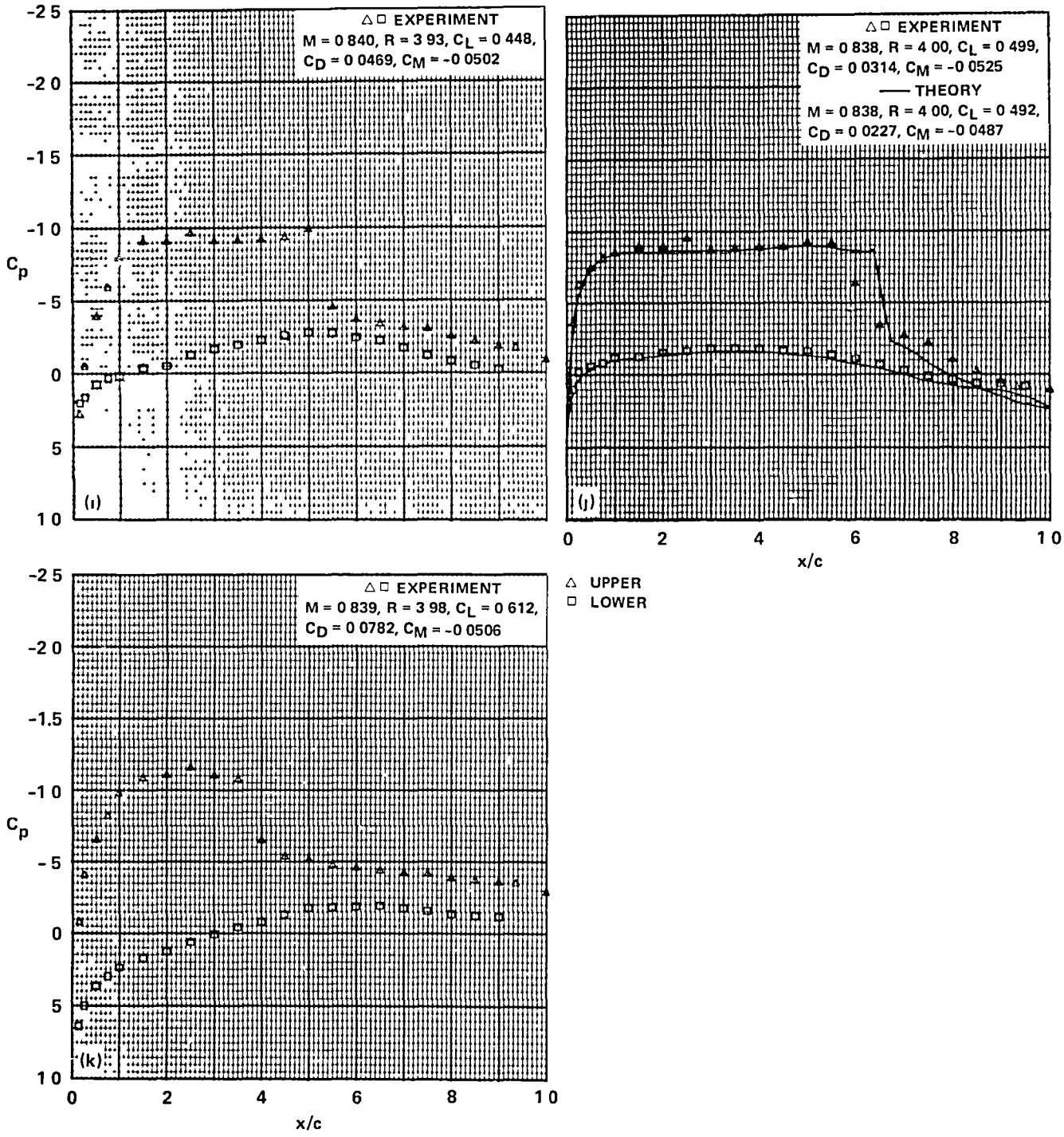

Figure 36.- Concluded.

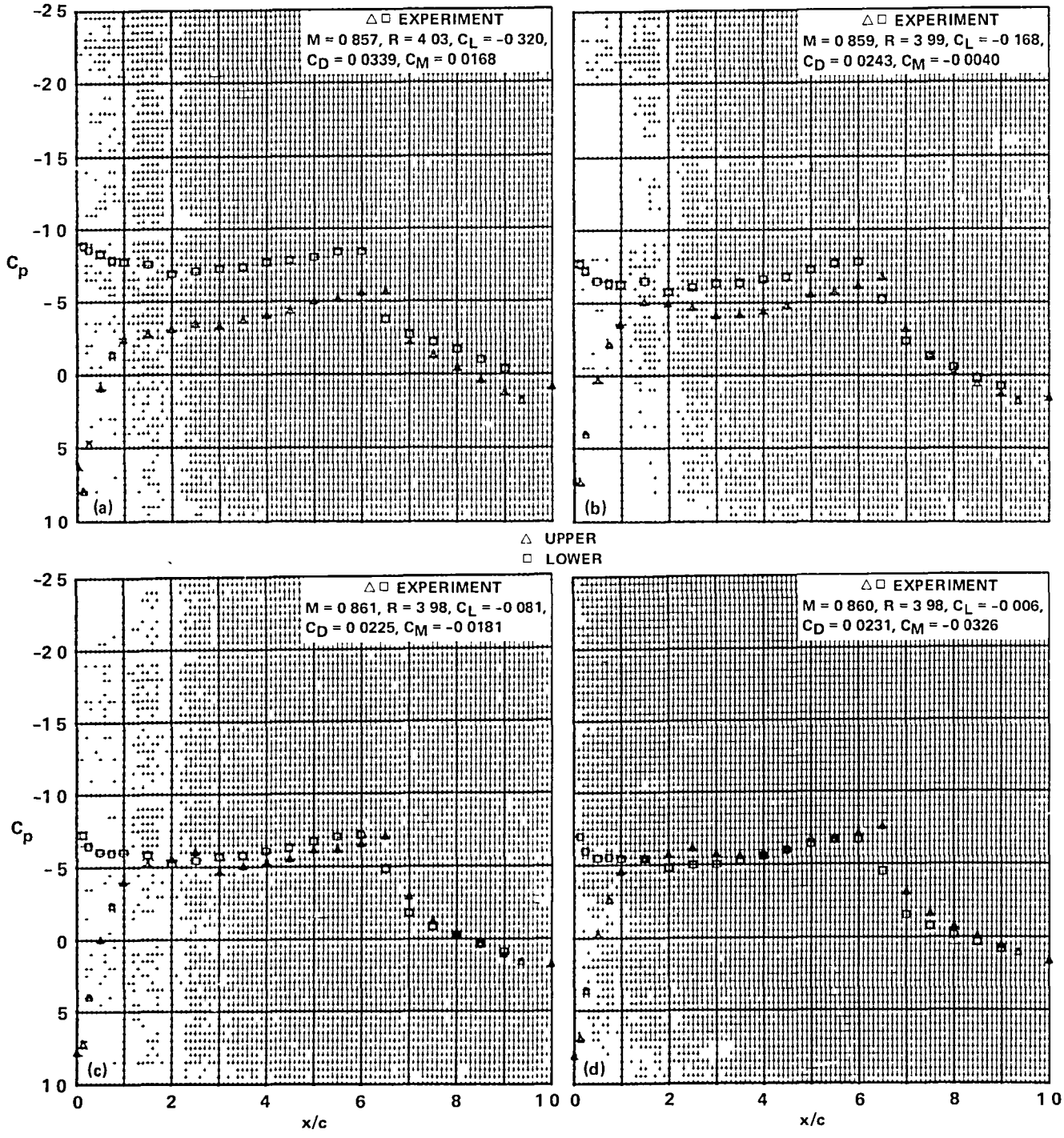

Figure 37.- Pressure distributions of the SSC-A09 airfoil, M_{set} = 0.86.

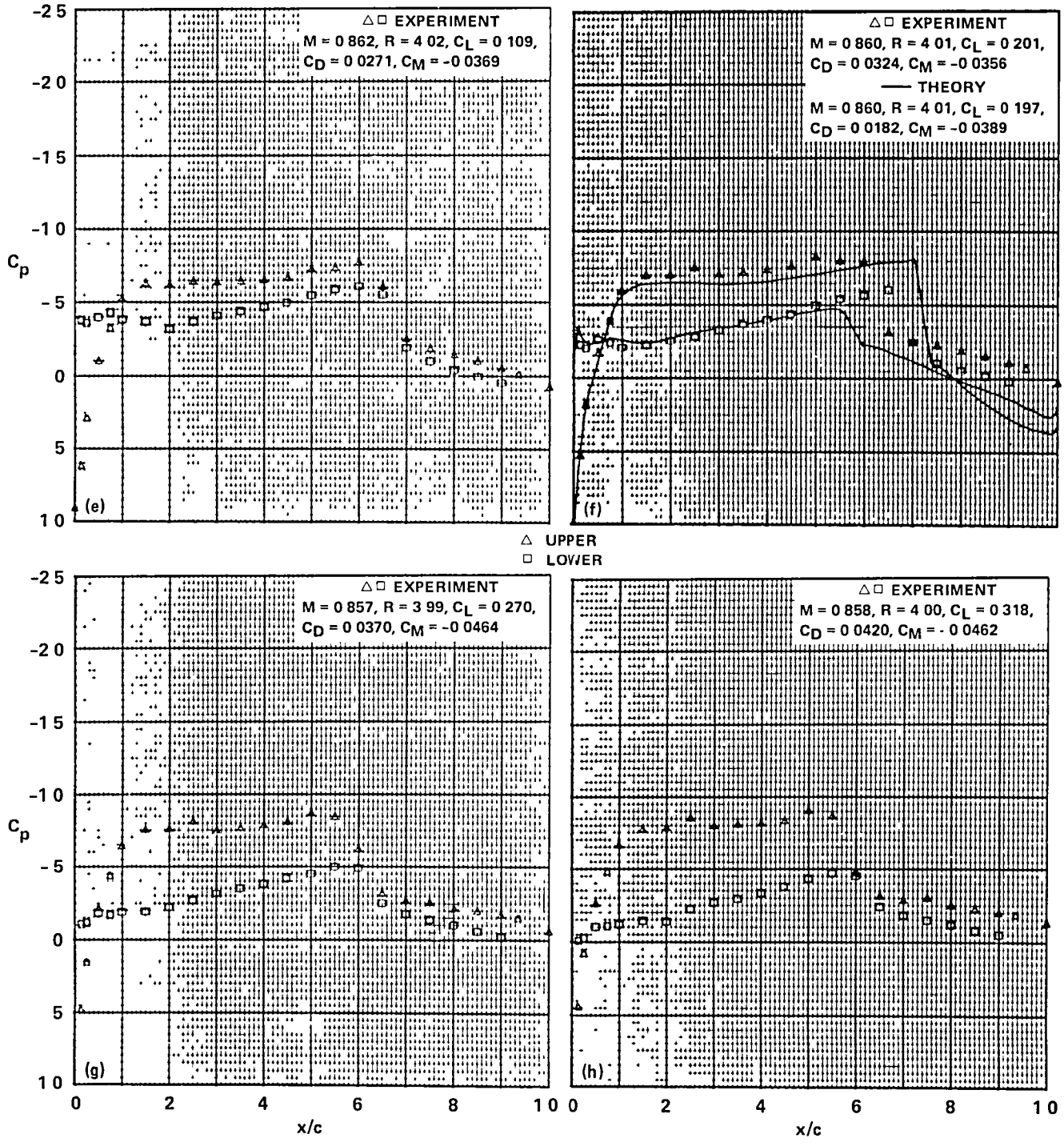

Figure 37.- Continued.

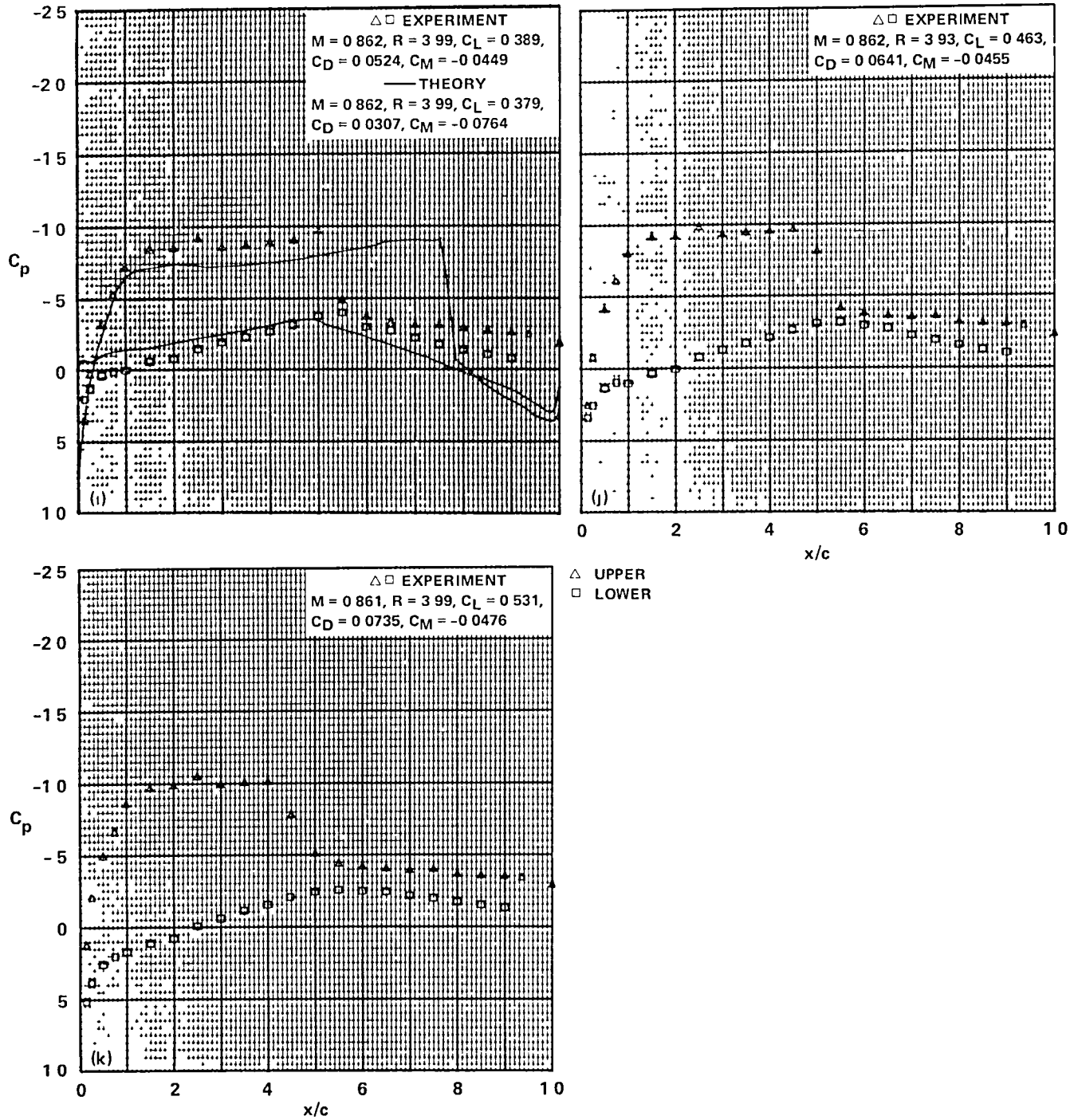

Figure 37.- Concluded.

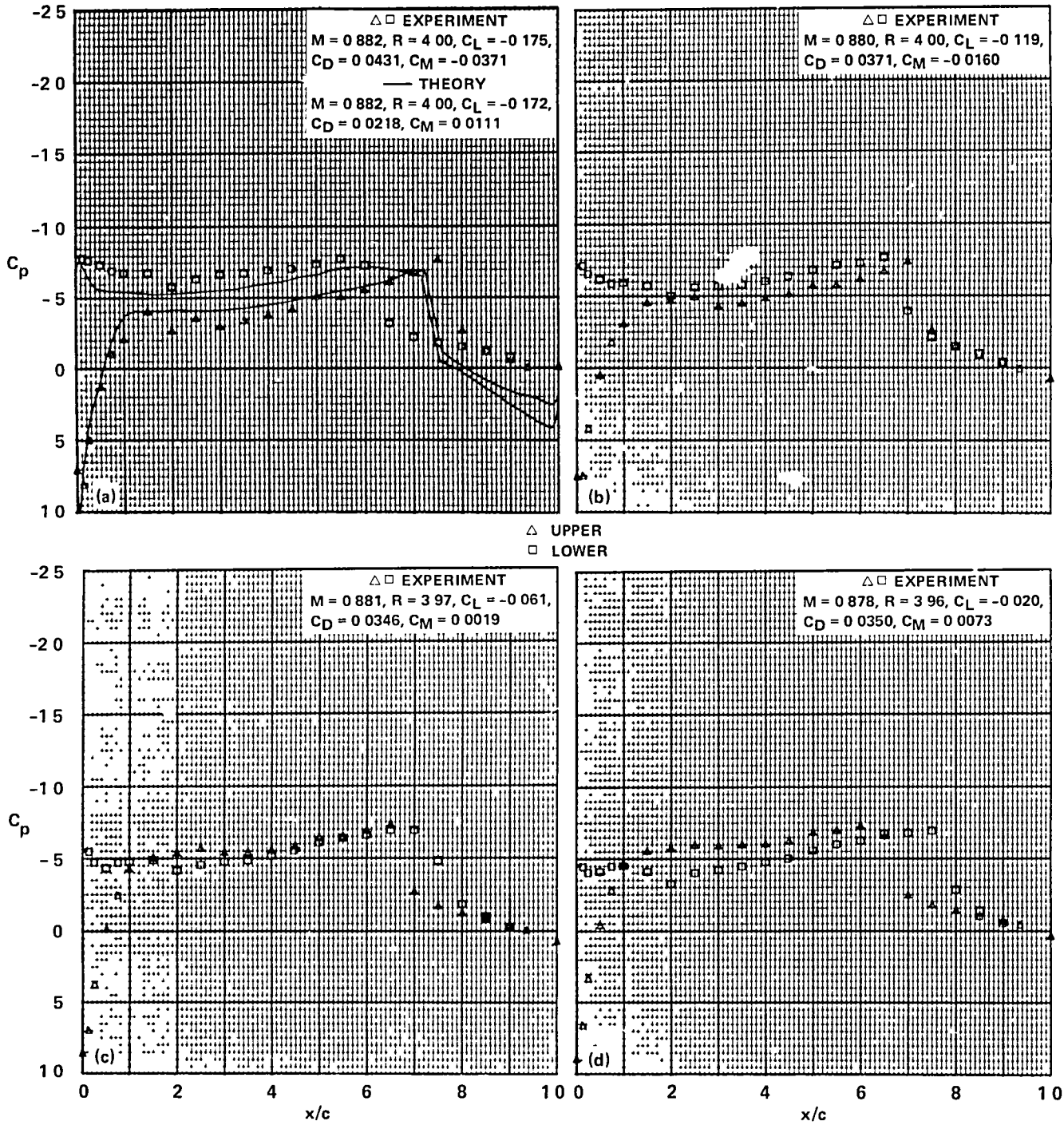

Figure 38.- Pressure distributions of the SSC-A09 airfoil, M_{set} = 0.88.

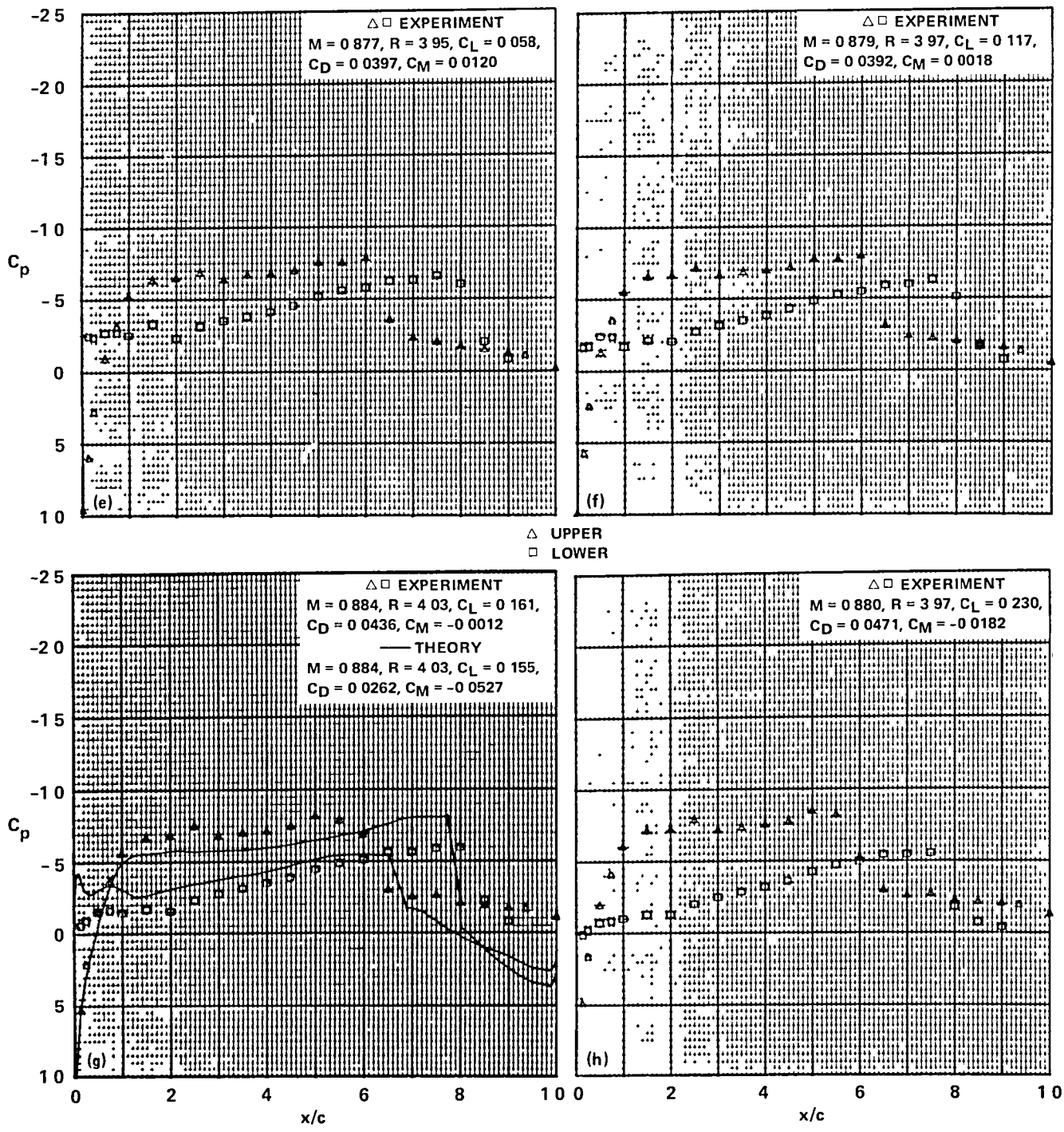

Figure 38.- Continued.

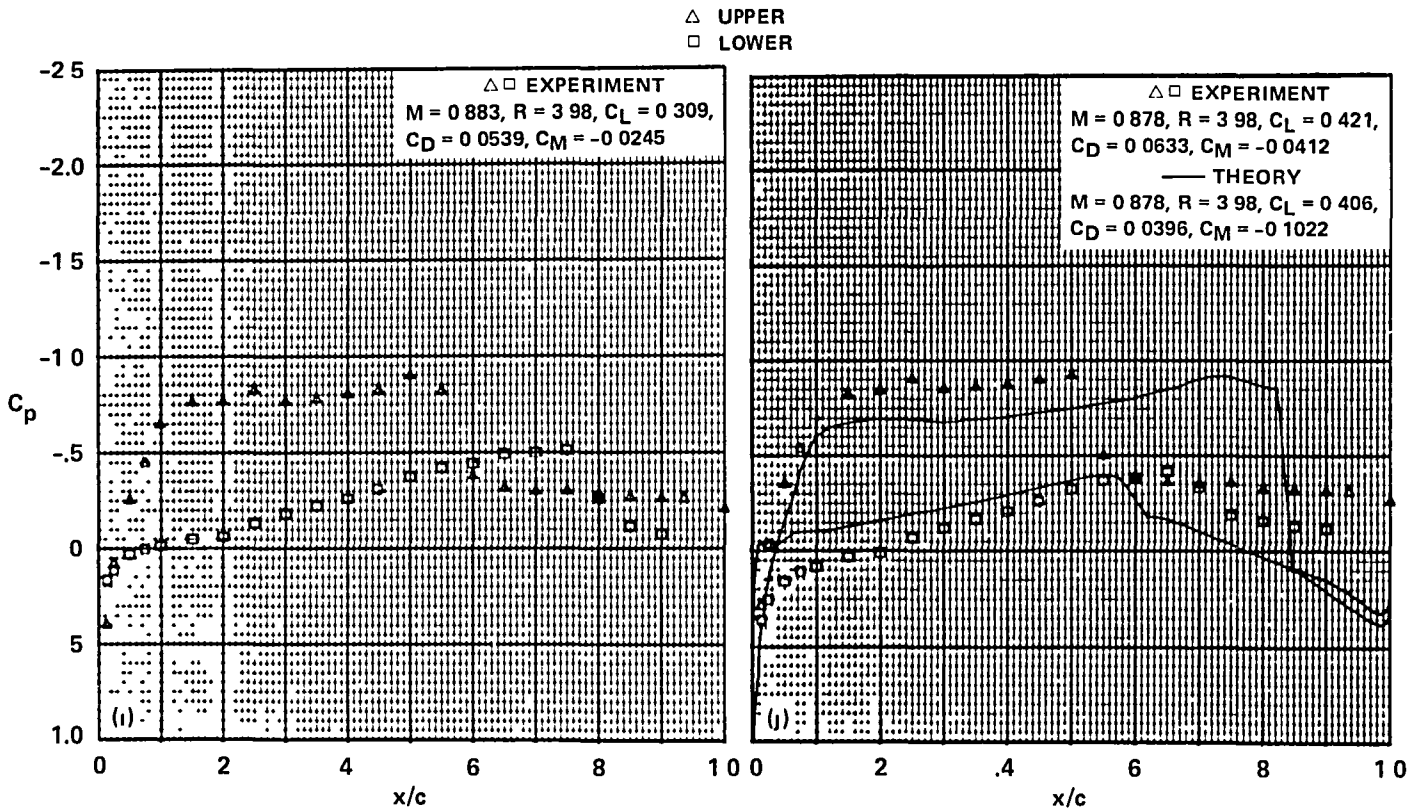

Figure 38.- Concluded.

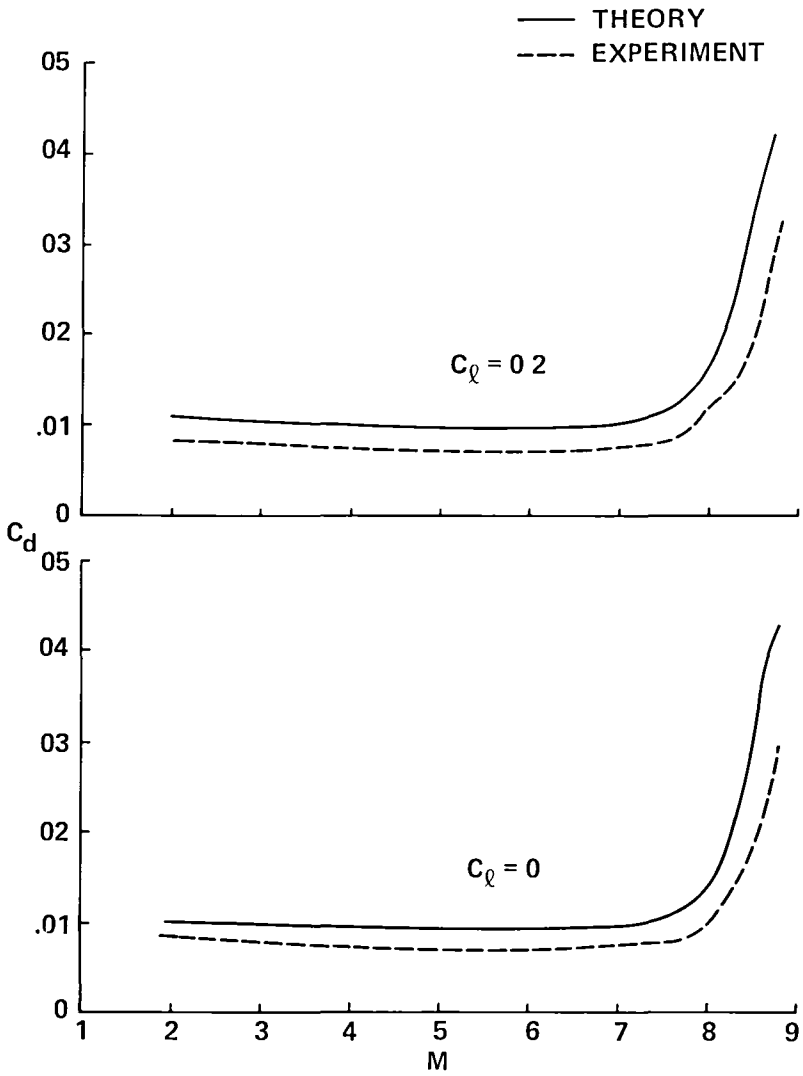

(a) SC-1095

Figure 39.-Variation of section drag coefficient with Mach number, transition fixed.

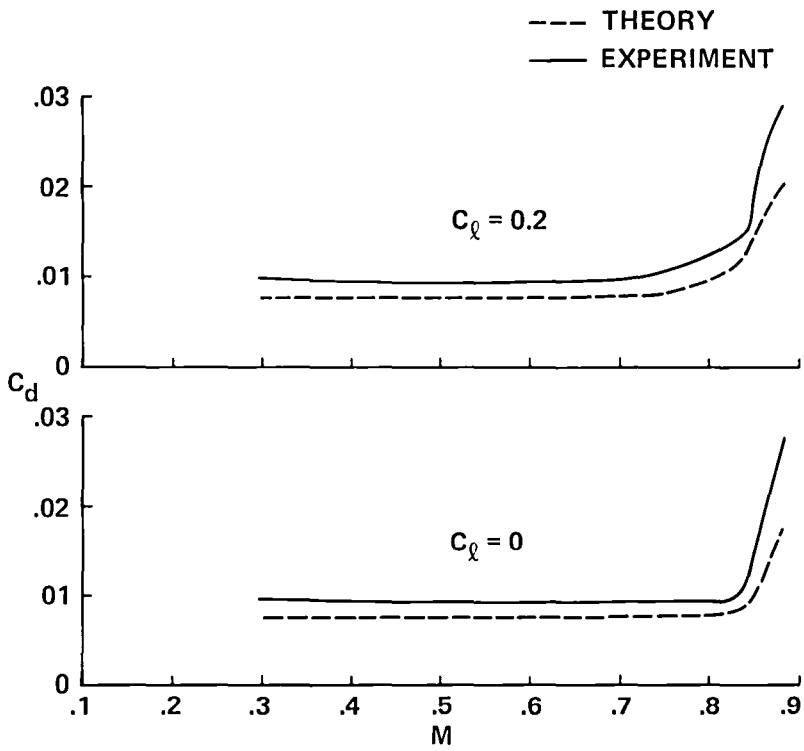

(b) A-2 AIRFOIL

Figure 39.- Continued.

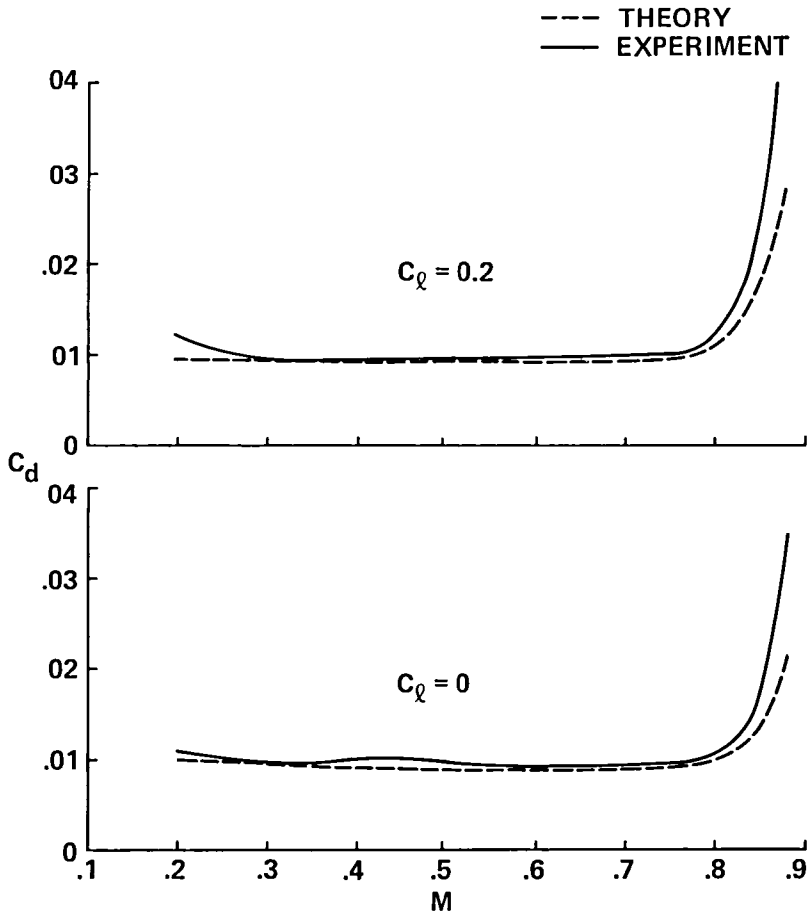

(c) SSC A09

Figure 39.- Concluded.

1 Report No	2 Government Accession No	3 Recipient's Catalog No
NASA TM-86719		

4 Title and Subtitle	5 Report Date
AN EVALUATION OF THREE HELICOPTER ROTOR SECTIONS	August 1985
	6 Performing Organization Code

7 Author(s)	8 Performing Organization Report No
Raymond M. Hicks and Leslie J. Collins (Informatics General Corp., Palo Alto, Calif.)	85219
	10 Work Unit No

9 Performing Organization Name and Address	11 Contract or Grant No
Ames Research Center Moffett Field, CA 94035	
	13 Type of Report and Period Covered
	Technical Memorandum

12 Sponsoring Agency Name and Address	14 Sponsoring Agency Code
National Aeronautics and Space Administration Washington, DC 20546	505-31-21

15 Supplementary Notes

Point of Contact: Raymond M. Hicks, Ames Research Center, MS 227-6, Moffett Field, CA 94035, (415) 694-5656 or FTS 464-5656.

16 Abstract

Three helicopter rotor sections were tested in the NASA Ames Research Center 2- by 2-Foot Transonic Wind Tunnel over a Mach number range from 0.2 to 0.88. The sections tested had maximum thickness/chord ratios of 0.078, 0.09, and 0.10. The thickest section was of early technology and had been tested previously in other wind tunnels. This section was included in the investigation to establish a basis for comparing the two thinner sections, which were of recent design. The results of the investigation showed that the pitching-moment characteristics for the three airfoil sections were acceptable. The drag divergence Mach numbers for the three sections were 0.80, 0.825, and 0.845 in order of decreasing thickness.

17 Key Words (Suggested by Author(s))	18 Distribution Statement
Airfoil Helicopter Wing Wind tunnel Rotor section	Unlimited Star category - 02

19 Security Classif (of this report)	20 Security Classif (of this page)	21 No of Pages	22 Price*
Unclassified	Unclassified	122	A06

*For sale by the National Technical Information Service, Springfield, Virginia 22161

End of Document